ADVANCED PHOTONIC METHODOLOGIES FOR THE *IN VITRO* MANIPULATION OF CELLULAR SYSTEMS

Craig McDougall

A Thesis Submitted for the Degree of PhD
at the
University of St. Andrews

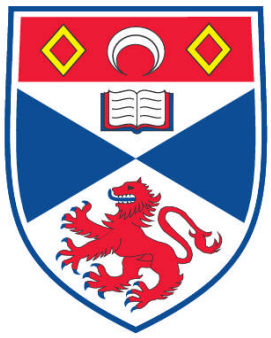

2011

Advanced photonic methodologies for the *in vitro* manipulation of cellular systems

Craig McDougall

A thesis presented for the degree of
Doctor of Philosophy

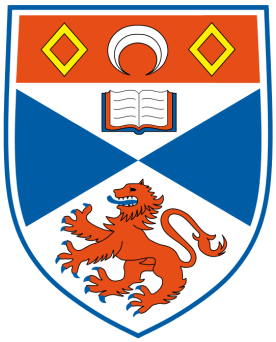

Ultrashort-pulse laser Group
School of Physics & Astronomy
University of St Andrews
United Kingdom

October 2010

Declarations

Candidate's declarations:

I, Craig McDougall, hereby certify that this thesis, which is approximately 35, 000 words in length, has been written by me, that it is the record of work carried out by me, and that it has not been submitted in any previous application for a higher degree. I was admitted as a research student in October 2006 and as a candidate for the degree of Doctor of Philosophy in October 2006; the higher study for which this is a record was carried out in the University of St Andrews between 2006 and 2010.

Date ..... Signature of Candidate .....

Supervisor's declarations:

I hereby certify that the candidate has fulfilled the conditions of the Resolution and Regulations appropriate for the degree of Doctor of Philosophy in the University of St Andrews and that the candidate is qualified to submit this thesis in application for that degree.

Date ..... Signature of Supervisor .....

Permission for electronic publication:

In submitting this thesis to the University of St Andrews I understand that I am giving permission for it to be made available for use in accordance with the regulations of the University Library for the time being in force, subject to any copyright vested

in the work not being affected thereby. I also understand that the title and the abstract will be published, and that a copy of the work may be made and supplied to any bona fide library or research worker, that my thesis will be electronically accessible for personal or research use unless exempt by award of an embargo as requested below, and that the library has the right to migrate my thesis into new electronic forms as required to ensure continued access to the thesis. I have obtained any third-party copyright permissions that may be required in order to allow such access and migration, or have requested the appropriate embargo below.
Access to printed copy and electronic publication of thesis through the University of St Andrews.

Date ..... Signature of Candidate .....

Signature of Supervisor .....

Dedicated to the benefit of all sentient beings...

(but especially Mum, Dad, Mark and Cat)

"Studying is a form of austerity. It is a process, like the bud unfolding into the beautiful fragrance spreading flower. Understanding this, we should approach our topic of study with love and patience."

Sri Mata Amritanandamayi, 29th May, 2010

Advanced photonic methodologies for the in vitro manipulation of cellular systems

Craig McDougall

Submitted for the degree of Doctor of Philosophy

October 2010

Abstract

This thesis investigates the application of a variety of optical techniques for the manipulation of single cells and their local micro-environment. The methodologies developed provide enhanced control over a single cell under study affording exquisite spatial and temporal control over biological processes of interest. The work presented within the thesis can be split into three distinct categories.

The first of these provides an investigation in light activated "caged" molecular probes. This work generated several new compounds which were then applied to providing control over processes involved in pain, mitochondrial intracellular signalling and memory processes in the central nervous system. Application of caged neurotransmitters then demonstrates the first *in vitro* wavelength orthogonal photolysis of biologically relevant substances. Such a technique has great potential in the study of fundamental interactions within the processes underpinning memory and cognitive function.

Secondly the application of optical injection techniques for the introduction of membrane impermeable species of interest is presented. An exploration of laser sources and optical systems has yielded two new strategies for optical injection. The targeted introduction of fluorescent stains, nucleic acids and gold nanoparticles to the interior of a live mammalian cells demonstrates the power of these techniques.

Thirdly, an investigation in optical trapping and optical injection provides simplified micromanipulation techniqes for application to biological studies. The use of capillaries as reservoirs for reagents of interest has realised a procedure for the reduction of large scale chemical assays to a single cell level in static flow. When this technique is combined with intelligent control over the trapping laser source's temporal behaviour, the interaction with the sample under study can be tailored for

biological amiability or sample ablation. In this way a single laser source can be employed for the optical trapping and nanosurgery of a biological sample.A final study is presented demonstrating initial results for the targeted optical injection of caged compounds into mammalian cells. This methodology draws on the strengths of optical injection and caging technologies and presents a significant step forward in the level of control afforded over a biological system under study by optical techniques.

The studies presented highlight the level of control and flexibility afforded by the application of optical manipulation and excitation strategies. Such optical methodologies extend the photonic tools available for enhanced studies in the life sciences.

Acknowledgements

I cannot believe that I am finally writing this section...that means that I must be finished writing my thesis, which has been made possible by the patience and generosity of a great many people. So before I reclaim my life outside a lab, I would like to offer my heartfelt thanks, gratitude and admiration to the following people.

First and foremost I would like to thank my supervisor Dr Tom Brown to whom I am greatly indebted. Thank you Tom for the fantastic opportunity to work in your group, your patience and support. More importantly thank you for the bacon rolls and coffee when I had been stuck in the lab all night! Also thanks for turning a blind eye if the surf report was looking particularly good and I am glad that we have not yet me under your coastguard persona...there is always time!

I also owe strong thanks to my second supervisor Dr Stuart Conway, who even after moving to Oxford University answers my elementary (sorry) chemistry questions. My understanding of biology would be far weaker if it were not for Dr Frank Gunn-Moore and his valuable advice, input and Monday meetings. Further gratitude is owed to Dr Nigel Emptage, for my introduction to working in a pharmacology lab and for hosting my visits to Oxford. Finally I wish to express my strong gratitude to Professor Kishan Dholakia for the opportunity to work within his optical trapping group.

So many people have helped me over the years and made my time in St Andrews so memorable that when I attempted to list everyone, this section of my thesis grew to around four pages. This is the heavily edited version.

Thank you to everyone in W-Squad for you help support over the past four years and your shared love of whisky, my Wednesdays will never be the same! Special thanks must go to Chris for teaching me how to build femtosecond lasers and more

importantly supportive talks when things were hard! Klaus Metzger, vielen Dank! Especially for always being up for “board” meetings and the lunches at the farm, I don’t think that our surf adventures have ended yet and I thank you for making hard times at work so much more enjoyable! I extend similar thanks to everyone in the optical trapping group. In particular thanks must be made to Dave Stevenson, you rock! I am also indebted to George Robb and his team in the mechanical workshop, who always managed to turn my scribbles into beautifully engineered masterpieces. Special thanks go to Stevie Balfor for always going beyond the call of duty!

Outwith the physics department, I need to thank all the chemists and biologists and pharmacologists who helped me out. In particular I must thank Nicos, Neil and Tom from the Conway group for your assistance. Extra special thanks go to Megan, who never lost patience with no matter how many questions I asked (or at what time!). I also have to thank my new boss for the time off work to finish my thesis off, greatly appreciated David. I am also forever grateful to the weather in St Andrews for bringing me waves to surf and wind to kitesurf when I needed an escape from the lab!

On a more personal note, I do not think that I can thank my family enough. Mum, Dad and Mark your endless support guided me through the duration of my PhD and without your kind words I would not be writing this now. Cat, you have no idea how much of a difference you made during my time in St Andrews but your hot chocolate and adventure skills in particular stand out. Thank you.

Thank you all for helping me through the last few years!

Publications

Peer Reviewed Publications

[1] M. Stanton-Humphereys, R. Taylor, C. McDougall, M. Hart, C. T. A. Brown, N. Emptage and S. .J. Conway *"Wavelength orthogonal photorealease of neurotransmitters in vitro"* In review.

[2] M. P. Van Ryssen, N. Avlonitis, R. Giniatullin, C. McDougall, J. L. Carr, M. N. Stanton-Humphreys, E. L. A. Borgström, C. T. A. Brown, D. Fayuk, A. Surin, M. Niittykoski, L. Khiroug and S. J. Conway *"Synthesis, photolysis studies and in vitro photorelease of caged TRPV1 agonists and antagonists"* Org.Biomol.Chem, 7, 4695 - 4707, (2009).

[3] C. McDougall, D. Stevenson, C. T. A. Brown, F. Gunn-Moore , K. Dholakia *"Targeted optical injection of gold nanoparticles into single mammalian cells"* J.Biophoton, 2(10), 736-743, (2009).

[4] N. Avlonitis, S. Chalmers, C. McDougall, M. N. Stanton-Humphreys, C. T. A. Brown, J. G. McCarron and S. J. Conway *"Caged AG10: new tools for spatially predefined mitochondrial uncoupling"* Mol.Biosyst, 5, 450 - 457,(2009).

[5] C. T. A. Brown, D. Stevenson, X. Tsampoula, C McDougall, A. A. Lagatsky, W. Sibbett, F. J. Gunn-Moore and K. Dholakia *"Enhanced operation of femtosecond lasers and application in cell transfection"* J.Biophoton, 1, (3):183-199 (2008).

Conference Proceedings

[6] C. McDougall, D. Stevenson, C. T. A. Brown, F. Gunn-Moore , K. Dholakia "Targeted optical injection of gold nanoparticles into single mammalian cells" . in CLEO, Munich, (WB1), 2008.

[7] C.T.A. Brown, C. McDougall, D. Stevenson, F.J. Gunn-Moore and K. Dholakia “Laser assisted delivery of membrane impermeable materials to targeted single cells” .

Abbreviations

AOD - Acousto Optical Deflector

ATP - Adenosine Triphosphate

Benzoin- 3,5-dimethoxybenzoin

Ca^{2+} - Calcium

CCD - Charge Coupled Device

CDMNB - DMNB-carbonate linker

CHO - Chinese Hamster Ovary

CMNB - 5-carboxymethoxy-2-nitrobenzyl

CO_2 - Carbon Dioxide

CLSM - Confocal Laser Scanning Microscopy

CLSRM - Confocal Laser Scanning Reflectance Microscopy

CNS - Central Nervous System

Cr:Forsterite - Chromium Forsterite

CW - Continuous Wave

DMNB - 2-nitro-4,5-(dimethoxy)benzyl

DNA - Deoxyribonucleic Acid

EMCCD - Electron Multiplying Charge Coupled Device

ER - Endoplasmic Reticulum

FCS- Foetal Calf Serum

FITC - fluorescein isothiocyanate

fs - femtosecond

GABA - γ-Aminobutyric acid

GLMT - Generalised Lorentz Mie Theory

GPCRs - G protein couped receptors

HEPES- 4-(2-hydroxyethyl)-1-piperazineethanesulfonic acid

HL-60 - Human Leukameia

HPLC - High Pressure Liquid Chromatography

HSP - Heat Shock Protein

IP_3 - inositol 1,4,5-trisphosphate

IPSP- Inhibitory PostSynaptic Potential

IR - Infra Red

Laser- Light Amplification by Stimulated Emission of Radiation

LG- Laguerre Gaussian

MEM - Modified Earles Medium

MeO - Methoxy

MPA - 4-methoxyphenacyl

mRNA - messenger Ribonucleic Acid

N.A - Numerical Aperture

Na^+ - Sodium

Nd:YAG - Neodymium Yttrium Aluminum Garnet

NIR - Near-Infa-Red

NMDA- N-Methyl D-aspartate

NMR - Nuclear Magnetic Resonnance

ns - nanosecond

OPO - Optical Paramteric Oscillator

PBS - Phosphate-Buffered Saline

ppm - Parts per million

RBC - Red Blood Cell

RNA - Ribonucleic Acid

ROI - Region Of Interest

RPMI - Roswell Park Memorial Institute

SERS- Surface Enhanced Raman Spectroscopy

SESAM - Semiconductor Saturable Absorber Mirror

TEM - Transverse Electro Magnetic

$Ti:Al_2O_3$ - Titanium Sapphire

TMRE- Tetramethylrhodamine, ethyl ester, perchlorate

TMS - Tetramethylsilane

TRPV1 - Transient Receptor Potential Vanilloid 1

UV - Ultra Violet

UV/Vis- Ultra Violet/Visible

Vis - Visible

Yb:KYW - Ytterbium Potassium Yttrium Tungstate

$\Delta\Psi$m - Mitochondrial mambrane potential

3D - Three Dimensional

Contents

Chapter 1

Light as a tool for the life sciences

1.1 Preface

Biochemical processes working on sub-micron spatial and sub-second temporal resolutions govern the health of all living organisms. Tools and techniques for the observation, probing and manipulation of these processes are crucial to maintaining healthy function. For over three hundred years photonic technologies have enabled researchers in the life sciences observe the results of their probing systems with a biochemical tool set and unravel some of the biochemical mysteries behind life functions. Over the past fifty years, the application of photonic technologies to the life sciences has advanced beyond the realm of passive observation to active manipulation and spawned the multidisciplineary field of biophotonics.

The same period has also seen powerful developments in the chemical probes used to investigate biological processes. In the 1970s chemists applied light activated chemical compounds known as "caged compounds" to biological systems for the first time. Subsequent caging of major biological affectors has provided researchers in the life sciences with a host of molecular tools for probing and controlling the mechanisms of complex cellular processes.

The theme of the work presented in this thesis is of developing and applying optical methodologies for enabling the advanced manipulation of biological samples. Techniques employing optical tweezers and a variety of laser sources for the active manipulation of biological samples is presented alongside the development of novel

caged compounds and intelligent photolysis methodologies for the control of cellular chemistry and local microenvironment. Such tools are necessary for the successful eludication and upkeep of healthy cellular function either in the investigation, diagnosis or treatment of disease.

1.2 Synopsis

This thesis is concerned with the use of optical techniques for the manipulation of single cells and consists of eight chapters.

The first chapter provides an introduction to using light as a tool in the life sciences and introduces the field of biophotonics. The motivations for advanced cellular manipulation and the key techniques involved in the work, optical tweezers, laser scalpels and caged compounds are introduced. As the techniques presented in this thesis are concerned with the manipulation of single mammalian cells, an introduction is given to the eukaryotic animal cell and its major constituents. The chapter concludes with a consideration of the interaction between laser fields and biological samples and the parameters controlling the interaction.

In chapter two, a brief review of the literature provides the theoretical basis for the optical tweezers and injection techniques employed in this thesis.

Chapter three covers the key experimental techniques employed throughout the thesis to prevent repetition. The design and construction of the ultrafast pulsed titanium sapphire laser used for the majority of the studies is presented alongside a general procedure for the construction of an optical tweezers arangement. The techniques associated with the preparation, handling and charaterisation of caged compounds is given, as is an overview of the biological techniques employed throughout the thesis.

Chapters four through seven describe the experimental work conducted in the laboratory.

More specifically, chapter four presents the development of caged molecular probes for enabling the control of cellular chemistry. Detailed charaterisation of the compounds is accompanied by a short summary of their biological application

Chapter five details the development of wavelength orthogonally caged neurotransmitters for application to studies in memory and cognitive function. Characterisation of the newly developed compounds is presented alongside the construction of the wavelength orthogonal photolysis microscope and the *in vitro* applicaiton of the new compounds.

Chapter six reports the development of advanced tehcniques for the optical injection facilitated delivery of membrane impermeable substances such as fluorescent stains, nucleic acids and gold nanoparticles to the interior of targeted mamallian cells.

The work introduced in chapter seven details simplified systems for the micromanipulation of single cells. These include a robust technique for the scaling of ensemble assays to single cells in static flow and a simplified arrangement for the optical tweezing and cellular surgery of a selected cell with a single laser source. A preliminary study into the optical injection of caged molecular probes is presented. Initial results are presented and future directions discussed.

The eighth and final chapter concludes the thesis with a summary of the presented work and consideration for future developments.

1.3 Motivation for advanced cellular manipulation

Living organisms are capable of reproduction, growth, metabolising and demonstrate responsiveness to their surroundings. Their constituent cells are elegantly orchestrated nanomachines that come together to form all living organisms. The processes underpinning cell function rely upon complex chemical signals, electric potentials, protein transfers and the correct translation of information stored in genetic archives being executed with critical timing and sub-micron spatial accuracy. Researchers in the life sciences work to uncover the mechanisms behind these processes. Malfunction of processes at the cellular level can manifest as diverse diseases ranging from diabetes to cancer. Understanding the processes behind cellular function is thus vital to assessing and treating disease.

Historically, biologists have utilised an arsenal of biochemical tools and increasingly powerful microscopes to elucidate the causes for breakdown of correct cellular function. There is great demand for new tools that provide greater temporal and spatial resolution for investigation. The work in this thesis seeks to meet some of these needs, providing novel tools for manipulating biological systems based upon light. Tools permitting controlled movement of cells under study, the delivery of membrane impermeable substances and the defined activation of biochemical affector compounds are presented.

1.4 Photonics in the life sciences: biophotonics

In the 1700s microscopes became advanced to a level where high magnifications were achievable and made it possible for biologists to see cells and internal structures for the first time [8]. More recently the development of the laser in 1960 [9] paved the way for a paradigm shift in application of photonic technologies from passive observation to active manipulation. Unlike filament or arc lamps laser radiation is a collimated, highly focusable source of light which is available at many different wavelengths. Intense development has lead to a plethora of laser sources operating across the electromagnetic spectrum, both CW and pulsed, being made available for application to the life sciences.

A watershed event in the relationship between photonics and the life sciences took place in the 1970s when Arthur Ashkin developed the first optical traps enabling non-contact manipulation of microscopic particles [10]. Optical tweezers utilise the piconewton forces imparted by the momentum of light to hold, translate and spin microscopic particles with unprecedented dexterity.

In the late 1960s Bessis used highly focused lasers to develop the “laser scalpel” [11]. The interplay between the laser field and sample was engineered for maximum interaction, resulting in ablation of the sample. The laser scalpel enabled sub-cellular nanosurgery in a non contact sterile manner permitting the perforation, cutting or even fusion of biological cells with great control .

The combination and application of such photonic technologies therefore provides

an attractive toolset. A single microscope can be used to image and physically manipulate a biological sample of choice in a sterile non-contact manner. With very little modification a standard laboratory microscope can be transformed into a photonic bioworkstation capable of imaging, cutting [12], fusing [13], stretching [14], rotating [15], modifying and translating biological samples.

The advantages offered by optical manipulation are sterile precision and control. Unrivalled spatial control is achievable when using a laser beam focused to its diffraction limit. The duration of the light-matter interaction can be easily controlled through the temporal switching of the laser beam. The nature of the interaction can be selectively scaled from non-destructive to ablation by varying, for example the peak power of the laser.

1.5 Caged compounds for control of cellular chemistry

Caged compounds are biological affector molecules where activity is disabled by the addition of a chemical group to a critical position on the molecule. As illustrated in figure 1.1, removal of this photolabile protecting group with light typically in the UV region of the spectrum returns functionality and generates a localised concentration jump of the affector. Exquisite control over compound delivery is afforded even once

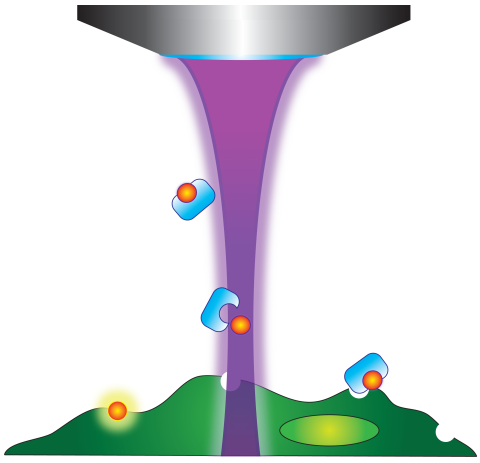

Figure 1.1: *Irradiation of a "caged compound" with light breaks the photolabile bond resulting in a highly localised concentration jump of the active molecule.*

delivered to the cell interior where control over traditional agents can be challenging.

Since the application of caged adenosine triphosphate (ATP) in the 1970s [16], numerous caged probes have been synthesised for application to biological studies including chelators, neurotransmitters, fluorescent stains, peptides, nucleotides and enzymes for which several exceptional reviews exist [17, 18]. The caged control of DNA transcription presents a powerful demonstration of the methodology [19].The methodology is advantageous for the study of any process which demands high spatial and temporal resolution such as the mechanisms of ligand-gated receptor channels.

Photolysis is commonly achieved using high power UV flashlamps, however, such broadband sources are inefficient and challenging to focus effectively [20]. Consequently the use of lasers to initiate photolysis has become more commonplace. Developments in photolysis technologies strive for finer spatial control over photorelease of the affector molecule. The application of multiphoton techniques yields femtolitre concentration jumps of effector molecules due to the highly localised excitation at the beam focus [21]. The improved axial confinement over single photon photolysis is illustrated in figure 1.2 Longer wavelength excitation can be advantageous

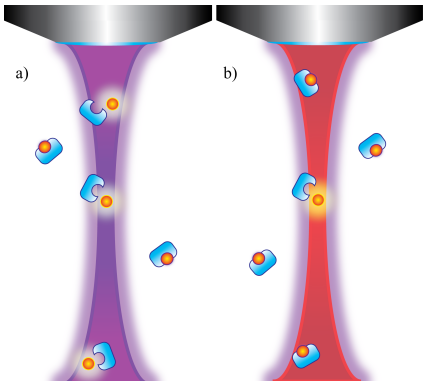

Figure 1.2: *Single photon UV photolysis (a) provides poor axial spatial resolution compared to Multiphoton IR photolysis (b). The intensity squared dependance for multiphoton absorption determines that photolysis only occurs at the focus of the beam (b).*

due to increased penetration depth and greater biological amiability. Unfortunately the modelocked femtosecond IR laser sources required are expensive and operator intensive. A lack of caged compounds with acceptable two-photon cross sections is also problematic. Another technique for improved spatial resolution is chemi-

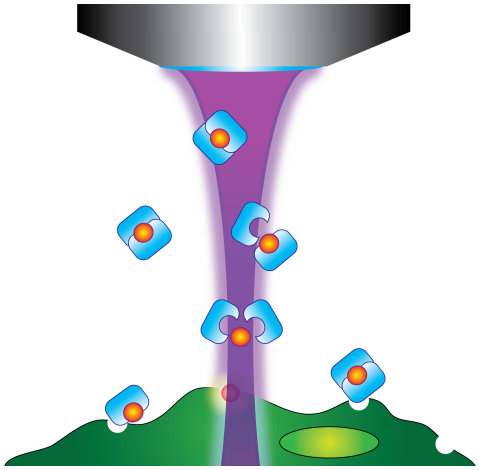

Figure 1.3: *Caging with two chemical groups provides an intensity squared dependence for photorelease of the affector compound under single photon illumination.*

cal two-photon photolysis [22]. As illustrated in figure 1.3 affector molecules are caged with two photolabile groups to achieve the same intensity squared condition for photolysis. Advantageously, chemical two-photon photolysis is a single-photon process based on more robust economical UV laser sources. Another drive in the development of photolysis methodologies is for multisite photolysis techniques. Here the application of advanced optical beam deflection techniques based on acusto optical deflectors (AODs) and spatial light modulators (SLMs) is revolutionising the photolysis of caged compounds.

The main barriers to more widespread implementation of caging technologies are complicated instrumentation and a reliance on commercially available caged probes. In this thesis, the development of new caged molecular probes for unmet biological problems and the establishment of a new methodology for enhanced investigation of neuronal systems is presented.

1.6 Nature's nanomachines; an introduction to the mammalian cell

The cell is the fundamental structural and functional unit of living organisms. There are two classes of cells, prokaryotic and eukaryotic. These share common features such as being bound by a semi-permeable plasma membrane enclosing a cytosolic

semi-fluid. Both also contain ribosomes for protein manufacture according to the genetic information encoded on chromosomes. There are substantial differences between the two.

Prokaryotic cells, approximately 1 - 10 μm in size, are basic structure and divide by binary fission. Organisms such as bacteria or archea are prokaryotic based. Eukaryotic cells are larger, approximately 10 - 100 μm in size with complex internal structure. Eukaryotic cells contain a true membrane bound nucleus, internal structure and specialised membrane bound organelles. Division is by the process of mitosis [23]. Larger complex organism such as plants, fungi and animals are formed from eukaryotic cells.

The presented techniques are for the study of single eukaryotic animal cells, though they also have the potential for application in other areas of biology. Successful manipulation requires a basic knowledge of the structure and constituents of the cell which are detailed here.

1.6.1 The structure of the eukaryotic animal cell

In simplifying biological problems the cell is often reduced to a sphere immersed in water and treated like a polymer colloid in solution. In reality, the cell is a complex and diverse light-sensitive structure with scattering centres, non-spherical morphology and adherent qualities. Understanding the composition and internal processes of a cell is vital to successful experiments. The exploded cartoon cross section of a generalised eukaryotic animal cell shown in figure 1.4 highlights the cellular components of interest to the work presented in this thesis.

The cytosol of the cell contains distinct membrane bound compartments known as organelles. Each plays a specific role in the internal workings of the cell, bound by a semi-permeable plasma membrane. In addition to the organelles there is an internal cellular network of fibres known as the cytoskeleton which maintains and alters the cell morphology.

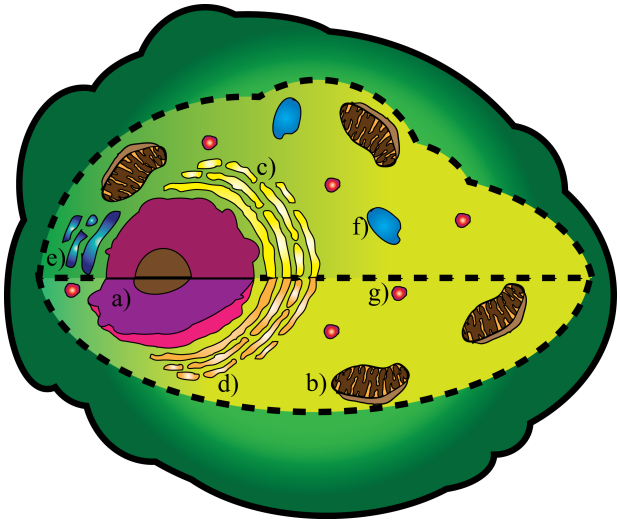

Figure 1.4: *An exploded cross section of the eukaryotic animal cell illustrating all the major organelles.*

1.6.1.1 The Nucleus

The largest and first organelle to be discovered was the nucleus (figure 1.4a). The majority of the genetic information in a cell is housed within the nucleus though a small amount is also located in the mitochondria [24]. The nucleus is comprised of a double membrane housing nucleoli and chromatin. The double membrane is perforated with pores and is continuous with the endoplasmic reticulum. It is the region where units of DNA called chromosomes are transcribed into messenger RNA (mRNA). Once translated from DNA, the mRNA passes into the cytoplasm ready for translation to proteins by ribosomes in the cytoplasm.

1.6.1.2 Mitochondrion

Mitochondria (figure 1.4b) are the respiratory powerhouses of the cell and are where energy is extracted from sugars and fats, combined with oxygen and converted to ATP in the Krebs cycle. They are 0.2 μm to 0.5 μm in length [24] and comprised of a double membrane with infoldings called cristae, all of which encloses a matrix. Mitochondria are self replicating and contain DNA and ribosomes permitting them to synthesise their own proteins.

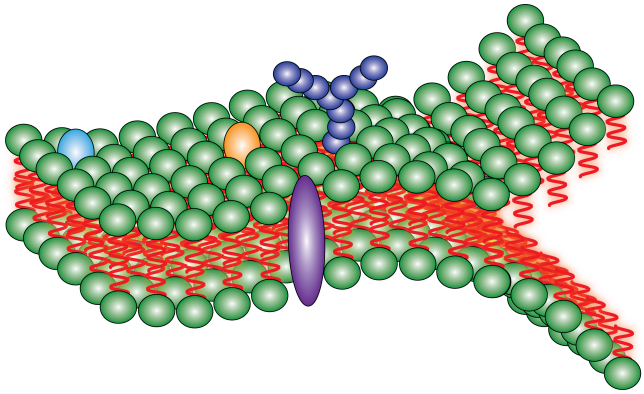

Figure 1.5: *The selectively permeable cell membrane is composed from a phospholipid bilayer (green & red) interspersed with transmembrane proteins (purple, yellow & blue) which control the passage of materials in and out of the cell and oligosaccharide carbobohydrate molecules (navy blue) which form the glycocalyc coat.*

1.6.1.3 Endomembrane system

The endomembrane system is comprised of the smooth and rough endoplasmic reticulum (ER), Golgi apparatus and lysosomes (figure 1.4c,d,e and f respectiveley). Together these organelles moderate the transport of proteins throughout the cell whilst performing vital metabolic functions. The smooth ER has many enzymes attached to it and produces steroid hormones and detoxifies fluids [23]. The rough ER is so called due to the ribosomes attached to its surface which in turn produce proteins. The Golgi apparatus stores, modifies and distributes the products of the ER. Lysosomes are single membrane sacs containing digestive enzymes which form the digestive system of the cell.

1.6.1.4 Peroxisomes

Peroxisomes (figure 1.4g) that are single walled vesicular sacs containing specific enzymes known as peroxidases are located in close proximity to mitochondria and perform oxidation and then detoxify the resulting hydrogen peroxide.

1.6.1.5 Membranes

The plasma and organelle membranes are comprised of a phosphlipid bilayer as illustrated in figure 1.5. The fluid mosaic model for the cell membrane was proposed in the 1970s by Singer and Nicholson [25]. The phospholipid molecules consist of

a hydrophobic heads on the exterior with hydrophillic tails on the interior. The bilayer is approximately 6-10 nm thick [23] and forms a selectively permeable layer to the cell interior and allows the cell to regulate the transport of materials into the cell. Lipid soluble materials can passively diffuse across the membrane whereas polar molecules rely upon proteins embedded in the membrane to facilitate active transport across the membrane. There is a layer of oligosaccharide carbohydrate enriched molecules covalently bonded to many of the proteins on the outer layer of the cell membrane known as the glycocalyx coat. The negative charge produced by the glycocalyx coat separates cells in multi cell layers and functions as a highly sensitive receptor surface. Chemical signals are carried on the surface of the coat which enable neighbouring cells to recognise the cell. The membrane forms an effective barrier to large and charged molecules such as DNA [23].

1.7 Light tissue interaction

The complex interaction between the biological sample and manipulation laser field is multi-faceted and depends upon several factors. Beyond the obvious relationship with applied laser power, the distribution of the radiation, wavelength and temporal emission characteristics of the laser play an important role in the interplay between the laser and biological sample as do the optical properties of the material. Such factors dictate how the incident light is absorbed, scattered, refracted or reflected in the bulk of the sample under study.

1.7.1 The effect of laser irradiance

Irradiance describes the light incident upon a surface as a function of power and exposure area and is commonly confused with intensity which describes energy flux in similar units. Intuitively, laser-induced photodamage scales with increasing irradiance and exposure time [26]. Greater damage is caused at increasing optical powers and with decreasing exposure areas. The laser irradiance within the focal volume of the system controls interaction between the laser radiation and biological sample [27]. The extent of the interaction is fundamentally related to how the

sample absorbs the incident light and dissipates the deposited energy. Absorption is a function of the how the energy is distributed, exposure time, wavelength and temporal characteristics of the incident beam. In extreme cases photodisruptive ablation of a sample can occur [28–33]. Absorption of the laser field can result in photothermal, single-photon photoablative or multiphoton plasma ablative processes [27]. Photoablation results from the absorption of a single photon promoting an electron from a bonding to nonbonding orbital resulting in dissociation of the molecule. Subsequently a highly disruptive mechanical pressure wave propagates in a process known as cavitation [34]. In plasma-induced ablation the multiphoton absorption of incident laser light and cascade ionisation processes result in generation of free electrons within the focal volume [30, 33]. At high irradiances a cavitation bubble may trigger similar to photoablation, however, the multiphoton ablation is more commonly associated with a plasma formation [30] which has been observed to cause less collateral damage to surrounding regions [35]. The key parameters governing which process occurs are laser irradiance, wavelength and temporal characteristics of the radiation.

1.7.2 The effect of laser wavelength

The principal absorbing constituents of a typical biological sample are water and pigments such as haemoglobin and melanin [27, 36]. The absorption spectrum in figure 1.6 illustrates a "diagnostic window" where a relative minimum in absorption between 0.6 μm and 1.2 μm provides favourable conditions for optical manipulation. Within this window the viability of biological samples has been shown to increase greatly compared to visible wavelengths [37]. This is attributed to increased absorption by proteins such as haemoglobin or melanin in the visible as illustrated in figure 1.6. Examples of photodamage and phototoxic effects within the visible and UV wavelength ranges are commonly reported in the literature. For optical tweezers applications strong absorbtion must be avoided but for cellular nanosurgery these wavelengths are of interest.

As early as 1912 Tschachotin had used intense UV light to destroy targeted regions of cells and embryos [38]. This implementation of the first microbeam scissors

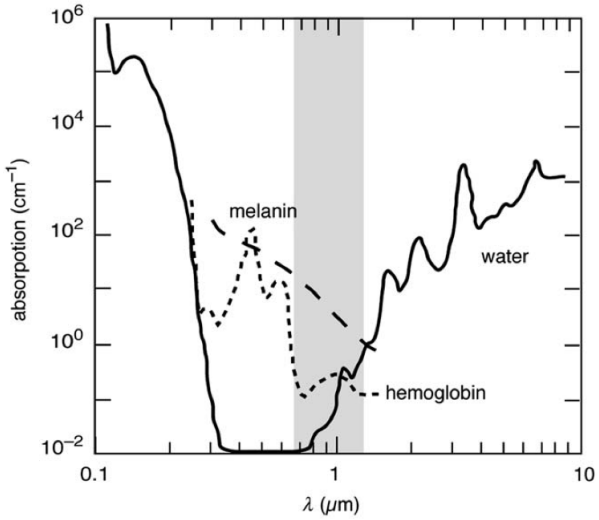

Figure 1.6: *A theraputic window exists between 0.6 μm and 1.2 μm where there is a relative low in absorption in the major constituents of biological samples; water, melanin and haemoglobin. Wavelengths in this window are ideal for the manipulation of biological samples. Figure from [36].*

far preceded the advent of the laser and development of laser scissors by Bessis in 1962 [11, 12]. Therefore, it can be seen that for the successful optical manipulation careful choices must be made with regards to wavelength.

Wavelength choice is often limited by availability of suitable laser sources. For optical trapping the laser source should emit in a single transverse mode (TEM_{00}) with good beam pointing and power stability. For studies in the IR, CW Ti:Al_2O_3, and Neodymium based laser sources are typically employed.

Ashkin observed "damage free" optical manipulation of biological samples using IR wavelengths [37]. Based on his work rigorous investigations into IR trapping of biological samples have been performed. There are no known nuclear chromaphores with absorption in the 700 nm to 1064 nm wavelength range, but mitochondria are known to exhibit strong absorption at 700 nm [26].

The work of Berns *et al* pioneered investigations into photoinduced damage in optical traps. Several investigations examine the action spectrum of wavelength as a function of photodamage. In 1993 whilst working with mitoic chromosomes, Berns' research group demonstrated wavelength specific formation of abnormal chromosome bridges. The most detrimental effects occurred at 760 nm [39]. Using CHO cells in 1996 , the Berns group employed a ND:YAG (1064nm) and a Ti:Al_2O_3 laser

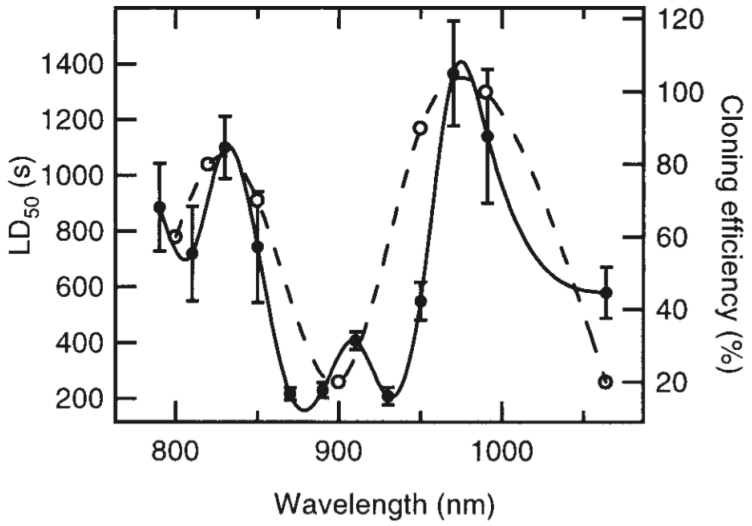

Figure 1.7: S*tudies into the effects of trapping cells with IR wavelengths demonstrated and action spectrum of wavelength against photodamage. The solid line represents studies undertaken by Neuman et al on the effects of optical trapping at different wavelengths in the IR upon the health of Escherichia coli. The dashed represents a similar study conducted by Liang et al upon CHO cells. Figure from* [26, 40].

(700-990 nm) to examine the effect of optical trapping upon the clonability of the cells [26]. Alongside a decrease in clonal growth for increasing exposure times and power densities, they observed an action spectrum of clonabilty with wavelength as illustrated by the dashed line in figure 1.7. Maximum clonability was observed for 950-990 nm whilst least at 740-760 nm and 900 nm. Alarmingly, as shown in figure 1.7, 1064 nm which is commonly used for the trapping of biological samples had a strongly detrimental effect upon the clonability of the cells [26].

In 1999 Neuman *et al.* performed a similar experiment with *Escherichia coli (E.Coli)* over the 790 - 1064 nm wavelength range [40]. As illustrated by the solid line in figure 1.7 observed minima in photodamage at 830 nm and 970 nm whilst identifying maxima in photodamage at 870 nm and 930 nm. Interestingly Neuman observed that under anaerobic conditions any damage was reduced to zero, implicating oxygen and the photodamage pathway. Furthermore, the intensity dependence of the photodamage was found to be linear, indicating a single photon process [40]. In 2002 Leitz *et al* studied the action spectrum of photodamage against wavelength on a heat shock protein (HSP) transgenic strain of the nematode *Caenorhabditis elegans* which expresses reporter gene when under stress [41]. In addition to increased

expression of the HSP reporter gene with increased power and exposure time, it was confirmed that the wavelength range between 700 nm and 760 nm is unsuitable for optical tweezers due to photochemical processes. Their work also reported a minimum in photodamage at 810 nm. It was also observed that although photochemical effects are reduced at longer wavelengths, photo-induced heating increases [41]. In 2004 Ramser et al demonstrated that red blood cells (RBC) were more sensitive to 1064 nm than 830 nm and also confirmed that the photo-toxic effects were minimised in anaerobic conditions [42]. A recent investigation in 2008 by Mirsaidov et al upon time-shared optically trapped bacteria in the wavelength range 840 - 930 nm reported a weak dependence upon wavelength but linear dependence upon laser peak power. This work implies a single-photon process for the observed photodamage [43] in agreement with the earlier work of Neuman [40].

The wavelength selected for manipulating a biological sample can have a profound effect upon the nature of the interaction with the sample under study. Even in the IR where viability is optimal there is an action spectrum of photodamage against wavelength as illustrated in figure 1.7. The studies described in this section are all based upon CW laser systems however, the temporal dynamics of the laser source can have a marked effect upon the light tissue interaction. With careful experimental design, the same wavelength can be used to obtain both optical tweezing and controlled cutting of the same sample by varying only the temporal dynamics of the beam as demonstrated in chapter seven of this thesis.

1.7.3 The effect of pulsed laser operation

The pulsed laser systems of interest in this work deliver pulses ranging from nanoseconds (ns) to femtoseconds (fs) in duration. The different temporal regimes elicit distinct interactions with biological samples. Optical photo-disruption is primarily controlled by the pulse energy which is a function of the irradiance, temporal pulse duration and pulse repetition rate at the sample plane.

Disruption can occur by means of photothermal, photo-ablative or plasma induced ablation and the degree of colateral damage varies with each mechanism. Typically the processes behind nanosecond and picosecond ablation are far more

aggressive that those associated with femtosecond irradiation, resulting in unwanted damage to the surrounding sample [31–33].

In 2003 it was demonstrated that colateral damage to a glass or soft sample as a result of photodamage shows a strong dependence upon the laser pulse energy [44]. It follows then that varying temporal operation of the laser from cw to pulsed and in this way varying the peak power of the laser pulses greatly affects the laser tissue interaction. In 2005 Heisterkamp *et al* performed experiments on a biological system and investigated the role of pulse energy in intracellular surgery using 1 kHz regeneratively amplified Ti:Al_2O_3 pulses. They derived optimal conditions for plasma-mediated surgery with minimum collateral damage operating 20% above the threshold for photobleaching [45]. Although it has been demonstrated that multiphoton absorption effects can occur in CW optical traps [46], the high peak powers associated with pulsed laser sources make multiphoton nonlinear absorption effects a critical issue for successful manipulation of biological samples in optical tweezers. However, it is these high peak powers which makes pulsed laser systems ideal for cellular surgery applications.

Recently in 2009, Zeigler *et al.* investigated cell viability in NG108 cells post cellular nanosurgery. Using UV pulsed nanosecond and IR femtosecond lasers single-photon UV nanosecond and femtosecond IR multiphoton ablative processes were contrasted. 3 ns pulses at 337 nm were compared with with 5 ms trains of 110 fs pulses at 770nm. 36 % viability was observed with the UV source and 79 % with the IR source 12 hours post exposure. The IR results were comparable to the control groups [34]. Increased viability with femtosecond IR pulses clearly highlights the reduced damage in nearby tissues when working with multiphoton plasma mediated ablation as opposed to aggressive mechanically mediated single photon photoablation generated by the UV pulses. Moreover, within the IR fs regime wavelength is still an important parameter as illustrated by studies by Chen *et al.* in 2002 in their work in multiphoton microscopy [47]. They observed suppressed plasma formation and significantly reduced absorption and auto-fluorescence when working with a longer wavelength Cr:Forsterite laser at 1230 nm compared to a Ti:Al_2O_3 laser operating at 800 nm. Reduced absorption longer wavelengths can also provide

increased penetration depth into samples permitting optical manipulations deeper within samples.

Laser repetition rate is also an important factor as lower repetition rates correspond to higher pulse energies. For precision nanoprocessing in the femtosecond regime, two distinct regions exist operating at repetition rates of 80 MHz and regeneratively amplified 1KHz. Each regime exhibits distinct mechanisms for ablation.

At 80 MHz, the dissection mechanism is believed to be mediated by free electron induced decomposition of chemical bonds and multiphoton induced chemical processes. Free electrons are generated by the formation of a low density plasma at the focus. Such a low density plasma forms well below the threshold for optical breakdown and only slightly higher than the intensity used for nonlinear imaging. The process has limited relation to thermoelastic stress or heating effects. In this regime detrimental effects such as lasting bubbles caused by accumulative heating and long lasting bubbles brought forth by tissue dissociation are only observed if the pulse energy is too high [30].

Varying the repetition rate from 80 MHz to 1 kHz increases the pulse energy by a factor of more than a hundred. Consequently the ablative process becomes far more aggressive being mediated by thermoelastically induced cavitation as opposed to low density plasmas. Although operating at 1 kHz is more aggressive than the 80 MHz regime, both methods of femtosecond cellular surgery provide 2-3 times improved spatial precision over CW laser modalities [30]. Figure 1.8 provides an overview of the phenomena associated with fs pulse laser tissue interactions.

In terms of non-destructive manipulation of biological samples based on optical tweezers, pulsed laser sources even in the IR are clearly unsuitable. The use of pulsed lasers does however provide opportunity for cellular nanosurgery. The works of Vogel *et al.* provide rigorous investigation of the mechanisms and characteristics of nanosecond and femtosecond laser-tissue interactions [29–33]. Their work probes damage ranges and examines means to reduce collateral damage in laser surgery. Information on operation regimes where it may be possible to obtain multiphoton like ablation through careful control of single-photon nanosecond processes is also given. Such developments are of great interest as femtosecond laser sources are

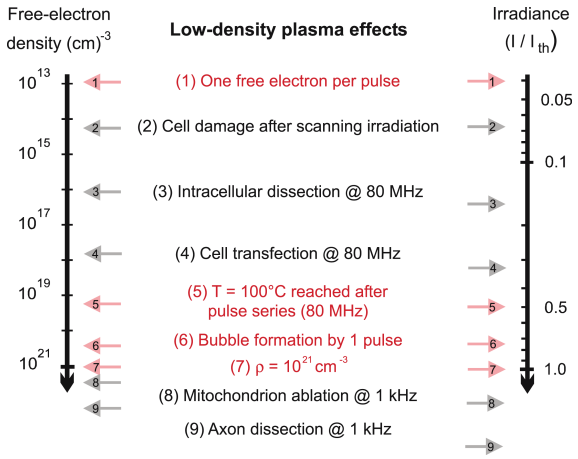

Figure 1.8: *An overview of the plasma mediated operations associated with fs laser interaction with tissues. Figure from [30]*

both expensive and difficult to maintain, as a result most commercial laser surgery systems are based upon ns laser systems.

1.8 Conclusions

The development and application of photonics techniques for the advanced manipulation of biological samples is the theme of this thesis. There is great demand for such tools to drive the eludication of subcellular processes in the life sciences. In this work light is applied to manipulate single cells with laser scalpels, optical tweezers and as a remote trigger for control of the intracellular chemical environment with caged compounds. The presented studies are concerned with the study of single cells which are complex structures highly sensitive to their environment.

Single cell studies are of interest as they may divulge information and trends masked by studies on global populations of cells, however, it should be highlighted that single cell studies may themselves mask the "network" effects of large groups of cells. The complex interaction between the laser field and cell under study has been shown to be greatly influenced by factors such as wavelength, irradiance and temporal beam characteristics and these dynamic relationships are further explored in the remainder of this thesis.

Chapter 2

The theoretical basis of optical manipulation

2.1 Optical tweezers for manipulation of matter with light

The term "optical tweezers" describes the method by which microscopic sized particles can be held and manipulated in three dimensions using light by exploiting the intense optical field in a tightly focused laser beam. The phenomenon originates from the interaction of microscopic particles with strong optical gradients generating an optically-induced force.

In 1986 Arthur Ashkin published his seminal paper on "optical tweezing", describing an investigation into the radiation pressure exerted by the transfer of momentum from photons to physical objects [48]. This paper instigated the birth of an entire new field of research, which has facilitated far greater understanding of fundamental physics and biology. To date several thorough reviews of optical trapping/tweezing exist in the literature [49–52].

2.1.1 Radiation pressure of light

The basis for optical tweezing can derived from a greater understanding of the radiation pressure of light. First outlined by Johanes Kepler in the 1700s whilst

observing the tail following a comet, described in the 19th century by Maxwell through his theory of electromagnetism [53] and finally demonstrated for the first time in 1901 by Lebedev [54], the radiation pressure of light describes the situation whereby a photon exerts a force upon an object through transfer of momentum. In the late 1960s Ashkin revisited the question of the radiation pressure of light armed with a microscope, the newly realised laser [9] and a knowledge of the quantum nature of light [55].

In 1969 Ashkin considered the interaction of light with a mirror, whereby incident light is reflected by the mirror [56]. Conservation of momentum demands that there must be a transfer of momentum between the light and mirror resulting in the light imparting a small force in the order of femtonewtons upon the mirror. Whilst this small force has little effect upon the macrosized mirror under everyday conditions, it becomes appreciable in the micrometer size regime. The advent of the laser provided access to light intensities which made the possibility of imparting forces on microscopic particles a reality.

Throughout the 1970s Ashkin thoroughly investigated the nature of the radiation pressure of light the transfer of momentum from light to solid matter. His work over the next 16 years involved development of three of the earliest trapping geometries [10, 48, 57].

2.1.1.1 Trapping regimes

The theoretical treatment of the optical trapping phenomena depends upon the relative sizes of the particle being trapped and the wavelength of the trapping beam. It is possible to describe two distinct regimes as illustrated in figure 2.1, the Mie regime where the particle size is much larger than a wavelength of the trapping light and the Rayleigh regime where the particle size is much smaller than a wavelength of the trapping light. At the sizescale of biological cells, around tens of microns (0.1 - 10λ) the explanation of the trapping mechanism falls between the Mie and Rayleigh regimes in an intermediate regime where a more complete electromagnetic treatment of the situation is appropriate for a rigorous description. The work presented in this thesis falls into both regimes.

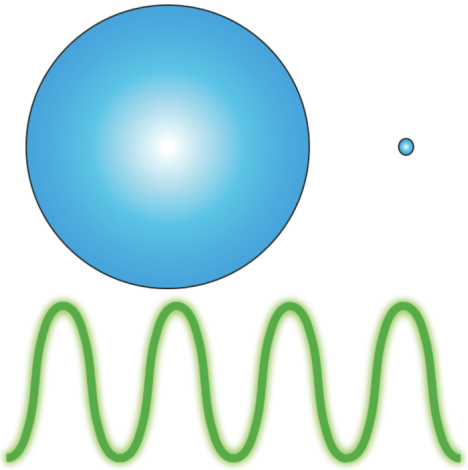

Figure 2.1: *The diameter of the Mie particle (left) is far greater than the wavelength of the incident light field (below) whereas the diameter of the Rayleigh particle (right) is much less than the wavelength of the incident light. The theoretical description of the interaction is determined by the relative size of the particle compared to the incident light field.*

2.1.1.2 Optical trapping in the Mie regime

In the Mie regime the particle being trapped is much larger than the wavelength of the trapping beam. As such, the whole wave has an effect upon the particle and a ray optics description of the trapping mechanism is appropriate.

Consider a small dielectric particle with refractive index higher than the surrounding medium, such as a micron sized silica particle in water or a mammalian cell in growth medium. Having a higher index of refraction than the immediate surroundings, the particle will cause incident light to refract and acts as a small lens. An incident Gaussian laser beam can be considered as a bundle of rays each weighted according to its intensity. These incident rays will experience a momentum change caused by interaction with the particle. Newton's third law of motion then dictates that the particle must experience an equal but opposite force. In the transverse trapping plane as illustrated in figure 2.2a, more intense rays in the centre of the incident laser beam will exert a larger force upon the particle than less intense outer rays. Consequently the particle experiences a strong net force towards the most intense portion of the beam, where the forces will balance and the particle will be held. Therefore the transverse trapping mechanism is due to the transverse gradient across the laser beam.

In the axial plane "z-trapping" as illustrated in figure 2.2b is realised by the

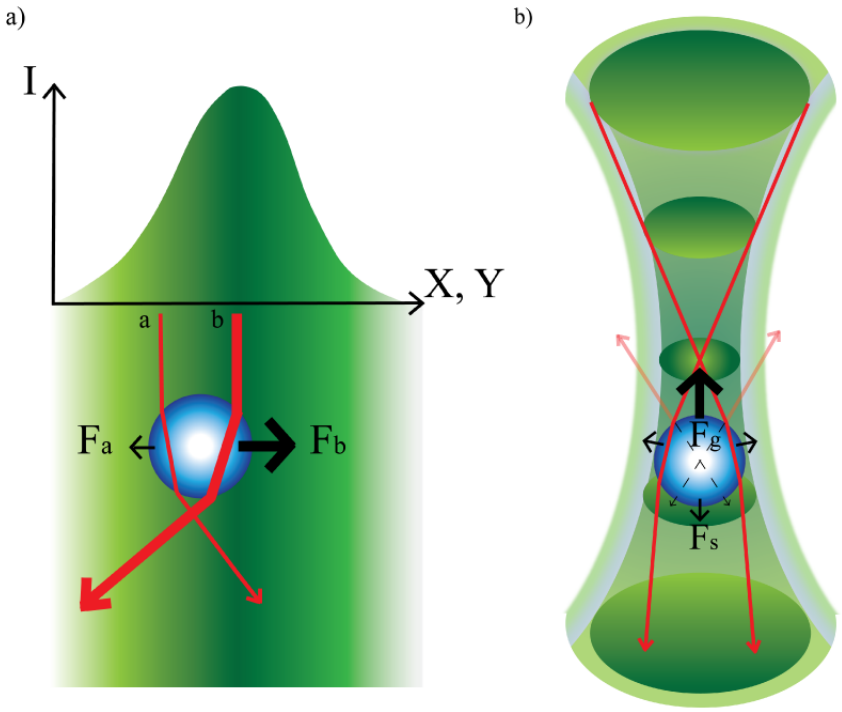

Figure 2.2: *In the X & Y planes, the particle is drawn towards the most intense portion of the beam by conservation of momentum generating a transverse gradient force (a). Intense portions of the beam are refracted more than the weaker components and consequently the force towards the most intense region of the beam is greatest (Fb > Fa). In the Z plane, an axial gradient force F_g generated by the downwards refraction of the incident beam draws the particle towards the focus of the beam when F_g overcomes the opposing scattering force along the optical axis F_s and the downwards draw of gravity.*

strong axial intensity gradient generated by the tight focusing of the beam with a high N.A objective lens. Aggressively focused off-axis rays encounter the particle and are refracted downwards. Conservation of momentum results in the particle being drawn upwards towards the focus of the objective. Competing with this axial gradient force are gravity and a radiation force originating from back-scattered on-axis rays which generate a net downwards force. Therefore it is imperative that high N.A optics are employed to achieve a strong enough axial intensity gradient to overcome the competing axial optical scattering force and downwards pull of gravity to trap the particle close to the focus of the laser beam. Further rigorous quantitative analysis of axial trapping in the Mie regime is possible by considering the Fresnel reflection and transmission coefficients [58].

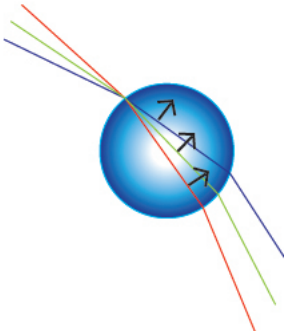

Figure 2.3: *Consideration of the Fresnel coefficients highlights the requirement for high N.A optics to provide tightly focussed trapping beams. It is the aggressively focussed exterior rays exhibiting the largest angle of incidence which provide the greatest vertical component of the resulting axial gradient force.*

Here, the gradient force is given by

$$F_g = \frac{n_m P}{c}\left(Rsin2\theta + \frac{T^2\left[sin\left(2\theta - 2\phi\right) + Rsin2\theta\right]}{1 + R^2 + 2Rsin2\phi}\right) \tag{2.1}$$

the scattering force by

$$F_s = \frac{n_m P}{c}\left(1 + Rcos2\theta + \frac{T^2\left[cos\left(2\theta - 2\phi\right) + Rcos2\theta\right]}{1 + R^2 + 2Rcos2\phi}\right) \tag{2.2}$$

and the total force by

$$F = \frac{Qn_m P}{c} \tag{2.3}$$

where F_s is the scattering force, F_g the gradient force, n_m the refractive index of the medium surrounding the particle, θ the angle of incidence, Φ the angle of refraction, R the Fresnel reflection coefficient, T the Fresnel transmission coefficient, P the photon momentum and Q the dimensionless trapping efficiency [58].

These equations demonstrate the greater the angle of incidence, the greater the vertical component of the resultant force as illustrated in figure 2.3. The equations highlight the dependence of successful axial trapping upon the angles of incidence and refraction. Whilst the formulas show that the axial force is independent of particle size, it is worth noting that the force of gravity puts an upper limit on the largest trappable particle as the mass of the particles scales with their radii cubed. In this discussion, consideration of optical trapping in the Mie regime has been limited to particles of higher refractive index than the surrounding medium.

Particles with a low refractive index relative to their surroundings which will be excluded from high intensity regions and therefore expelled from laser beams with a Gaussian intensity profile. Such particles can be trapped by employing Laguerre-Gaussian (LG) beams. These "doughnut ring" beams can trap low index particles in their dark cores. Furthermore, it is worth noting that use of LG beams to trap high index particle results in enhanced axial trapping due to minimisation of the radiation force resulting from back scattered axial rays. It can be seen that the key factors for achieving robust three dimensional optical trapping in the Mie regime are strong gradients in the axial and transverse intensity fields. These gradients work together to overcome scattering induced radiation pressures and gravity to hold the particle close to the most intense part of the beam.

2.1.1.3 Optical trapping in the Rayleigh regime

When trapping a Rayleigh particle, the wavelength of light is large compared to the particle dimensions and only a small portion of the light interacts with the particle. As such a ray optics description is inappropriate and it is more accurate to consider the forces in terms of the electric field which is imposed upon the particle by the light.

In the presence of a light field, a small polarisable Rayleigh particle will develop an electric dipole moment as the electric field component of the light wave will induce a polarisation in the atoms which make up the particle. Considering the particle and light field as a closed system, the polarised particle will experience a Lorentz force and be drawn to the region of highest field intensity which will be the local minimum in potential energy. As such the particle will move to minimise the energy of the whole system.

Therefore in a uniform field such as an unfocused light beam such as that shown in figure 2.4a, there will be no electric field gradient and hence no force upon the particle. As illustrated in figure 2.4b, a strong electric field gradient can be introduced by tightly focusing the light beam. The particle will then be trapped at the focus of the light beam. As in the Mie regime, the gradient force described above which is responsible for the optical trapping phenomenon is counteracted by a scattering

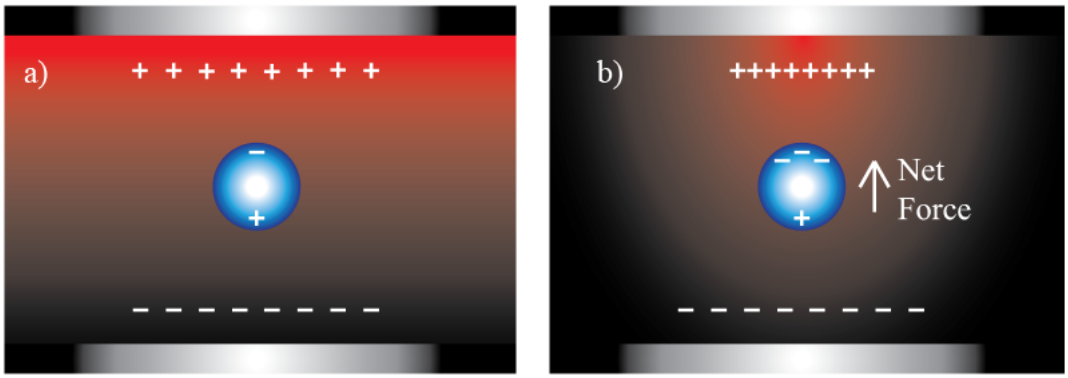

Figure 2.4: *A dipole is induced in a dielectric particle placed in an external field. When the eternal field is uniform (a) there is no net force upon the particle, however in a non-uniform field (b) the particle is drawn along the field gradient to the most intense region of the field.*

force which in the Rayleigh regime originates from the absorption and re-emission of the light by the induced dipole. This will result in a net force in the propagation direction of the light. As such the scattering force will work to counteract the gradient force and push the particle away form the focus of the light.

More rigorous quantitative analysis of optical trapping in the Rayleigh regime describes the gradient force (F_{grad}) experienced by the particle as

$$F_{grad} = -\frac{n_m}{2}\alpha\nabla E^2 = -\frac{n_m^3 r^3}{2}\left(\frac{m^2-1}{m^2+2}\right)\nabla E^2 \tag{2.4}$$

where n_m = refractive index of the medium surrounding the particle, α= Polarisibility of the particle, E = Electric field vector, r = particle radius and m = effective refractive index of the particle [48]. Note the proportionality to the polarisability of the particle a. Similarly the scattering force working to push the particle away form the focus can be described as

$$F_{scat} = \frac{n_m P_{scat}}{c} \tag{2.5}$$

which can in terms of incident field intensity intensity I_0, can be described as

$$F_{scat} = \frac{I_0}{c}\frac{128\pi^5 r^6}{3\lambda^4}\left(\frac{m^2-1}{m^2+2}\right)^2 n_m \tag{2.6}$$

For the particle to be held trapped at the focus of the laser beam the ratio of gradient force to scattering force

$$\frac{F_{grad}}{F_{scat}} = \frac{3\sqrt{3}}{64\pi^2} \frac{n_m^2}{\left(\frac{m^2-1}{m^2+2}\right)} \frac{\lambda^5}{r^3\omega_0} \tag{2.7}$$

where ω_0 = size of the Gaussian beam waist must be greater than one. Equation 2.7 describing the ratio of these forces has several implications . Firstly it suggest that the ratio is independent of laser intensity, although real world considerations like Brownian motion acting upon the particle make this untrue. Furthermore the direct proportionality between the ratio and the trapping wavelength which implies longer wavelengths are more suitable for trapping. However, longer wavelengths cannot be focused as tightly as shorter wavelengths as described by

$$d = \frac{1.22\lambda}{2N.A} \tag{2.8}$$

where d is the diameter of the smallest resolvable spot achievable focusing a light of wavelength λ, with a lens of a given N.A also suggests that this implication is also untrue. The ratio described by equation 2.7 is also inversely proportional to beam waist, therefore necessitating the use of high N.A optics to provide as small a waist as possible. Finally the ratio is also shown to be inversely proportional to the particle size, implying that the smaller the particle the more robust the trapping. It is worth noting however that when the particle size drops to around 18 nm and below, the number of polarisable atoms becomes too low to sustain a gradient force making it impossible to trap a particle of infinitely small dimensions [59].

The treatment of the mechanisms underpinning optical trapping in the Rayleigh regime highlights the importance of a strong gradient field and the minimisation of scattering forces, similar to the Mie regime. Again, this underlines the necessity of employing high N.A optics to achieve tight focusing and access the strong optical gradients which underpin the successful optical trapping of particles.

2.1.1.4 Optical trapping in the intermediate regime

The mechanism for trapping for particles of this size can be modelled with a generalised Lorentz Mie theory (GLMT) [60] which develops Lorentz-Mie theory [61]

from a treatment using plane waves to that of focused wavefronts.

The theory describes the behaviour of the electric field surrounding the particle which is immersed in light of wavelength approximately equal to its dimensions. The treatment takes the particle size, refractive index and the wavelength of light being used to trap the particle into account. In this way diffraction of the light by the particle and the optical field of the trapped particle are included. Such calculations can be computationally intensive and much work goes into developing effective techniques and algorithms of successfully modelling particle systems in this regime to the point where computational toolboxes are available for common modelling programmes such as matlab [62].

The particles under study being optically manipulated in this thesis fall either into the Mie regime (cells 10-15 μm in size in IR wavelengths) or Rayleigh regime (nanoparticles of 100 nm in IR wavelengths) described previously. However, during the construction of the optical tweezers silica and polystyrene spheres in the intermediate size range (around 1 μm in IR wavelengths) are used to assess the alignment of the trap.

2.1.2 Trapping geometries

As illustrated in figure 2.5 several distinct optical trapping geometries exist, all of which are based upon the radiation pressure of light and mostly developed by Ashkin and colleagues in the. 1970-80s. Early experiments investigating the radiation pressure of light revealed a transverse light pressure, a gradient force which drew the particle towards the centre of the beam. This force forms the basis of the dual two beam trap illustrated in figure 2.5a.

A particle is held at an equilibrium point between two diverging counter-propagating beams [10]. Such as trap is of particular interest for the probing of biological samples as the sample is not held near the most intense region of the trapping beam.

The first single-beam optical trap exploits the optical radiation pressure and holds a particle levitated against gravity as shown in figure 2.5b [57].

The geometery of most relevance to the work presented in this thesis is the single-beam gradient trap, commonly referred to as “optical tweezers” which are

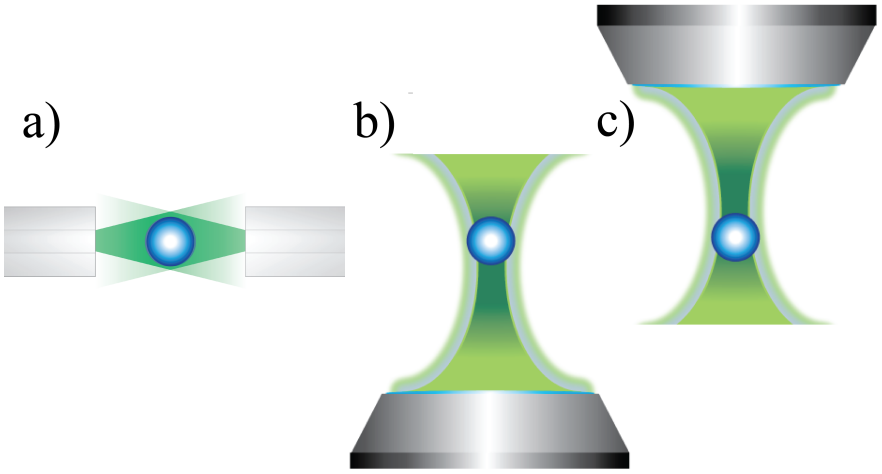

Figure 2.5: *The earliest stable optical trap was the dual beam trap (a) [10] where the particle is trapped between two opposing diverging beams. Such a trap is of particular interest for the trapping of biological samples. The single beam levitation trap (b) [57] employs the radiation pressure of light to hold the particle against gravity. The single beam gradient trap (c) [48]holds the trapped particle by balancing the gradient and scattering forces of light against gravity. Commonly reffered to as "optical tweezers" this trap forms the basis of the presented work.*

illustrated in figure 2.5c [48].

Much later, the first interferometric tweezers from two propagating beams were developed [63]. This idea which has now been extended to multiple beams providing optical lattices [64]. The 3D optical tweezers trap forms the basis of the optical manipulation techniques presented in this work.

2.2 Optical injection for cellular processing

Optical injection is the act of employing a laser transiently to permeabilise the membrane of a cell to allow impermeable species to be internalised. In this way theraputic agents may be introduced to the interior of dysfunctional cells. In the literature it appears under many guises such as optoinjection, laser injection, optoporation and photoporation. In this thesis I use the term optical injection.

If the membrane impermeable substance delivered into the cell interior is a nucleic acid species such as DNA or mRNA and the cell subsequently produces the protein coded for by the nucleic acid, then transfection may be said to have taken place. This process of optical injection mediated transfection also has many names

in the literature such as optical transfection, optotransfection, laserfection, laser transfection, phototransfection and laser assisted transfection. For consistency, I use the term optical transfection in this thesis.

It is important that the distinction is made between optical injection and optical transfection and their relative efficiencies. Optical injection of a nucleic acid whilst maintaining post injection viability does not guarantee a successful transfection event.

2.2.1 Theoretical basis of injection mechanism

Since the first demonstration of optical transfection in the early 1980s [65], various approaches for optical injection have been investigated and reviewed in the literature [66,67]. The underlying theme shared by all mechanisms is stressing the cell but in a controlled manner to permeabilise the membrane whilst not compromising viability.

Different laser operation parameters determine distinct laser sample interactions. It therefore seems intuitive that the mechanism behind UV nanosecond optical injection is most likely to be different to that of femtosecond IR optical transfection. The injection mechanism is driven by the laser sample interaction, so again the main criteria affecting the interaction are the laser irradiance, wavelength and operating modality. At present, the main mechanisms for optical injection are thought to be, heating, thermoelastic stress, bubble formation and generation of free electrons in low density plasmas although all processes are most likeley associated with some form of photochemical reaction.

2.2.1.1 Heating

Heating is typically associated with wavelengths which are readily absorbed by the sample under study, such as those in the UV and visible (Vis) wavelength ranges. The mechanism is thought to be driven by a localised heating of the plasma membrane. It is typically associated with single-photon processes but no work has been undertaken to asses the role of multiphoton heating effects. Consequently, heating is mostly associated with optical injection using CW UV lasers [68–72] where it provides the primary mechanism for injection .

It has been shown that events based purely on heating effects can be enhanced through the addition of an absorbing chemical to the culture medium [69, 72, 73]. Heating is also believed to play a role in ns optical injection although the primary mechanism is believed to be thermoelastic stress.

2.2.1.2 Thermoelastic stress & bubble formation

Thermoelastic stress and bubble formation are closely related and associated with more aggressive optical injection using. Such injection is achieved using nanosecond Hz repetition rate and femtosecond KHz repetition rate laser sources. At these repetition rates the pulse energies are orders of magnitude higher that those used for fs optical injection. Focusing such a laser into a sample volume results in heating, bubble formation and subsequent shockwaves of thermoelastic stress which propagate through the sample [32].

The shockwave is thought to mediate the optical injection and is why low repetition rate lasers yield largely untargeted injection of blanket regions of cells surrounding a "dead zone" where the laser pulse instigated bubble formation. Successful injection has been reported with nanosecond lasers operating in the UV [65, 74–77], visible [78, 79]and IR [80, 81] wavelength ranges.

2.2.1.3 Generation of free electrons

This effect is exclusively associated with high repetition rate ultrashort pulsed lasers operating at NIR wavelengths in the MHz regime generating pulses around 100 fs. Optical injection is believed to be mediated by the photochemical dissociation chemical bonds in the plasma membrane caused by free electrons generated by a low density plasma originating at the laser focus.

This technique is highly targeted and well suited for application to single cell optical injection offering high selectivity and viability. Consequently femtosecond optical injection is rapidly becoming the preferred technique for optical injection of biological samples . It is noteworthy that for generation of a low density plasma suitable for optical injection an objective lens of N.A greater than 0.9 is required [29, 33].

2.2.2 Efficiency of the optical injection process

The figure of merit for optical injection is often taken as the injection efficiency, which is assessed inconsistently by different groups. Some only count cells which remain viable throughout the entire process whereas others take account of all cells which were targeted during the process, whether they remain viable or die. Of those who take the viability of the cells correctly into account, viability is measured differently. Some use exclusion of membrane-impermeable dyes (trypan blue or propidium iodide) as an indicator of maintained viability, however, a cell in the early stages of apoptosis may still exclude such stains. The only real indicator of viability is continued cell division. Whilst appropriate for optical injection, cell division introduces a problem in correctly calculating transfection efficiencies in optical transfection experiments as the number of cells is constantly growing.

In the literature the majority of experiments deal with optical transfection. In such reports no distinction is made between the optical injection and transfection efficiencies. As described previously, a successful optical injection event may not yield successful transfection of the cell. Therefore such efficiencies will be lower than the actual optical injection. It is possible to decouple the injection and transfection efficiencies through addition of a non-toxic membrane impermeable stain such as lucifer yellow to the transfection medium permitting optical injection to be assessed in parallel with transfection. Such an approach gives a more complete indication of the process understudy.

In spite of this variation in technique there are observable trends in efficiencies in the literature. Typically the highest efficiencies are associated with femtosecond IR lasers operating in the MHz regime. Here peak efficiencies range from 70% upwards. Shorter wavelenghts in the UV are commonly associated with high levels of photodamage and see greater absorption in the sample. Coupled with the aggressive nature of ns optical injection, UV nanosecond optical injection exhibits relatively low efficiencies (~10%) when compared with femtosecond injection [76]. In the visible typically around 532 nm nanosecond pulses efficiencies which range from 30 % to as high as 80% [78, 79]. Even at IR wavelengths which are not readily absorbed by the sample, injection efficiences of as high as 60 % were reported [80].

These results further implicate thermoelastic shockwave as the mechanism driving ns optical injection over thermal effects.

It is also worth highlighting again that in general the femtosecond injection is towards targeting single cells whereas nanosecond is less selective and targeting colonies of cells. Therefore if the user is more interested in throughput as opposed to specificity, cheaper ns sources may be employed. For CW optical injection, recent work has concentrated upon the use of short wavelength UV laser diodes with reported efficiencies up to 40% [72]. Like femtosecond MHz injection this method is also highly targeted however it relies solely upon heating by single photon absorption as the mechanism. Interestingly no work exists using CW 532 nm lasers, which the nanosecond injection indicates could possibly provide a higher success rate. The lower efficiencies of nanosecond and cw laser optical injection do not solely indicate that these regimes lead to less injection that femtosecond optical injection, but rather that fewer cells remain viable.

2.3 Conclusions

The theoretical bases of the techniques developed within the thesis has been presented. It has been shown that through careful laser operation parameter selections the laser field can be used to translate or perform surgery upon a cell. The process of an incident photon resulting in the liberation of the affector molecule from the caged precursor has also been considered.

Chapter 3

Experimental techniques

The key systems and techniques underpinning the experimental work reported in this thesis are presented here. These include the design considerations for a range of photonics systems including femtosecond lasers and optical tweezers, the techniques used for examining the response of caged organic molecules to photolysis light sources and a final section describing the standard techniques used in the biological experiemnts reported in the remainder of the thesis.

3.1 Photonic Systems

The design, construction and characterisation of a near-infared (NIR) femtosecond laser is presented alongside the principals behind the design and construction of an optical tweezers.

3.1.1 Design & construction of a femtosecond laser for optical manipulation of biological samples

Much of the work reported in this thesis relies upon multiphoton effects that are made accessible through the high peak powers and photon densities achievable by tightly focusing femtosecond laser beams with high numerical aperture objective lenses. Therefore, a modelocked femtosecond laser source was necesarry for the majority of the work presented in this thesis. It was decided to construct a modelocked

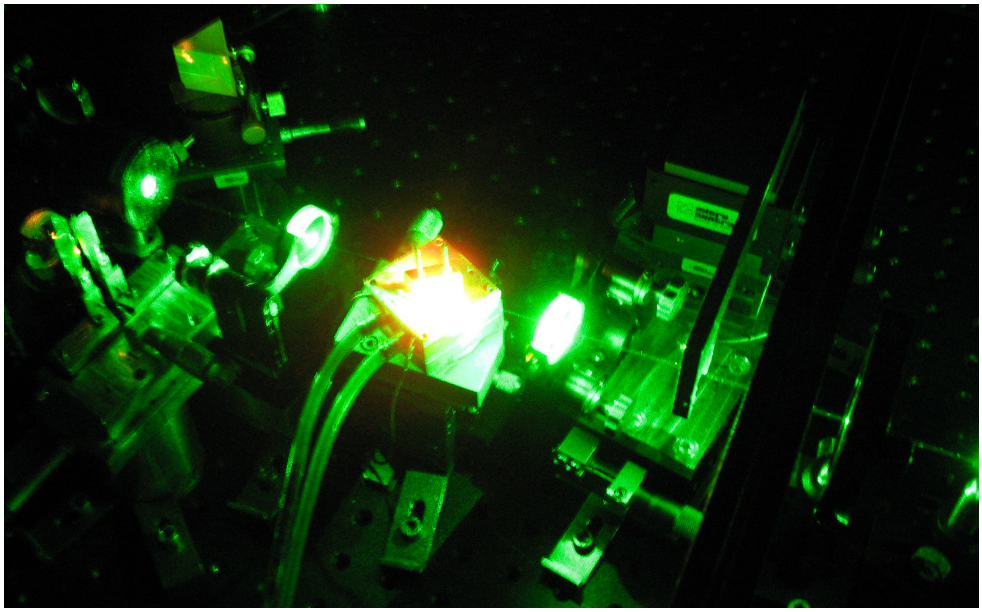

Figure 3.1: *The constructed Ti:Al_2O_3 oscillator in operation. The water cooled Brewster cut crystal (center) was pumped at 532 nm in a z-fold cavity configuration.*

laser as home built system is more flexible to design changes than a commercially purchased one. Ti:Al_2O_3 was chosen as the gain material as it supports femtosecond pulses and exhibits a degree of tunability. Furthermore the IR output of the laser source is well suited to biological applications as described in chapter 1. Here, the design and construction of a femtosecond titanium:sapphire (Ti:Al_2O_3) laser is presented.

3.1.1.1 Design considerations

When constructing a new femtosecond laser system the gain material, pump source, cavity configuration and modelocking mechanism are major considerations. Ti:Al_2O_3 exhibits a double-structured absorption band between 400 and 600 nm with peaks at 485 nm and 550 nm [82]. A 532 nm CW neodymium:vanadate solid-state diode pumped laser (Verdi V5, Coherent and later Millennia V5, Spectra Physics) was chosen as the pump laser source. A "z-fold" cavity was chosen to minimise astigmatism introduced by the use of a Brewster-cut laser crystal within the cavity used to minimise intracavity losses [83,84]. The cavity length was designed to produce a repetition rate of 83 MHz and was calculated to be 1.815 metres. The cavity illustrated lasing in figure 3.1 was designed by examining relevant cavity designs [85, 86]. The

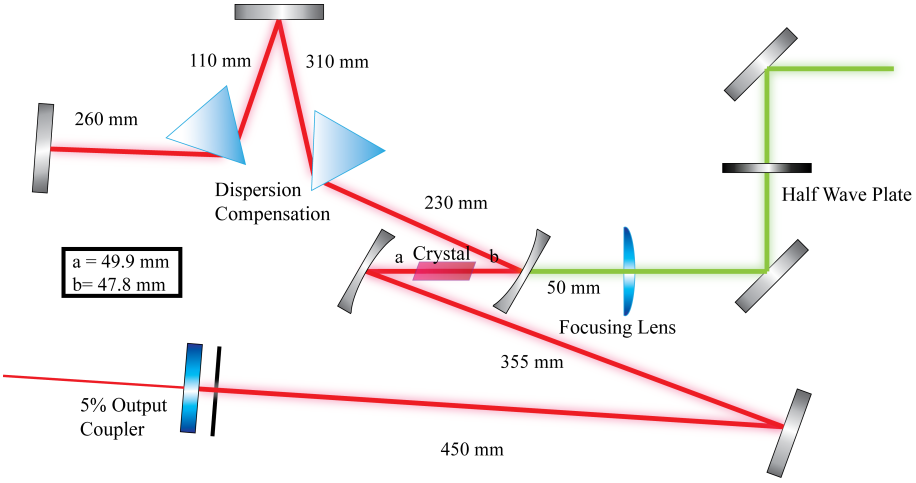

Figure 3.2: *The laser cavity was designed by ABCD matrix modelling of the cavity parameters using the program "LCAV". The 1.815 m cavity length results in a 83 MHz repetition rate. The modelocked laser produced 95 fs pulses at 780 nm at 700 mW average output power.*

laser cavity design software "LCAV 1.0" which models the laser cavity stability using ABCD matrix propagation analysis for a Gaussian beam within the cavity [85, 87] was then used to determine the optimum relative positions and angles of the cavity components. To achieve modelocking by means of hard aperture Kerr-lens method a slit was introduced to provide preferential discrimination to pulsed operation.

3.1.1.2 Laser construction

To allow for the laser to be portable it was constructed on a breadboard 900mm x 600mm. Two steering mirrors where used to deliver the 532nm pump beam to the correct height on the breadboard with a degree of flexibility. A half-wave plate was used to control the polarisation of the pump beam and two irises were installed to allow realignment of the pump if the laser was relocated. This also allowed the pump laser to be exchanged at a later date.

The laser was constructed to the dimensions detailed by the ABCD matrix modelling of the cavity illustrated in figure 3.2 with high quality components mounted on precision translation mounts to allow for optimisation of the system. A 100 mm focal length lens was used to focus the pump beam ($\omega_0 = 31$ μm to provide optimum pump/laser mode overlap) in a water-cooled 10 mm Brewster-cut Ti:Al_2O_3 laser rod. The folding mirror angles were 20° and their radius of curvature 100 mm.

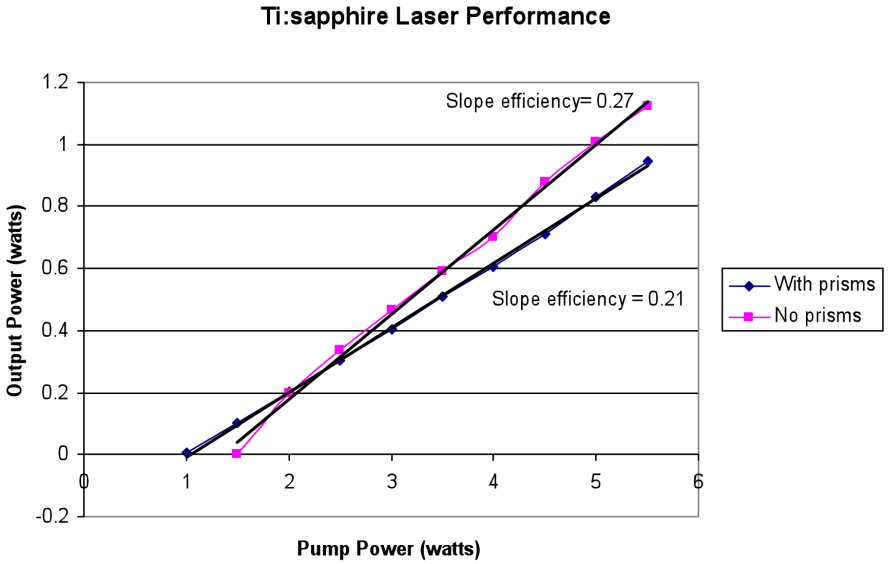

Figure 3.3: *Dispersion compensation prism insertion caused the expected drop in output performance.*

All optics were antireflection coated and all mirrors high-reflection dielectric coated.

Once continuous wave (CW) operation of the laser had been optimised the dispersion management prisms were inserted into the long arm. The prism separation to provide the correct amount of negative dispersion was calculated using accepted dispersion theory [88] to be 42cm. Hard aperture Kerr-lens modelocking was chosen as it is easier to achieve than soft aperture Kerr-lens modelocking which demands critical alignment of the laser cavity modes. To achieve hard aperture modelocking a knife edge slit was installed close to the 5% output coupler.

3.1.1.3 Laser characterisation

The output power from the laser was measured using a Melles Griot 3396 broadband power meter. Care was taken to ensure that the entire output beam was incident upon the detector head and an appropriate filter was employed to remove any residual pump beam.

Once satisfactory CW performance had been obtained, Brewster-angled dispersion compensation prisms made from SF10 glass where installed within the cavity. The introduction of these prisms was expected to cause a minor reduction in performance which was observed as illustrated in figure 3.3. To achieve modelocking, the second cavity folding mirror position was adjusted to bring the laser to the edge

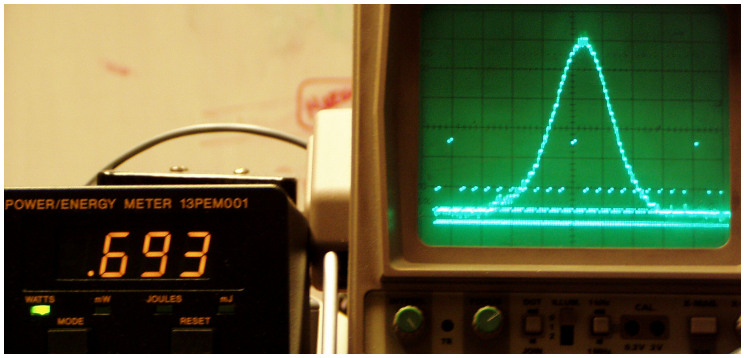

Figure 3.4: *Critical alignment of the laser cavity realised modelocked operation by the Kerr lens hard aperture method. Autocorelation measurements determined 95 fs pulses at 700 mW of output power.*

of stability for CW operation whilst adjusting the position and size of the hard aperture situated next to the output coupler.

The output of the laser system was monitored both by the power meter and a visible-IR IST-Rees spectrum analyser that allowed the output wavelength of the laser to be monitored. As the cavity is moved towards the edge of the stability region for CW operation, mode competition could be observed in the output spectrum of the laser. As the slit size and amount of dispersion compensation were altered the degree of mode competition could be seen to increase dramatically until upon introduction of a noise spike modelocking was achieved. As illustrated in figure 3.4, the output spectrum of the laser changed from a series spikes demonstrating many longitudinal modes competing to a Gaussian curve indicating that the longitudinal modes had modelocked together.

Interferometric and intensity autocorrelation measurements (Timewarp, Elliot Scientific) recorded bandwidth limited pulses of 95 $\pm$14 fs at output powers of 700 mW operating around a central wavelength of 790 nm. The laser remained modelocked for several hours at a time until temperature change in the lab or mechanical disturbance caused a loss of the modelocking and initiation with a new noise spike was required.

As illustrated in figure 3.5 the output beam was characterised using a beam profiler (Coherent, USA). The output was shown to be TEM_{00} and demonstrate an approximately 93 % Gaussian intensity profile. The M^2 beam parameter of the laser output was determined to be 1.2.

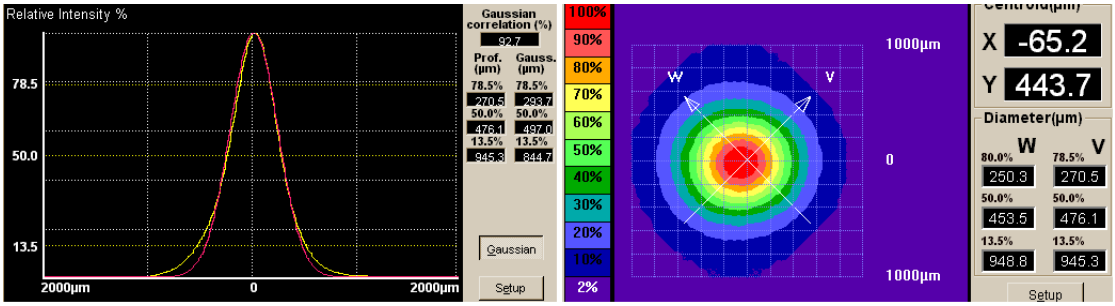

Figure 3.5: *Beam profile measurements determined the laser operated with TEM_{00} output with 93 % Gaussian profile.*

A Ti:Al_2O_3 laser oscillator has been successfully constructed and modelocked employing the hard aperture Kerr-lens modelocking technique. The system operates at a repetition rate of 83 MHz and has been observed to produce sub-100 femtosecond pulses at output powers of up to 700 mW operating around 790 nm. The home built nature of this system affords flexibility with regards to reconfiguring the cavity. At a later date the Coherent V5 Verdi pump source was replaced with a similar Spectra Physics Millennia 5 pump source and comparable laser operation was observed.

3.1.2 Construction of optical tweezers for interrogation of biological systems

Several optical tweezers systems were constructed for the work presented in this thesis. The primary design considerations and generic construction protocol for a typical tweezers arrangement common to all systems employed are discussed here.

3.1.2.1 Design & typical construction

Several comprehensive guides exist detailing the construction of the many functional forms of optical tweezers setups [89–91]. When constructing any optical tweezers system the major concern is how to obtain a strong optical gradient with a light field which is not harmful to the sample under study. The trap geometry, microscope objective and laser source employed for trapping are therefore important considerations.

The laser irradiance at the focus of optical tweezers can reach megawatts per

square centimeter [92]. Such high irradiances can give rise to heating effects, through water absorption of the IR trapping radiation. Tweezers are flexible, compatible with microscopy and easily be used for optical tweezing or cellular nanosurgery by intelligent laser selection.

Objective lens considerations

Strong optical gradients are achieved through the use of high N.A optics, typically 0.7 – 0.9 N.A (50x magnification and greater) for the trapping of Mie particles and 1.2 - 1.4 N.A (typically 100x) for the trapping of Rayleigh particles. Such objectives generate strong optical gradients due to the steep angle at which off-axis rays come into focus at the sample.

As discussed in chapter one laser choice is a major consideration. Careful choices of wavelength, temporal operating regime and irradiance must be made for successful optical manipulation of biological samples.

The typical upright optical tweezers configuration optical trap is illustrated in figure 3.6.

Preparation and delivery of the trapping beam

The laser beam is first expanded by a telescope (L1 & L2) which enlarges the beam to overfill the back aperture of the microscope (typically ~ 7mm). This first telescope also ensures that the beam is correctly collimated. Collimation was verified by use of IR viewer card, IR camera and also by the use of a shear plate (Melles Griot).

The beam is then elevated to working height by using a pair of highly reflecting mirrors (M1 & M2) which form a periscope. The expanded, collimated beam then passes through a relay telescope (L3 & L4). For the infinity corrected objectives employed which require a 200 mm tube lens, 200 mm focal length lenses are ideal for the relay telescope. However, due to practicality of setup size on optical bench 100 mm focal length lenses were used at the expense of sharper steering angles.

The relay telescope ensures that the steering mirror M2 is now a conjugate plane with the back aperture of the infinity corrected objective lens in a 4 f conjugate pair system. Consequently the two planes at M2 and the objective back aperture are

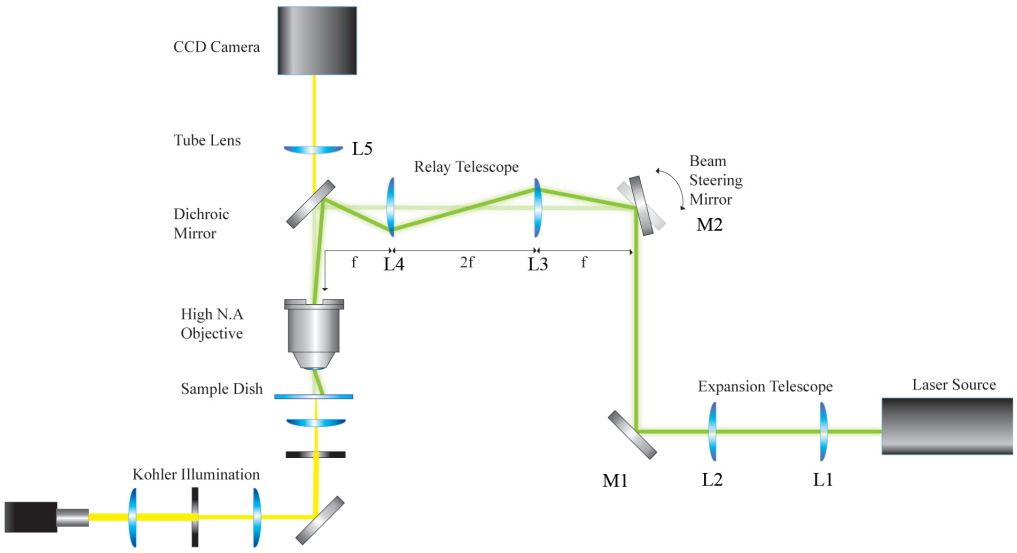

Figure 3.6: *An upright optical tweezers system forms the foundations of much of the work presented within this thesis. The expansion telescope conditions the laser beam to match the diameter of the back aperture of the objective lens providing the optical gradient demanded for optical trapping. The relay telescope prevents the beam becoming misaligned by adjustment of the beam steering mirror. The Köhler illumination provides uniform illumination at the sample plane. The CCD camera is used to capture images of the interactions at the sample plane.*

optically equivalent. As shown in figure 3.7 this arrangement prevents misalignment of the beam with respect to the back aperture when the steering mirror is adjusted.

Following the relay telescope the beam is directed through the infinity corrected objective by a dichroic mirror at 45 ° which reflects the laser beam but allows the image from the sample plane to pass through it. The bundle of parallel rays produced by the infinity corrected objective lens are then focused by the tube lens L5 (typically f=200 mm for objectives employed) which forms an image of the sample plane on the charge coupled device (CCD) camera sensor. The sample is translated on a precision xyz stage (Newport, USA), in effect moving the sample chamber around the trapped particle held close to the beam focus.

Sample illumination

The sample is illuminated by a white light Köhler illumination arrangement as illustrated in figure 3.8. Achieving uniform illumination over a sample was traditionally a problem as the filament of the light source was imaged to the sample plane. To overcome this, August Köhler introduced the use of a 4f optical system which images

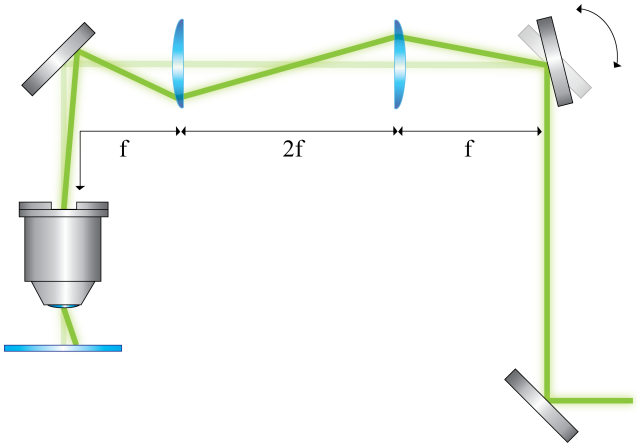

Figure 3.7: *Use of a 4f optical system prevents misalignment of the trapping beam with the back aperture of the microscope objective. The beam steering mirror (top right) is a conjugate optical plane with the back aperture of the objective, consequently any angular displacement of the beam at this mirror becomes an angular displacement at the focal plane of the objective lens and the optical system remains aligned.*

the field diaphragm and not the light source element to the sample plane. In this way, uniform illumination of the sample is achieved. By adjustment of the field and condenser diaphragms the quality of the image may be improved.

The detailed system is a very basic example of an optical tweezers arrangement suitable for the optical manipulation of biological samples. Each individual system constructed is described in more detail in the relevant experimental section.

3.2 Caged compounds for light-initiated control of cellular microenvironment

The use of caged compounds for the control of the cellular microenvironment was introduced in chapter one. Part of the work in this thesis deals with the development of new caged molecular probes in chapter six and the development of a new photolysis methodology in chapter seven. Experimental techniques common to both chapters are described in this section and include the assessment of absorption characteristics, laser photolysis studies and subsequent quantification.

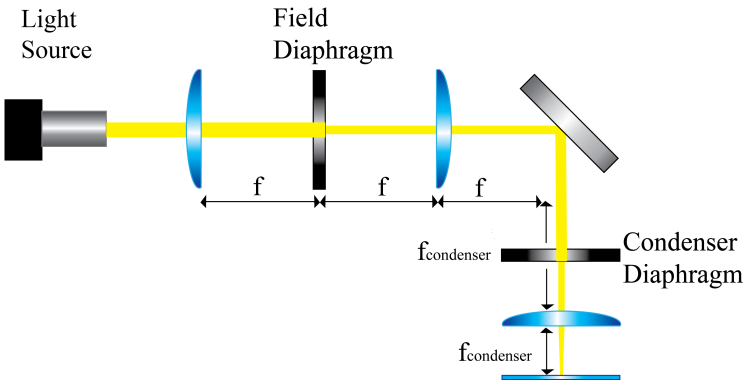

Figure 3.8: *Köhler illumination de-couples the light source and imaging planes by making use of a 4f optical system which images the field diaphragm to the image plane. The field diaphragm controls image contrast by eliminating excess illumination outside the region of interest. The condenser diaphragm controls the resolution. This arrangement provides uniform illumination at the sample plane.*

3.2.1 General sample handling

All samples were prepared using a four point digital balance (Sartorious cp64) for measuring masses of solids. Volumes were measured using volumetric flasks and Gilson pipetteman micro-pipettes. When required for biological studies, samples were prepared under sterile conditions in a laminar flow hood and all equipment was sterilised in an autoclave.

The light-sensitive nature of the compounds demanded the prevention of exposure to any light capable of causing unintentional photolysis. Care was taken to protect the solution from exposure to background UV irradiation and sample preparation and experiments were conducted under a red safety light. Where possible compounds were prepared fresh for each experiment. When this was not possible the compounds were stored at -20 $^{\circ}$C to prevent degradation due to chemical decomposition. For transport between labs samples were always shielded from light with aluminium foil.

3.2.2 Assessment of absorption characteristics

Following the synthesis of the caged compounds the first stage was to assess the UV/Vis absorption characteristics of the compound to indicate of which wavelengths were most likely to evoke photolysis. The UV/Vis absorption spectra were obtained

using a spectrophotometer (Lambda 950, Perkin Elmer).

A solution of the caged compound was prepared and placed in a high quality quartz cuvette (Perkin Elmer). A second cuvette containing the solvent used to dissolve the compound was used as a reference cell in the spectraphotometer.

The spectra generated by the spectraphotometer plot absorbance (A) as a function of wavelength (nm). Absorbance is defined as

$$A = -\log_{10}(\frac{I}{I_0}) \tag{3.1}$$

where $\frac{I}{I_0}$ is the transmittance of the sample determined by I_0 and I being the incident and transmitted intensities respectively. Such plots are dependant upon the concentration of the solution under study. The different caged compounds under study exhibit different solubilities and can not always be made up to the same concentration.

Beer's law for a solute in a non-absorbing solvent [93] relates A to the molar absorption coefficient ε (also known as extinction coefficient) by

$$A = \varepsilon lc \tag{3.2}$$

where c is the concentration of the solution and l is the interaction length of the interrogating light beam and solution in cm. Therefore the absorbance is converted to the concentration independent extinction coefficient ($Lmol^{-1}cm^{-1}$) permitting the spectra of different compounds to be readily compared as illustrated in figure 3.9.

3.2.3 Laser photolysis studies

Laser photolysis studies were required to assess which compounds might be applicable to biological systems. In this way it was possible to assess the behaviour of the caged compounds before application to the biological system of interest. Due to the volumes of liquid required for NMR analysis, it was necessary to perform these experiments in bulk solutions in cuvettes, therefore the photolysis times required were far longer than those commonly employed in biological application which employ

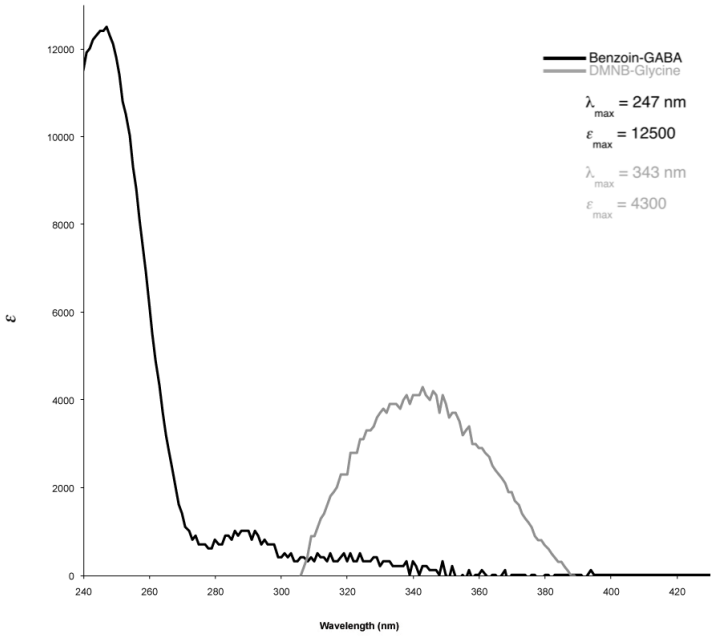

Figure 3.9: *Absorption characteristics of the caged compounds under study were obtained with a UV/Vis spectraphotometer and plotted as a function of molar absorption coefficient ϵ against wavelength. In this way the absorption characteristics of different samples could be readily compared. Here the absorption spectra of DMNB caged glycine are compared with those of benzoin caged GABA.*

far smaller volumes. The absorption and uncaging behaviour of the compounds was observed to be consistent between the two regimes.

Sample preparation

For the general laser photolysis procedure a solution of the caged compound was prepared. During photolysis experiments, aliquots (1 mL) of the solution were placed into UV transmitting cuvettes (101-QS, Hellma) and exposed to radiation from the given laser source for fixed time durations as illustrated in figure 3.10. Care was taken to ensure that the laser beam (diameter ~ 4mm) passed through the the solution in the cuvette at the lowest point possible. Experiments with caged fluorescein indicated that this caused sufficient mixing of the compound to negate the need for magnetic stirring.

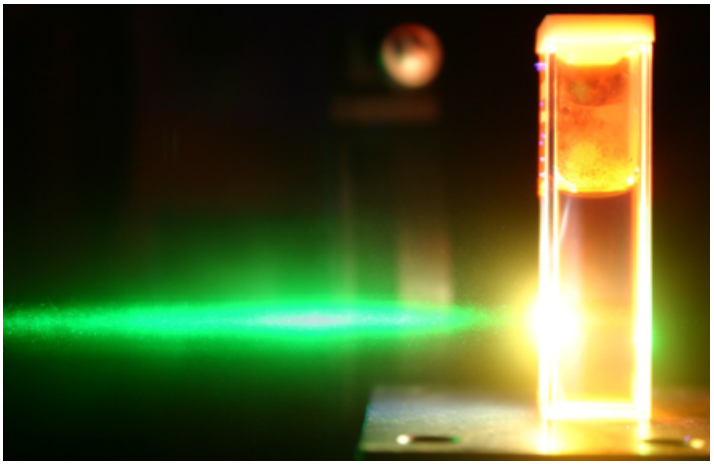

Figure 3.10: *Laser photolysis studies were undertaken by exposing a solution of the compound contained in a quartz cuvette to laser light. The appropriate photolysis wavelength was selected based upon the observed absorption characteristics of the compound.*

Photolysis light sources

Photolysis light sources included a CW 405 nm laser diode (i-Beam, Toptica) and an optical parametric oscillator (Panther EX OPO, Continuum) that was pumped at 355 nm by a frequency-tripled Nd:YAG laser (Surelite, Continuum). The pulses produced by the OPO were tunable through the wavelength range of 200 - 2000 nm, had a duration of ~4 ns at a repetition frequency of 10 Hz. The pulse energy varied depending on the wavelength in use but was typically in the order of tens of millijoules.

3.2.4 Photolysis quantification

After exposure to laser radiation the photolysis solution was analysed using nuclear magnetic resonance (NMR) spectroscopy and/or high pressure liquid chromatography (HPLC). It is widely accepted that HPLC exhibits greater sensitivity than NMR. This was found to be the case, however, both techniques indicated similar results. Consequently NMR was used to quantify the majority of the work presented in this thesis due to simpler sample processing and ready availability of this technique.

NMR spectroscopy is a non-destructive method for determining the structure of organic compounds. It relies upon the property of nuclear magnetic resonance

whereby, in the presence of a strong magnetic field, the degenerate spin states of atomic nuclei of interest split. This is known as the Zeeman effect. In this case, the nucleons are then probed using a second perpendicular electromagnetic field which is absorbed when in resonance with the energy gap giving rise to a NMR signal. The acquired signal is plotted as a function of chemical shift measured in parts per million (ppm).

To avoid the NMR spectra being dominated by the solvent spectra, NMR photolysis samples must first have the solvent which photolysis was conducted in removed and replaced with deuterated solvents. The solvent is initially evaporated off in a controlled manner through nitrogen bubbling. The samples are then exposed to a high vacuum (10^{-3} mbar) for 24 hours to ensure complete dessication. The samples were then re-suspended in deuterated solvents for NMR processing.

To allow quantitative analysis a small volume of 30 mM hexamethyldisiloxane (Fluka) was added prior to NMR spectra acquisition as an internal standard. Hexamethyldisiloxane exhibits a singlet transition around 0 ppm distinct from any peaks from the caged compound spectra. The standard therefore provides a calibration peak to measure the changes in caged compound peaks due to photolysis. In this way a photolysis percentage yield was determined.

For NMR the photolysis samples were placed in suitable sample vials and spectra were obtained using a 400 MHz spectrometer (Avance II, Bruker, Germany) using deuteromethanol as a reference for internal deuterium lock and tetramethylsilane (TMS) as a reference for the chemical shift. The resulting spectra were analysed using the Topspin software package.

HPLC is a chromatographic technique for separating mixtures of compounds. If differs from standard liquid chromatography through use of a pump to drive the mobile phase and analyte through a high density column. The increased density is provided by use of smaller particles which results in increased separation. A detector provides the retention time for the analyte. HPLC was performed by my collaborators in the Conway group using Gilson equipment detecting at 255 nm and a Phenomenex Gemini 5 μm C18 110A column.

3.2.5 Interpretation of NMR spectra

NMR spectra were typically employed to assess the photolysis of the caged compounds. Different characteristic peaks in the the NMR spectra can be attributed to different compounds present in the photolysis sample. Disappearance of peaks associated with the caged compound and appearance of peaks associated with the free compound was interpreted as photolysis of the caged compound generating the desired free compound.

Figure 3.11 demonstrates typical NMR spectra to be expected form a photolysis experiment. These spectra show the photolysis of a DMNB caged TRPV1 antagonist compound (DMNB capsaicin analogue) with 8 mw of 374 nm laser light at periods of 5, 10, 15 and 30 minutes through the irradiation with time increasing through the NMR stack.

The photolysis was identified by changes within the methoxy (MeO) region of the spectra between 3.3ppm and 4ppm on the "chemical shift" x-scale of the NMR spectra. By mixing caged and uncaged capsaicin together in unequal ratios it was possible to determine which methoxy peaks correspond to the presence of caged and uncaged compound. As a result it was possible to determine that the appearance of a peak at 3.81ppm on the spectra corresponds to the appearance of free capsaicin analogue. In this way the laser-induced photolysis can be qualitatively studied.

For quantitative assessment of the photolysis an internal standard must be added to the NMR sample to calibrate the varying photolysis spectra peaks against. For the DMNB caged TRPV1 agonist example 2,4,6-trimethoxy-myo-inositol-1,3,5-orthoformate was chosen as the standard for quantitative NMR as it has 3 MeO groups for comparison to the capsaicin MeO groups.

Figure 3.12 illustrates how the characteristic peaks of the spectra can be attributed to the different compounds present allowing quantification to be made against the internal standard. Integration of the peaks using the Topspin analysis software provides information on the amount of each compound that is present. The spectra has been annotated for ease of understanding.

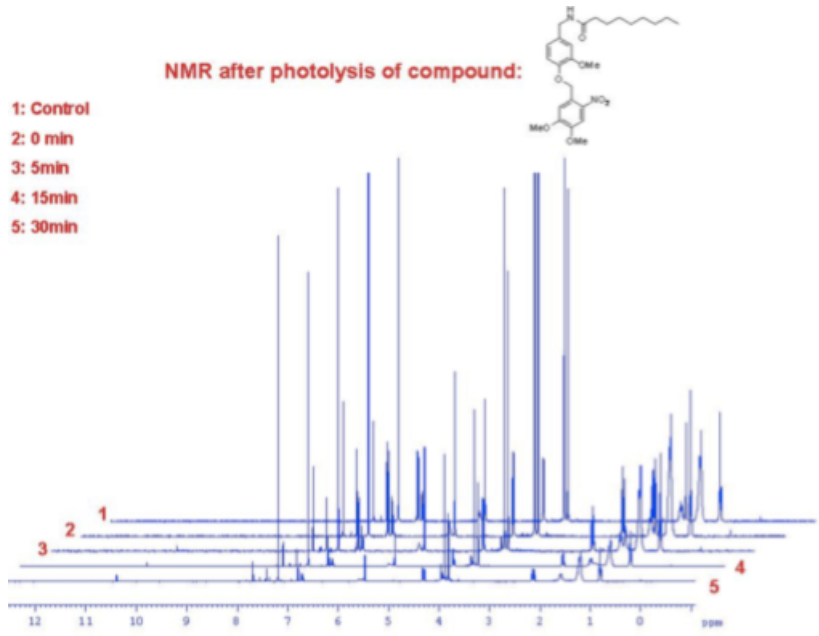

Figure 3.11: *Representitive NMR spectra such as these were used to characterise photolysis experiments. Reduction of peaks associated with the caged compound and subsequent increase of peaks associated with the free material was interpreted as photolysis of the caged compound generating the free active compound of interest.*

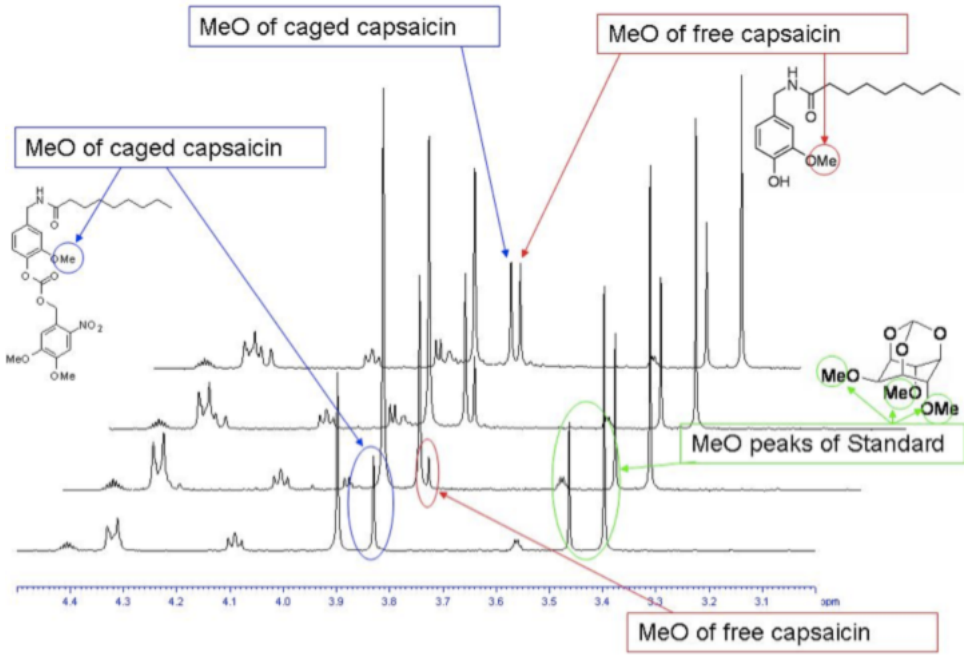

Figure 3.12: *Addition of a known internal standard permitted calibration of the NMR siganl peaks. Peak integration provided quantification of the photolysis experiments indicating how much free material was generated by laser irradiation.*

3.3 Biological Techniques

The most commonly employed biological techniques throughout the studies are presented here. Protocols specific to individual experiments are detailed in the relevant sections.

3.3.1 Aseptic technique & tissue culture

For ethical study of biological systems in the lab, model cell systems were cultured *in vitro*. Prevention of infection in any of the biological samples under study was paramount. Correct aseptic technique can prevent contamination with bacteria, fungi, mycoplasma or cross contamination with other cell lines. It was crucial to successful experimentation that good sterile aseptic technique was strictly adhered during the culturing of cells for experimentation.

All cell culture and sample preparation was performed within a sterile cell culture lab following standard aseptic cell culture protocols [94, 95]. These techniques ensured that there was a continual supply of cells for experimentation.

3.3.2 Viability assessment

Common techniques such as Trypan blue or Propidium iodide exclusion assays were initially used to asses cell viability. Healthy cells continue to exclude membrane impermeable stains and dead cells do not. Following laser exposure, apoptopic mechanisms have been shown to slow a cells metabolic response. Therfore any test immediately following an experiment would be premature as a cell in the early stages of apoptosis may still exclude such stains. The gold standard for assessing whether or not a cell has maintained viability is whether or not it goes on to divide. This was the method chosen for assessing the viability of any sample presented in this thesis.

3.3.3 Cell sample chambers

For micro-manipulation of biological samples, two sample chamber configurations were employed. Both worked in a sandwich configuration where a volume of liquid

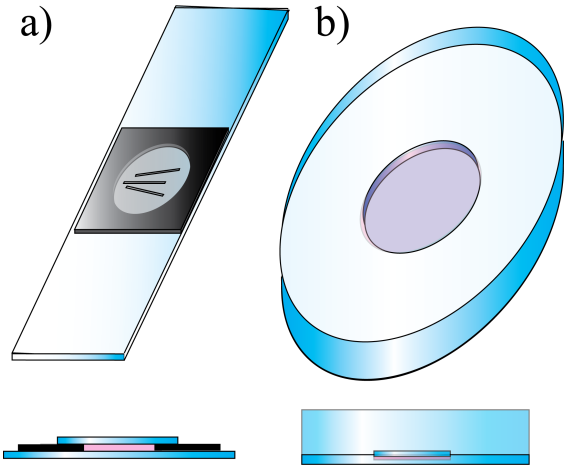

Figure 3.13: *Sample chambers for micromanipulation were prepared under aseptic conditions. The first chamber (a) is of use when recovery of the biological sample is not important and is constructed from a vinyl spacer sandwiched between two glass microscope slides forming a well for manipulation. The second chamber (b) was of use when the biological sample under study had to be recovered or stored in an incubator and comprised of a round bottomed culture dish sealed with a type 0 round coverslip.*

containing the manipulation sample was encompassed between two layers of glass. The two different sample chambers are illustrated in figure 3.13. All samples were prepared under full aseptic conditions with all component parts being sterilised.

In the first of these configurations (a) the chamber was fashioned by adding a 12 mm diameter, 100 mm high vinyl spacer (Gerber, USA) to a 76 X 26 X 1 mm glass microscope slide. The chamber area was then pacified by the addition and removal of Sigmacote, and 50 µl of cell solution was added. The chamber was then sealed with a 23 mm diameter type-0 coverslip was placed on the top of the microchamber. This chamber was typically used when the biological sample did not have to be stored in the incubator and when post experiment recovery of the cells was not essential. Due to the thickness of the bottom coverslip high N.A optics could not access the bottom of the sample. This sample chamber was found to be most useful for experiments using non adherent cell types.

In the second configuration (b), cells were seeded on the bottom of a 30 mm diameter glass bottomed culture dish with a usable working area of 23 mm (World precision instruments, Stevenage, UK) and incubated for a period of 24-48 hours for adherent cell lines. A floating cover slip was used to provide the top interface for the microscope objective. Upon completion of the experiment the floating coverslip

was removed with great care and the manipulation medium replaced with 2 ml of growth medium before returning the sample to the incubator. This chamber was most suitable if the sample had to be stored in the incubator and if the recovery of the biological material was important. Very quickly the second configuration became the standard for experiments and the majority of the described work was conducted in such chambers.

3.3.4 Conclusion

The key systems and techniques employed throughout the thesis have been introduced. The design, construction and characterisation of a femtosecond Ti:Al_2O_3 laser which was heavily utilised throughout the studies has been presented. The fundamental considerations for the construction of an optical tweezers have been discussed. Techniques for the handling and characterisation of caged compounds have been detailed. Finally a comprehensive account of the techniques required for the preparation and handling of the biological samples under study was given.

Furthermore, the reasoning for using certain systems or methods was presented. For example it was chosen to construct modelocked Ti:Al_2O_3 laser because a femtosecond laser was required and the wavelength of this material well suited to biological applications. Optical tweezers were chosen for the manipulation of biological samples since the technique is easily integrateable with common microscopes and permits the aseptic handling of biological media. NMR was chosen for non-destructive analysis of caged compounds as this technique was readily available and shown to give similar results to the more sensitve HPLC.

However, this chapter does not go into detail why certain broader approaches were taken. For example, the merits of optical injection over competing methods such as electroporation [96] or gene gun bombardment [97] or the advantages of caged compounds over other chemical delivery systems was not discussed. Rather the objective of this chapter was to describe the equipment and methods used within the work presented in the thesis to avoid repetition.

Chapter 4

Caged molecular probes for controlling cellular chemistry

Cellular function is dependent upon the local microenvironment, control of which is crucial to the successful probing of a biological process. Reagents must be delivered to the cell interior with a high level of spatial and temporal control akin to the process under study. A major failing of conventional chemical tools is that control is lost upon entering the cellular environment. In this chapter the use of light as a precise trigger for caged bio-active compounds is investigated. In this way spatial and temporal control over the cellular microenvironment can be maintained following delivery of the compound to the cell interior.

The rationale and basis of caged compounds were introduced in chapter one. The work presented in this chapter is to do with the development of novel molecular probes for unmet biological problems. All of the caged compounds work presented in this thesis is based upon single-photon photolysis as this is most accessible to the biological community.

The development of the compounds presented in this chapter was undertaken between disciplines. Chemical design and synthesis of all the presented compounds was undertaken by colleagues in the Conway group at the School of Chemistry at the University of St Andrews who have now moved to the University of Oxford[1].

[1]Dr Stuart Conway, Department of Chemistry, Chemistry Research Laboratory, University of Oxford, Mansfield Road, Oxford, OX1 3TA, UK.

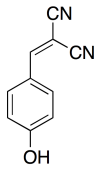

Figure 4.1: *Chemical sturcture of the protonophore AG10 which acts to decouple the mitochondrial membrane.*

Biological application of the compounds was carried out by a range of collaborators detailed in the appropriate sections.

My role was to apply photonics techniques for the characterisation of the developed compounds. This work involved performing UV/Vis absorption studies of the compounds under development and using these results to perform NMR quantified laser photolysis studies. These techniques were detailed in chapter three. This work fed back into to compound design and indicated which compounds might be suitable for biological application. In this way it was possible to optimise the photolysis systems for the most controlled and efficient compound release *in vitro*.

In this chapter the development of caged AG10 derivatives for spatially predefined mitochondrial uncoupling [4], TRPV1 agonists and antagonists [2] and caged lidocaine for highly localised anaesthesis in neuroscience are presented. Full descriptions of the work are available in the literature as indicated.

4.1 Caged AG10 for spatially predefined mitochondrial uncoupling

In this section the development of caged AG10 derivatives for selective depolarisation of mitochondria in localised regions of the cell is presented [4].

4.1.1 Introduction

AG10 has a chemical structure that is illustrated in figure 4.1. This molecule is a tyrosine phosphorylation inhibitor (tyrphostin) which acts as a protonophore. As such, AG10 promotes the transport of protons across lipid bilayers such as that of the cell membrane resulting in depolarisation of the membrane.

As discussed in chapter one, the mitochondrion is a vital organelle of the eukaryotic cell which plays a central role in controlling cellular function. To investigate the role mitochondria play in cellular function, it is necessary to have the ability to selectively inhibit mitochondrial activity. Whilst whole cell mitochondrial disruption is easily achievable through chemical treatment, there are few examples of targeted, localised inhibition of mitochondria or sub-poulations of mitochondria within selected intracellular regions [98, 99]and these require expensive multiphoton laser systems. Caged AG10 is an ideal candidate for such selective spatial control for the inhibition of subcellular populations of mitochondria by uncoupling the mitochondrial membrane potential ($\Delta\Psi$m). Here the synthesis, characterisation and biological application of the first pair of caged AG10 derivatives is presented.

4.1.2 Synthesis & structure

Quenching the ability of AG10 to act as a protonophore was achieved by caging of the important phenol group. Figure 4.2 shows the structure of the two caged AG10 compounds, 2-nitro-4,5-(dimethoxy)benzyl (DMNB) AG10 (a) and DMNB-carbonate linker AG10 (CDMNB AG10) (b) . The DMNB caged AG10 was synthesised by reaction of 4-hydroxy-benzaldehyde and 4,5-dimethoxy-2-nitrobenzyl bromide with K_2CO_3 in dimethylformamide at 40 °C (51% yield) of the DMNB benzaldehyde derivative, which was then under condensation with malononitrile, in the presence of piperidine in ethanol under reflux, produced DMNB-caged AG10 (70% yield).

The CDMNB AG10 was produced by reaction of DMNB acid with phosgene. The resulting DMNB chloroformate was reacted with AG10 in the presence of three equivalents of trithylamine to produce the DMNB carbonate AG10. The carbonate linker was designed to promote greater solubility of the compound for biological application.

4.1.3 Characterisation

Prior to application to *in vitro* biological systems, the photochemical properties of the compound were evaluated by the techniques discussed in chapter three. The ab-

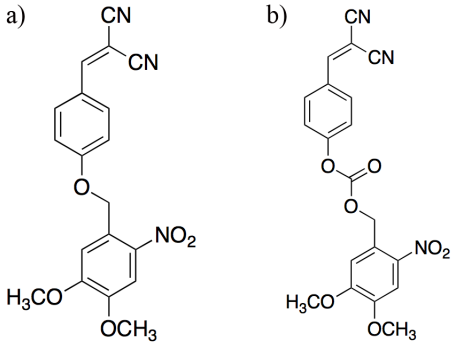

Figure 4.2: *Chemical structure of DMNB (a) and CDMNB (b) caged AG10 derivatives.*

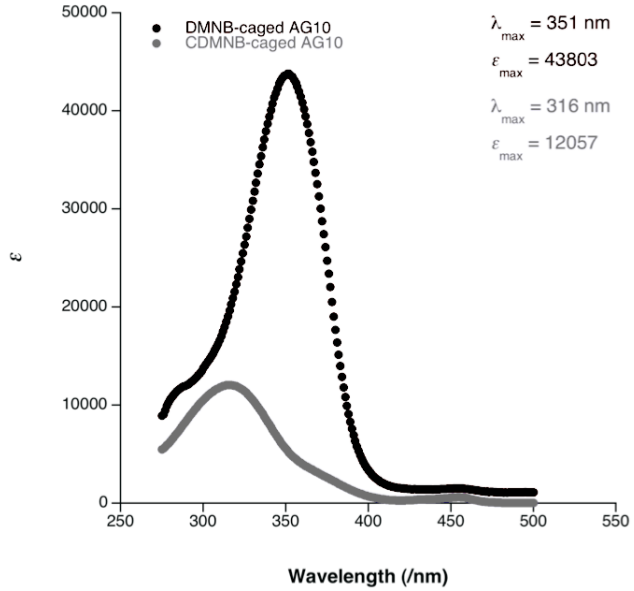

Figure 4.3: *Absorption characteristics of the DMNB and CDMNB caged AG10 derivatives. The dimensionless extinction coefficient (ϵ) is plotted against wavelength to indicate where the compound absorbs most strongly.*

sorption characteristics of the molecule illustrated in figure 4.3 showed that DMNB AG10 demonstrates a λ_{max} of absorption at 351 nm and extinction coefficient (ε) of 43803. The CDMNB AG10 exhibited a λ_{max} at 316 nm with ε of 12057. Full laser photolysis studies were undertaken using the 355 nm nanosecond pulses provided by the third harmonic of a Nd:YAG laser (Surelite, Continuum). These studies were used to determine whether photolysis of the photolabile protecting group occurred at this wavelength and also the nature of the products that were formed when the compound was illuminated.

The development of the characteristic AG10 peaks at 6.9 ppm and 7.85 ppm

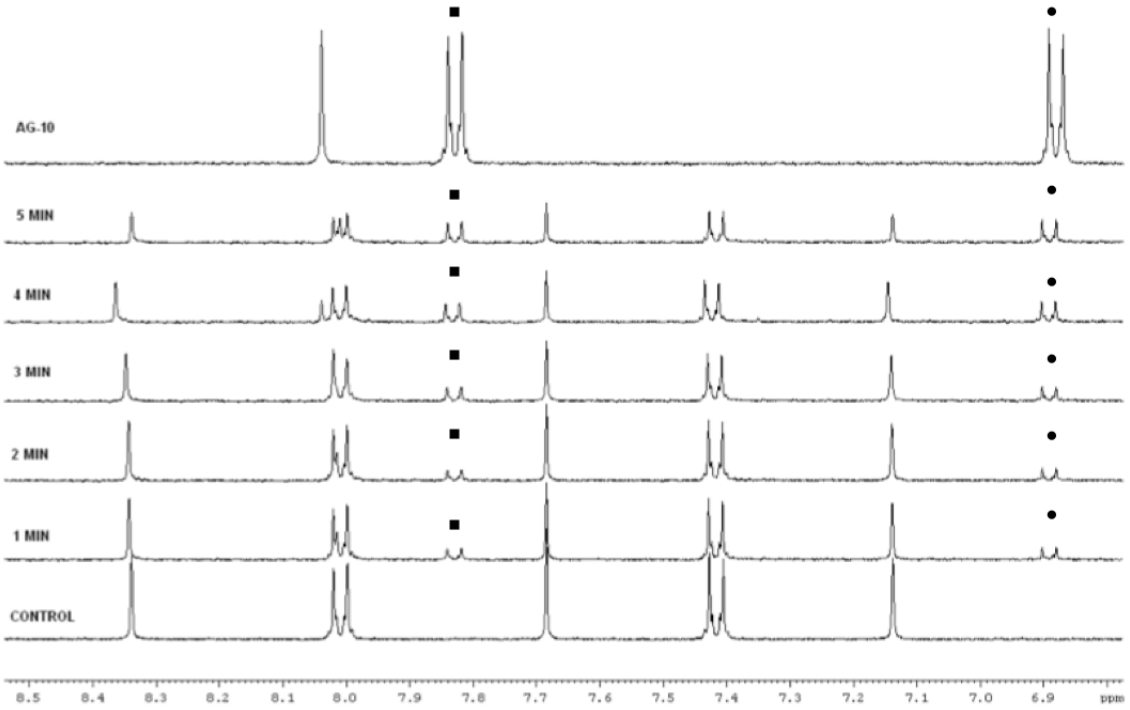

Figure 4.4: *Partial NMR spectra of a control sample, photolysis samples (1 - 5 minute exposure times) and free AG10. Comparison between spectra indicate that free AG10 has been generated as a result of laser irradiation. Loss of caged material and the appearance of free AG10 is indicated by the twin peaks at 6.9 (•) and 7.85 (■) ppm. Figure modified from [4].*

in the partial ^{1}H NMR spectra in figure 4.4 indicate the generation of free AG10 form the DMNB caged precurser. As detailed in chapter three, an internal standard (hexamethyldisiloxane) was used to determine the amount of caged and uncaged material present in the photolysis samples. For photolysis quantification by HPLC a previously measured calibration curve was used.

Figure 4.5 illustrates a graphical summary of the ^{1}H NMR and HPLC results for the DMNB and CDMNB caged compounds. The DMNB-AG10 compound was photolysed by the laser irradiation to give the expected AG10. After 5 minutes irradiation ^{1}H NMR showed 35% of the total initial material comprises the uncaged product and HPLC showed 46%. The CDMNB AG10 caged compound also photolysed to give the expected AG10. After 5 minutes irradiation ^{1}H NMR showed 26% of the desired AG10. It is generally accepted that HPLC analysis is more sensitive than ^{1}H NMR analysis for undertaking quantitative data although it is a more complex and time consuming process to undertake. More AG10 (produced by

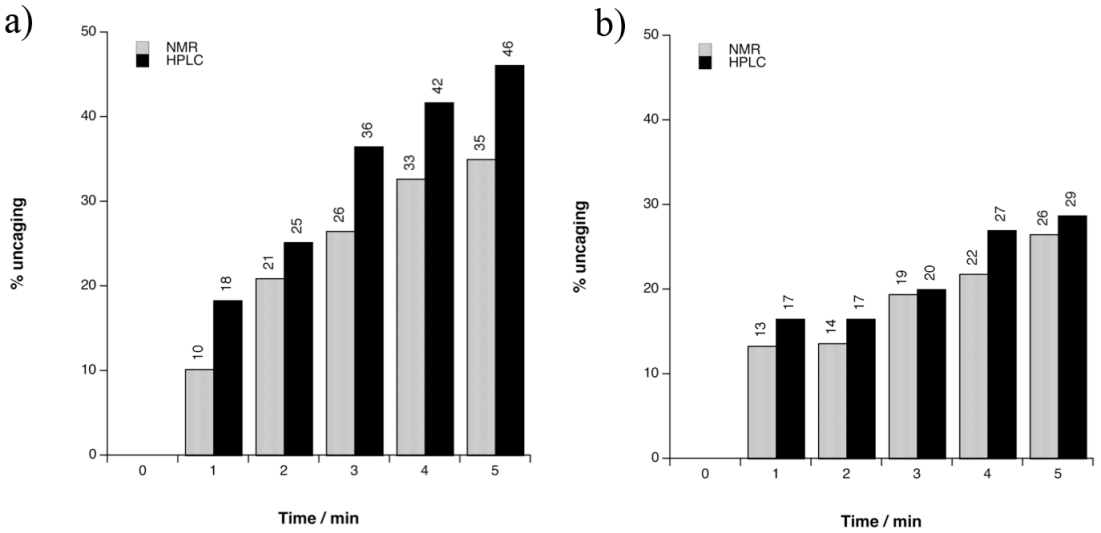

Figure 4.5: *Quantified NMR and HPLC reveals the percentages of free AG10 generated by the photolysis of DMNB (a) and CDMNB (b) AG10. Figure modified from* [4].

photolysis) was detected by HPLC than was detected by ^{1}H NMR and hence greater values for the percentage of AG10 present that were observed could be explained by the sensitivity difference in the detection method. However, the general trends in amount of photolysis were similar for both methods of detection.

Detection by^{1}H NMR demands larger volumes and hence longer exposure times than those typically used in biological experiments. Whilst the explicit details may vary between these large scale bulk and biological experiments the trends indicated by such studies are a valuable indicator to the behaviour in biological systems. The trend identified in these studies is that the DMNB caged compounds photolyse more efficiently than the CDMNB caged molecules. The large volumes and exposure times used in these make it difficult to extrapolate the results of these experiments to *in vitro* studies.

4.1.4 Biological application

Biological application of the compounds was undertaken by the McCarron group at Strathclyde University[2] and a brief summary of their results are presented here.

[2]Dr John McCarron, Strathclyde Institute of Pharmacy and Biomedical Sciences, University of Strathclyde, John Arbuthnott Building, 27 Taylor Street, Glasgow, UK G4 0NR

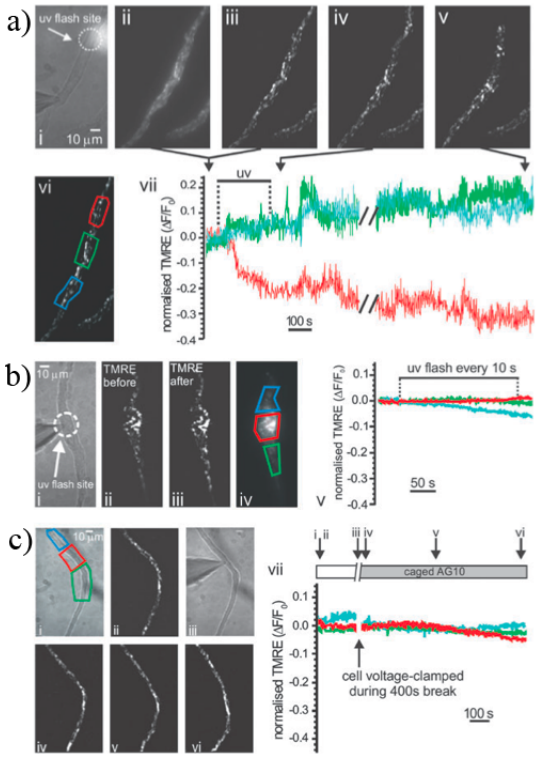

Figure 4.6: *In vitro photolysis of DMNB AG10 results in localised mitochondrial depolarisation. Figure modified from [4].*

The full report can be found in the literature [4]. The objective of these experiments was to assess the suitability of the caged compounds as molecular probes.

In vitro freshly isolated smooth muscle cells were loaded with 10 nm tetramethylrhodamine, ethyl ester, perchlorate (TMRE) a fluorescent stain commonly used to visualise $\Delta\Psi$m. When the $\Delta\Psi$m is decoupled the fluorescence signal is diminished. It was first demonstrated that synthetic AG10 depolarised $\Delta\Psi$m as as reported in the literature [100]. It was then demonstrated (from n=13) that intracellular localised photolysis of DMNB caged AG10 evoked a sustained (over 20 minutes) and localised $\Delta\Psi$m depolarisation.

Figure 4.6a shows the targeted photolysis of a selected region of smooth muscle cell and the consequent loss in TMRE fluorescence indicating depolarisation of the mitochondira at the photolysis site. Repeated exposure to flashes of UV light by a in the absence of any caged compound did not cause any depolarisation as shown in figure 4.6b. Application of the DMNB group alone, also produced no effect as illustrated in figure 4.6c. Photolysis of CDMNB AG10 illustrated in figure 4.7 also

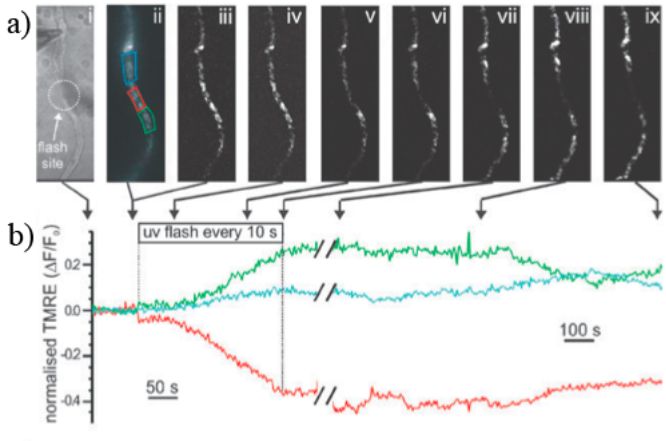

Figure 4.7: *In vitro photolysis of CDMNB causes localised mitochondrial depolarisation. Figure modified from [4].*

demonstrated to evoke more rapid $\Delta\Psi$m depolarisation than DMNB caged AG10 as indicated by figure 4.7. Increased solubility of this compound in the water-DMSO solution permited a concentration of 62 µM to be loaded into cells as opposed to the 25 µM possible with the DMNB AG10 compound. This was most likely responsible for the more rapid response.

4.1.5 Summary

Bulk photolysis experiments in the laser lab indicated that both DMNB and CDMNB caged compounds had the potential to act as molecular probes. Biological studies employing isolated smooth muscle cells then demonstrated that both compounds were highly suitable *as in vitro* molecular probes and caused the desired depolarisation of $\Delta\Psi$m upon photolysis. As intended, the CDMNB caged compound was found to have far greater solubility than the DMNB caged AG10, which compensated for the less efficient photolysis revealed in bulk laser photolysis studies.

The DMNB and CDMNB caged AG10 molecular probes developed provide for the first time the ability to direct targeted, localised $\Delta\Psi$m depolarisation with hitherto inaccessible spatial and temporal control. In this way researchers may begin to eludicate the role mitochondria play in the cell in a controlled and more specific manner. For example the compounds may find application in the study of Ca^{2+} signalling channels especially in the endopasmic reticulum (ER) and sarcoplasmic

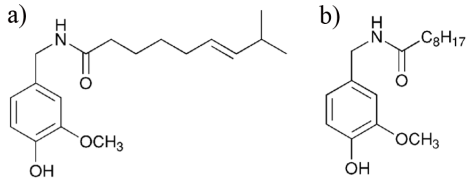

Figure 4.8: *The chemical structures of capsaicin (a) and nonivamide (b) which both act as TRPV1 agonists.*

reticulum (SR, part of the smooth endoplasmic reticulum) in which mitochondria have been implicated

4.2 Transient receptor potential vanilloid subtype 1 (TRPV1) caged agonists and antagonists

The development of caged TRPV1 agonists and antagonists are presented here for application to studies of the ligand gated TRPV1 channel [2]. The work was driven by the requirement for a higher degree of spatial and temporal control and a lack of caged antagonist compounds to enable more precise studies of TRPV1 receptor dynamics. The reported caged antagonist compounds are the first to appear in the literature and the caged agonist structures are of differnet structure to those already reported. As in the previous section the molecules were designed and synthesised by the Conway group. In this case the biological experiments were carried out by the Khiroug group at the Univeristy of Helsinki[3].

4.2.1 Introduction

Capsaicin, with a chemical structure illustrated in figure 4.8a is the active component of chili peppers responsible for their perceived spiciness when eaten and irritation upon application to the skin or eyes. Nonivamide with a structure illustrated in figure 4.8b is a similar compound which is synthetically far easier to produce than capsaicin, yet yields pharmacologically similar effects [101–103]. The main sensation

[3]Dr Leonard Khiroug,Neuroscience Center, University of Helsinki, Viikinkaari 4, FIN-00014, Helsinki, Finland

experienced following exposure to these compounds is heat and subsequent numbing of the exposed area. As such, capsaicin and similar derivatives are involved in the therapeutic treatment of chronic pain such as arthritis and skin conditions such as psoriasis [104].

Such biological activity is realised upon activation of the TRPV1 receptor which was both identified as the molecular target of capsaicin and subsequently cloned in 1997 by Julius *et al* [105]. TRPV1 is a protein located in the plasma membrane of sensory neurons and acts as a non-selective cation channel activated by capsaicin, acidic pH below 5.5 and temperatures above 42 °C. Location on the sensory neurons makes TRPV1 useful in studies of nociception [106], urinary urge incontinence, chronic cough and irritable bowel syndrome (IBS) [107]. Consequently, there has been great interest in the development of TRPV1 agonists and antagonists for use as drugs in the treatment of such conditions.

The development of several caged TRPV1 agonists is detailed in the literature. In 2003 the first of these employed a 2-nitro-4,5-(dimethoxy)benzyl (DMNB) caging group for application of caged capsaicin to studies of ion channel gating [108]. At a similar time photolysis studies of biologically inactive caged capsaicin derivatives was reported by Katrizky *et al.* [109]. Building on this work 4'-(methoxy)phenacyl and DMNB caged TRPV1 caged agonists and their application to the study of dorsal root ganglion neurons was reported by researchers at the University of St Andrews in 2006 [110]. In the same year Kao *et al.* also reported the development of several caged TRPV1 agonists [111] and Hagen *et al.* reported the caging of TRPV1 agonists with both DMNB and coumarin derived caging groups [112]. Interestingly, the courmarin group exhibit enhanced solubility and two-photon cross sections making these compounds possible candidates for two-photon photolysis.

In this section, the synthesis, characterisation and biological application of several 4'-(methoxy)phenacyl and DMNB caged TRPV1 agonists and, for the first time, antagonists are presented.

4.2.2 Synthesis & structure

Nonivamide was chosen as the starting compound for the synthesis of the caged compounds as it exhibits a simpler synthesis procedure than capsaicin. Alkylation of the phenol group of the vanilloid moiety of capsaicin was demonstrated to yield a successful caged capsaicin derivative and TRPV1 agonist by *Walpole et al.* in 1993 [103]. As such a similar strategy was adopted here. Appendino *et al.* demonstrated that halogenation of nonivamide yields TRPV1 antagonists and forms the basis of the presented caged TRPV1 antagonist through halogenation with bromine [113, 114].

4.2.3 Characterisation

The photochemical properties of the synthesised compounds were evaluated prior to *in vitro* application to biological systems. The absorption characteristics illustrated in figure 4.9 were obtained as detailed in chapter three to indicate which wavelengths might lead to most successful photolysis.

DMNB caged agonist (a) was observed to have a λ_{max} in absorption at 345 nm and extinction coefficient (ε) of 7191. The DMNB caged antagonist (c) exhibited a λ_{max} at 345 nm with ε of 6728. The CDMNB caged agonist (b) exhibited a λ_{max} at 343 nm with ε of 5804. The CDMNB caged antagonist (d) exhibited a λ_{max} at 342 nm with ε of 6107. Full laser photolysis studies were then undertaken to determine whether photolysis of the photolabile protecting group occurred and also the nature of the products that were formed.

For photolysis quantification by ^{1}H NMR, the procedure described in chapter three was followed. The earlier work on AG10 caged compounds in section 4.1 demonstrated that whilst NMR is less sensitive than HPLC, the trends observed are consistent between the two detection methods.

A graphical summary of the photolysis of the TRPV1 caged compounds is shown in figure 4.10. The DMNB-caged agonist (a) was photolysed by the laser irradiation to give the expected TRPV1 agonist. After 5 min, 61% of the total initial material comprises the uncaged product and there is approximately 4% of the caged mate-

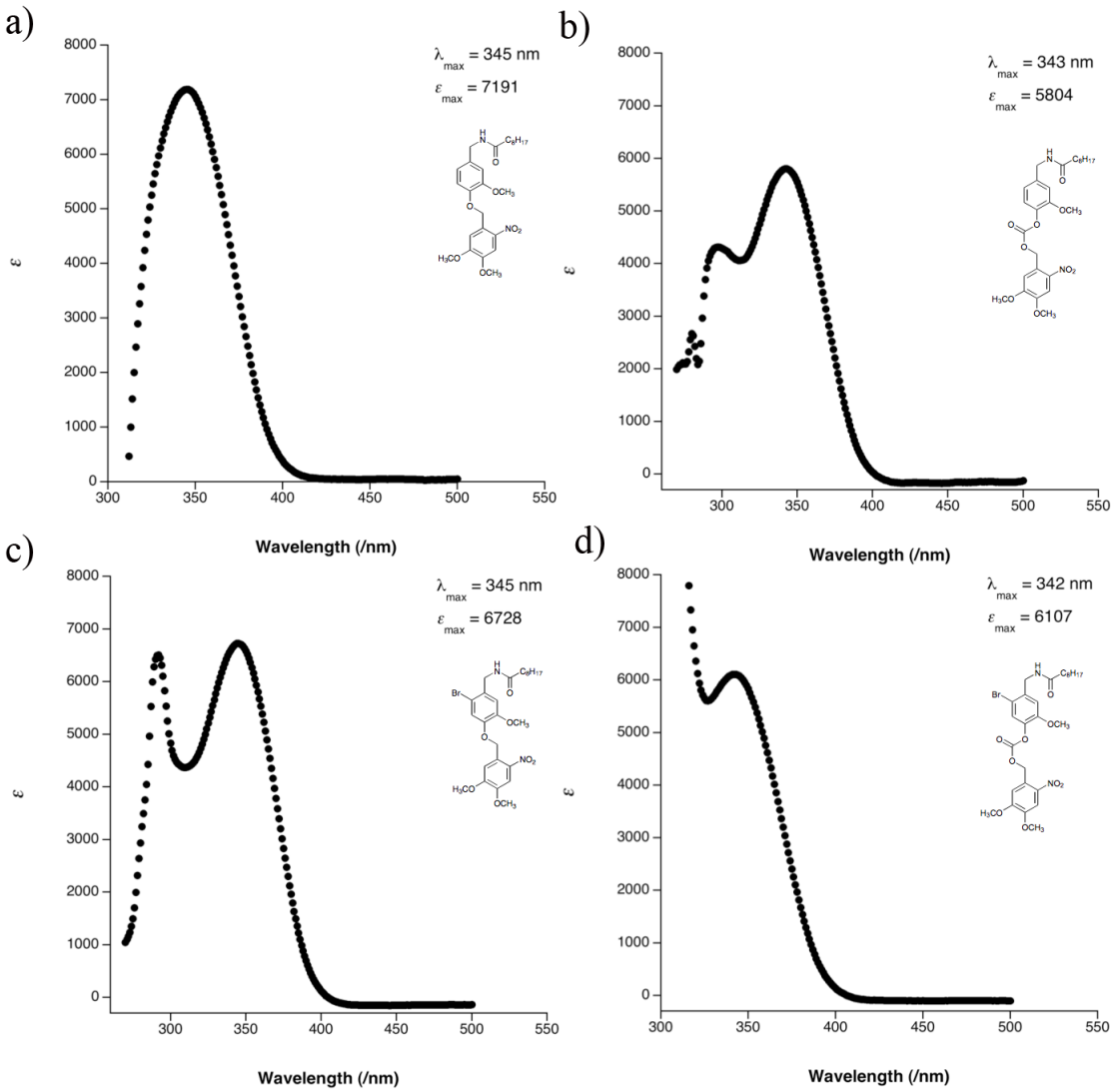

Figure 4.9: *Absorption properties and chemical structures of the caged TRPV1 agonists (a-DMNB, b-CDMNB) and antagonists (c-DMNB, d-CDMNB). The dimensionless extinction coefficient (ϵ) is lotted against wavelength to indicate where the compounds absorb most strongly. Figure modified from [2]*

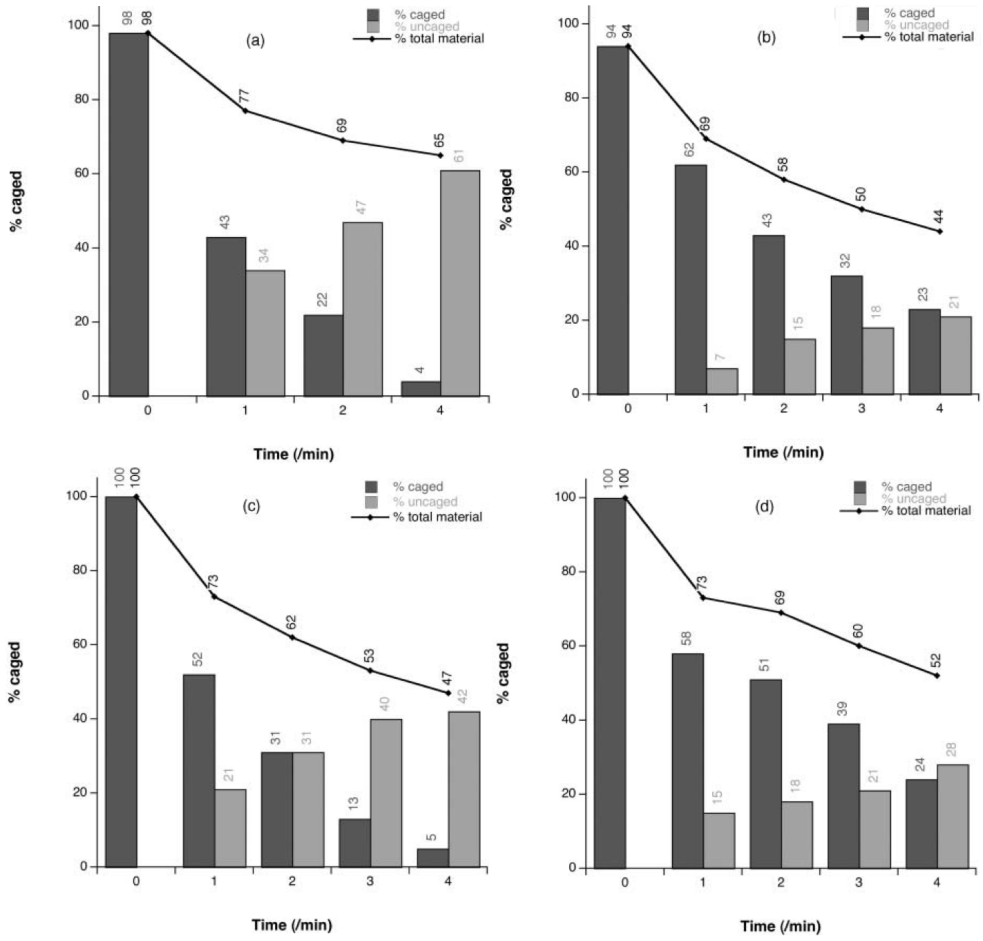

Figure 4.10: *Graphical summary of the quantified laser photolysis studies of TRPV1 agonist (a-DMNB, b-CDMNB) and antagonist (c-DMNB, d-CDMNB) compounds. Figure modified from [2].*

rial remaining. The CDMNB-caged agonist (b) was photolysed less efficiently, to give 21% of the desired TRPV1 agonist with 23% of the caged material remaining after 5 min. The DMNB-caged antagonist (c) released 42% of the desired TRPV1 antagonist upon photolysis, with 5% of the caged material remaining after 5 min. Similar to the agonist compound, the CDMNB-caged antagonist (d) was photolysed less efficiently, with 28% of the desired TRPV1 antagonist released after 5 min and 24% of the caged material remaining.

In all cases, the sum of the caged and un-caged material present at the end of the photolysis experiment was always found to be less than the total amount of caged material present at the beginning of the experiment. Given that the control samples contain approximately all of the material expected, attributing this loss to

experimental handling seems unsatisfactory. Therefore, it seems that an unwanted photodegradation of either the caged material or the uncaged product is occurring.

To investigate whether the uncaged material was further degrading the pure photolysis products were irradiated for 4 min with a 355 nm with 95 mJ pulse energies. Irradiation did not generate loss of material suggesting that the desired product is photostable once produced. It therefore may be the case that there is more than one photodegradation pathway for the caged material with one path yielding the desired material and one an unidentified by-product. Alternatively, it may be possible for the by-products of the caging group to interact with the desired products of photolysis, leading to degradation of the material. Finally, the observed photodegredation may be an artifact of the experimental conditions employed, which are different to those for irradiating cells *in vitro*.

The trend identified in these studies is that the DMNB caged compounds photolyse more efficiently than CDMNB where the DMNB moiety is attached by a carbonate linker.

4.2.4 Biological application

The objective of the experiments was to assess the suitability of the compounds as molecular probes for *in vitro* studies. To this end it must be demonstrated that the photorealease of the caged compounds produced the desired TRPV1 activation and deactivation for agonist and antagonist respectively in cells whilst not compromising cell viability. It is also crucial that the caged compounds themselves or the light evoking photolysis do not cause such an effect.

In vitro experiments were conducted on subpoulations of trigeminal neurons which are known to express TRPV1 receptor channels [115]. Upon agonist binding such cells exhibit a depolarisation of the membrane leading to an influx of Ca^{2+}. As such whole cell patch clamp and Ca^{2+}were utilised to indicate TRPV1 activation.

The DMNB caged agonist compound was shown to cause no reaction when introduced to the cells. As illustrated in figure 4.11 a and b, upon irradiation with a 50 ms flash of UV light (15 mW at 375 nm) a similar electrophysiological response to that of capsaicin was observed. The signal was agrogated in the presence of the

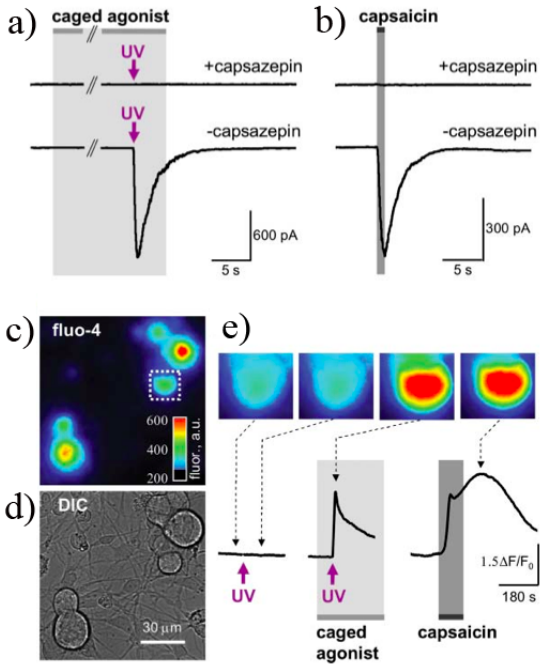

Figure 4.11: *In vitro photolysis of the DMNB agonist compound evokes a localised response similar to the applicaiton of capsaicin. The antagonist capsazepine was shown to agrogate the response. Figure modified from [2].*

antagonist capsazepine in agreement with the literature [116]. The same response was observed when fluo-4, the Ca^{2+} fluorescent stain was loaded into the cells to act as an indicator. Figure 4.11c shows cells loaded with the dye of which figure4.11d is a DIC brightfield view. The cell highlighted by the dashed line is targeted for photolysis. Figure 4.11e shows that the UV flash itself with no caged compound present causes no response whereas UV flash in the presence of the caged agonist evokes a signal similar to the application of capsaicin. Such a response was observed in 50% of cells (n = 145) over nine separate experiments. Taken together, this evidence demonstrates the suitability for the DMNB caged compound as an agonist of TRPV1 receptors. No biological application of the DMNB carbonate caged compound was undertaken.

The DMNB caged antagonist was found to have a solubility too low to render it useful for *in vitro* biological studies. The CDMNB caged compound was shown to exhibit higher solubility for *in vitro* application, unfortunately the compound was found to be toxic to the cells under study. As such neither of the caged antagonists were pursued as a viable molecular probe for *in vitro* application.

4.2.5 Summary

Bulk photolysis experiments in the laser lab indicated that all four caged compounds had the potential to act as a molecular probe releasing the desired TRPV1 ligand upon photolysis . However, biological studies employing subpoulations of trigeminal neurons demonstrated that the *in vitro* solubility of the DMNB caged antagonist made it unsuitable as a molecular probe. The CDMNB caged antagonist was found to have suitable solubility in DMSO but preliminary tests revealed that the antagonist was toxic to the cells under study resulting in progressive irreversible cell depolarisation. The caged antagonist compounds were shown to be unsuitable for use as molecular probes. The DMNB caged agonist was shown to be an ideal molecular tool for application to TRPV1 studies. No biological studies were conducted with the CDMNB caged antagonist. However, based on previous work this compound may exhibit higher solubility compensating for the relatively inefficient photolysis when compared to the DMNB caged compound.

More work remains in eludicating the source of toxicity of the antagonist compounds and if this is true in all cell types exhibiting TRPV1 receptors. A full biological study of the DMNB carbonate caged agonist would also be valuable as it may be a more successful probe than the DMNB caged compound.

The DMNB caged agonist based on nonivamide has been shown to be a highly appropriate molecular probe. It has been shown to be relevant for the *in vitro* activation of TRPV1 receptors with superior spatial and temporal control over existing application methodologies. In this way it may find application a useful probe specific to TRPV1 receptor studies, as well as in the study of Ca^{2+}signalling in general.

4.3 Caged lidocaine for highly localised anaesthesis

In this section, the development of a caged lidocaine compound is presented. The work was driven by the requirement for precise sub-cellular anaesthesis of selected areas in pharmacological studies.

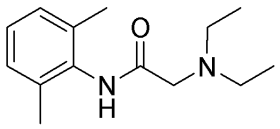

Figure 4.12: *The chemical structure of lidocaine.*

4.3.1 Introduction

Lidocaine, the chemical structure of which is shown in figure 4.12 is a common local anaesthetic. Biological function is mediated through blocking of sodium (Na^+) channels preventing depolarisation of the postsynaptic neuron. Consequently, transmission of an action potential fails. The motivation for development of a caged lidocaine molecular probe was to provide selective release of an anaesthetic.

Caging of lidocaine was achieved with the commonly employed DMNB caging group. Here the characterisation of DMNB lidocaine is presented alongside a preliminary biological study conducted by collaborators in the Emptage group at the University of Oxford [4].

4.3.2 Characterisation

As illustrated in figure4.13, DMNB caged lidocaine was observed to have a λ_{max} in absorption at 341 nm and extinction coefficient (ε) of 4411. Full laser photolysis studies were then undertaken to determine whether photolysis of the photolabile protecting group occurred and also the nature of the products that were formed.

Laser photolysis and NMR quantification procedures discussed in chapter three were employed. The time course in figure 4.14 illustrates partial 300 MHz ^{1}H NMR spectra of DMNB-caged lidocaine being photolysed. The control received no exposure to UV light and the sample spiked with commercially available free lidocaine illustrates the expected spectrum of the uncaged compounds.

As can be seen by the the disappearance of peaks from the caged compound (at 0.8 ppm) and the appearance of peaks from what appears to be free lidocaine (at 1.1 ppm) a degree of photolysis has been achieved. However, it does not appear to

[4]Dr Nigel Emptage, Department of Pharmacology, University of Oxford, Mansfield Road, Oxford, OX1 3QT, UK

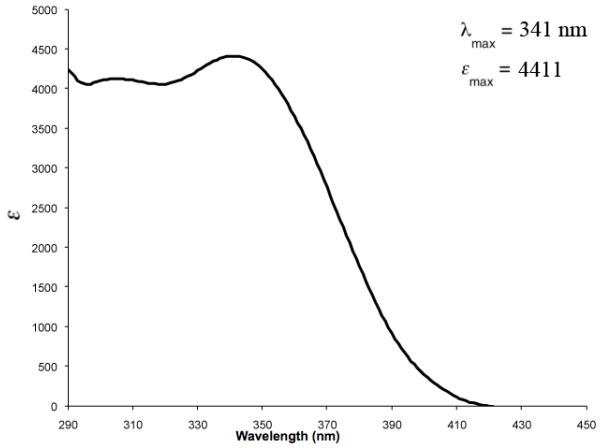

Figure 4.13: *Absorption characteristics of DMNB caged liocaine. The dimensionless extinction coefficient (ϵ) is plotted against wavelength to indicate where the compound adsorbs most strongly.*

grow with time. Figure 4.14 numerically surmises the results for DMNB lidocaine photolysis. As seen in the NMR traces, the release of free lidocaine from the DMNB caged compound was observed. However, the amount of free lidocaine did not grow beyond approximately 50 % beyond the one minute time.

Detection by ^{1}H NMR demands larger volumes and hence longer exposure times than those typically used in biological experiments. Whilst the explicit details may vary between these large scale bulk and biological experiments the previous work described in section 4.1 has shown that the trends indicated by such studies are a valuable indicator to the behaviour in biological systems.

4.3.2.1 Assessment of suitability to biological application

Preliminary biological application was on hippocampal pyramidal cells. A 1mM concentration of the DMNB lidocaine was applied to the cells. The membrane potential of the cell was observed to remain at a stable -70 mV throughout the experiments. Figure 4.15a demonstrates that current injection under control conditions results in an action potential firing. Figure 4.15b illustrates that following addition of DMNB lidocaine prior to UV light exposure, no further action potentials could be euldicated in response to the same current injection. DMNB caged lidocaine itself produced a biological effect.

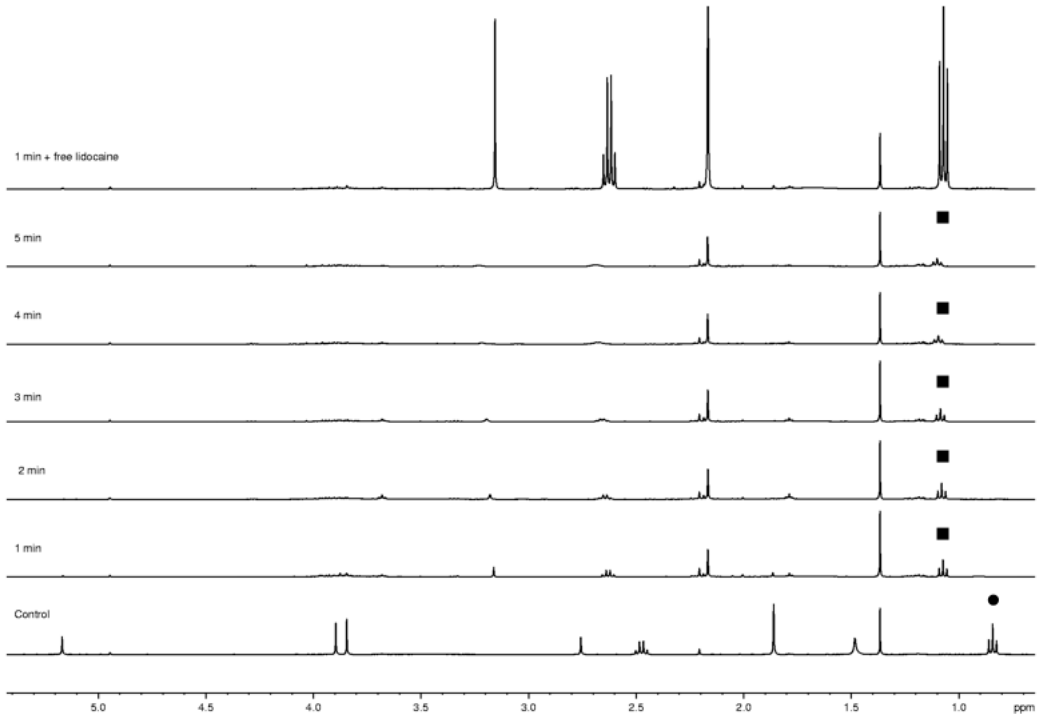

Time (min)	Caged (× 10^{-3} mmol)	% Caged	Uncaged (× 10^{-3} mmol)	% Uncaged
1	0.2001	7	1.5247	51
2	0.0146	0.5	1.7257	58
3	-	-	1.6983	57
4	-	-	1.6817	56
5	-	-	1.5905	53
Control	3	100	-	-

Figure 4.14: *NMR qanitification of the laser photoysis of DMNB lidocaine demonstrated rapid photolysis as indicated by the disappearance of the peaks attributed at the caged compound at 0.8 ppm (•) and the appearance of peaks attributed to free lidocaine at 1.1 ppm (■). The amount of free lidocaine generated never exceeded around 50%.*

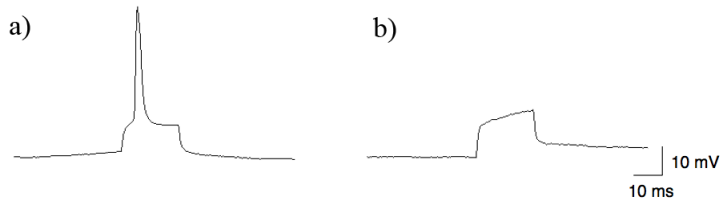

Figure 4.15: *Representative whole cell patch clamp recordings from application of the DMNB lidocaine to hippocampal pyramidal cells demonstrated that DMNB lidocaine realised biological activity in the absence of photolysis light. As such the compound was unsuitable for use as a caged molecular probe.*

4.3.3 Summary

Laser photolysis studies demonstrated that the DMNB lidocaine could be photolysed by intense UV light to yield free lidocaine. Unfortunately, preliminary biological experiments in hippocampal pyramidal cells indicated that the DMNB lidocaine itself exerts an anaesthetic effect and is therefore unsuitable for use as a molecular probe for biological studies. Future work must be done to investigate whether caging of the molecule at another location may achieve a functional caged molecule suitable for application as a molecular probe.

4.4 Conclusions

The work presented in this chapter has demonstrated the development and *in vitro* application of several new light-activated photochemical molecular probes

The development and *in vitro* photolysis of caged AG10 demonstrated the first example of a caged mitochondrial uncoupler for the selective and targeted disruption of mitochondria. Such a tool is essential for the eludication of the role mitochondria play in intracellular signalling processes.

The presented caged TRPV1 agonists will prove highly useful in the study of TRPV1 receptors and study of Ca^{2+} signalling in general. Further work must be undertaken to investigate the unexpected toxicity of the caged antagonist compounds.

Unfortunately caged lidocaine was found to be unsuitable for biological application as *in vitro* studies revealed that the caged compound itself generated a biological response. Future work would involve caging the compound at a different position to see if biological activity could be successfully quenched.

Future work for the development process of the caged compounds should involve a rigorous study into the factors affecting the efficiency of the photorelease of the compounds. Studies into the quantum efficiencies of the presented compounds would also be highly desirable.

All of the presented work was concerned with the single-photon photolysis of caged compounds. It has been demonstrated that light can be used as a highly precise remote trigger for the photochemical manipulation of *in vitro* biological systems.

The development of several caged molecular probes for application to biological systems has been detailed and future aims to investigate the efficiency of the release from the caged precursor molecule outlined.

Chapter 5

Wavelength selective activation of caged compounds compounds for neuroscience applications

5.1 Introduction

A major limitation of the caging technologies described in chapter one is that control over the biological affector molecule is lost upon photolysis. For example in the study of receptor dynamics, once a channel under study is activated by localised photolysis it will remain open as there is no means to achieve deactivation. The lack of an "off switch" is a major failing of the currently available caged molecular probes.

However, if the agonist of a target process is caged with a compound sensitive to one wavelength and the antagoinist compound caged with another compound sensitive to a different wavelength then it becomes possible to activate and deactivate a process under study. By using the two different wavelengths the agonist and antagonist compounds may be released in the presence of each other. Illumination of the system with one wavelength activates the target by photorelease of the agonist molecule, whereas illumination with a second wavelength deactivates by the target by photorelease of the antagonist molecule. Discrimination is therefore achieved by wavelength selection. Such a technique is known as "orthogonal" photolysis since the compounds can be independently released form their cages in the presence of

each other.

Here, the development of a wavelength selective system for enhanced control over neuronal processes is presented. This new methodology provides enhanced control of *in vitro* subcellular biochemistry and provides many experimental opportunities [17].As with the work presented in chapter four the compounds presented in this chapter were designed and synthesised by collaborators in the Conway group at the University of Oxford. The biological application of the compounds was carried out by collaborators in the Emptage group at the University of Oxford . My role was to apply photonics techniques discussed in chapter three for the characterisation of the developed compounds and to design and construct the photolysis systems used to perform the *in vitro* studies in Oxford.

5.2 Historical development

Wavelength differentiation between caging groups in the same system was first realised ten years ago in the work of Bochet *et al.* The principle was proven with caged dicarboxylic acids of no biological relevance in organic solvents [117–120]. The technique has since been utilised in solid phase synthesis [121] and lithography [122].

In the literature there is only one other example of the *in vitro* wavelength orthogonal photolysis of caged compounds. Kantevari *et al.* [123] claimed to demonstrate optically independent two-colour two-photon photolysis of caged neurotransmitters. However, selectivity is achieved by manipulation of compound concentration, optical power of the photolysis source and region selective photolysis biased towards the desired receptor type rather than by wavelength differentiation.

In the work presented in this chapter, development and *in vitro* single-photon photolysis of wavelength orthogonal caged neurotransmitters is demonstrated. This work has the long term goal of enabling new studies to be carried out in fundamental studies of learning and memory.

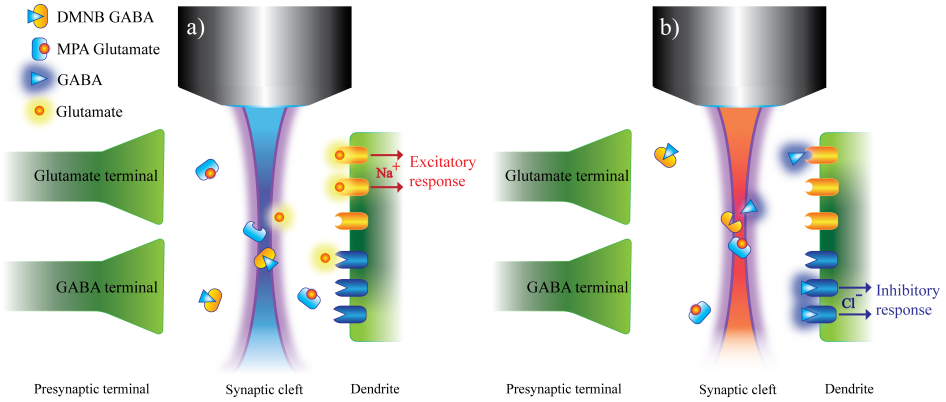

Figure 5.1: *A cartoon representation of the principal of wavelength orthogonal photolysis. Photolysis of individual compounds from a mixture of caged GABA and glutamate in a synaptic cleft can be achived by varying the excitation wavelength. Irradiation with shorter UV wavelengths (a) produces only free glutamate generating an excitatory reponse in the dendrite. Irradiation with longer UV wavelengths (b) produces only free GABA generating an inhibitory response.*

5.3 Development of compounds for the orthogonal toolkit

The design and characterisation of agonist and antagonist compounds where activation was selectively differentiated by the wavelength of illumintion was the first undertaking. The prominent excitatory and inhibitory neurotransmitters γ-aminobutyric acid (GABA), glutamate and glycine were chosen for application to studies of the central nervous system (CNS). Figure 5.1 illustrates the basis of the orthogonal toolkit. Photorelease of the agonist compound by illumination of a particular wavelength generates an excitatory response in the target dendrite (figure 5.1a). Illumination with a different wavelength generates an inhibitory response caused by the release of the antagonist compound (figure 5.1b).

Combinations of GABA, glutamate and glycine with a variety of caging moieties including 2-nitro-4,5-(dimethoxy)benzyl (DMNB), 3,5-dimethoxybenzoin (benzoin) and the 4-methoxyphenacyl (MPA) groups were investigated. It was paramount that the absorption of the paired caged compounds did not overlap as to provide selective differentiation. The DMNB caging moiety typically exhibits a long λ_{max} whereas the benzoin and MPA groups typically demonstrate much shorter λ_{max} [18]. The pairing of the DMNB moiety with one of the others provides an ideal system

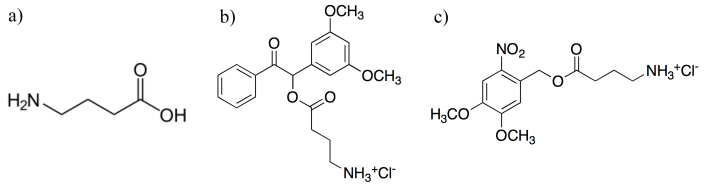

Figure 5.2: *Chemical structures of GABA (a), Benzoin caged GABA (b) and DMNB GABA (c).*

for achieving orthogonality.

5.3.1 Caged γ-aminobutyric acid (GABA) for orthogonal wavelength selective photolysis

GABA, with a chemical structure is illustrated in figure 5.2a is the chief inhibitory neurotransmitter in the CNS. GABA exerts its action by ligand gated chloride channels and G-protein-coupled receptors (GPCRs). Two caged GABA compounds were developed by the Conway group. The first of these utilised a DMNB caging moiety and the other a 3,5-dimethoxybenzoin (benzoin) cage. The structure of the two caged compounds, benzoin GABA and DMNB GABA are shown in figure 5.2b and 5.2c respectively.

As illustrated in figure 5.3 DMNB GABA was was observed to have a λ_{max} in absorption at 342 nm demonstrating an extinction coefficient (ε) of 6042. The benzoin GABA exhibited a λ_{max} at 247 nm with ε of 12500. Laser photolysis studies revealed irradiation of the compounds at the appropriate wavelengths generated free GABA.

5.3.2 Caged glycine for orthogonal wavelength selective photolysis

Glycine, with a chemical structure illustrated in figure 5.4a is an amino acid which acts as an inhibitory neurotransmitter in the CNS. Upon triggering activation of glycine receptors an inhibitory postsynaptic potential (IPSP) is generated by an influx of chloride ions. Glycine acts in tandem with glutamate as a co-agonist for N-methyl D-aspartate (NMDA) receptors responsible for synaptic plasticity in memory

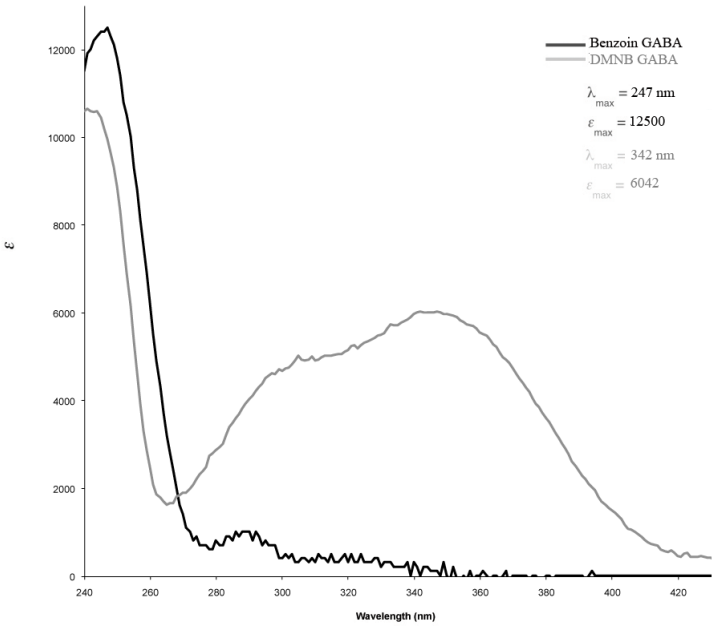

Figure 5.3: *Absorption characteristics of DMNB and benzoin caged GABA. The dimensionless extinction coefficient (ϵ) is plotted against wavelength to indicate where the compounds adsorb most strongly. Of the two compounds the DMNB GABA exhibits greatest absorption at the shortest wavelengths suggesting it would be highly suitable to an orthogonal pairing with a compound which photolyses at longer wavelengths.*

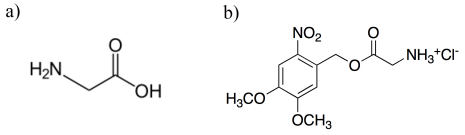

Figure 5.4: *The chemical structures of glycine (a) and DMNB caged glycine (b)*

function. Glycine was caged with a DMNB caging moiety as illustrated in figure 5.4b

As illustrated in figure 5.5 DMNB glycine was was observed to have a λ_{max} in absorption at 343 nm demonstrating an extinction coefficient (ε) of 4300. Laser photolysis studies revealed irradiation of the compound with the appropriate wavelength generated free glycine.

5.3.3 Caged glutamate for orthogonal wavelength selective photolysis

Glutamate, with a chemical structure shown in figure 5.6a is an amino acid and is the most abundant excitory neuron in the CNS. Biological function is exerted by

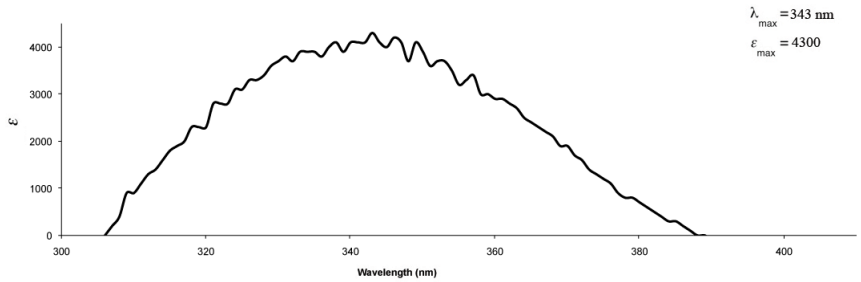

Figure 5.5: *Absorption characteristics of DMNB caged glycine. The dimensionless extinction coefficient (ϵ) is plotted against wavelength to indicate where the compound adsorbs most strongly.*

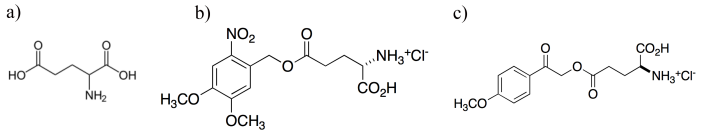

Figure 5.6: *The chemical structures of glutamate (a), DMNB caged glutamate (b) and MPA caged glutamate (c).*

activation of glutamate receptors comprising of ligand gated cation channels and G-protein-coupled receptors (GPCRs). Glutamate plays a major role in synaptic plasticity regulating cognitive processes such as learning and memory [124, 125]. Two caged glutamate compounds were developed, the first compound employed a DMNB moiety (5.6b) which exhibits a relatively long wavelength λ_{max} in absorption, whereas the second utilised a 4-methoxyphenacyl (MPA) moiety (5.6c) with a much shorter λ_{max}.

As illustrated in figure 5.7 DMNB glutamate was was observed to have a λ_{max} in absorption at 272 nm demonstrating an extinction coefficient (ε) of 12000. The MPA glutamate exhibited a λ_{max} of 283 nm with ε of 13648. Laser photolysis studies revealed irradiation of the compound with the appropriate wavelength generated free glycine.

5.3.4 Photolysis studies and application to *biological systems*

True wavelength orthogonal control requires that the discrimination between the compounds is achieved by wavelength choice only. Either a benzoin or MPA molecule

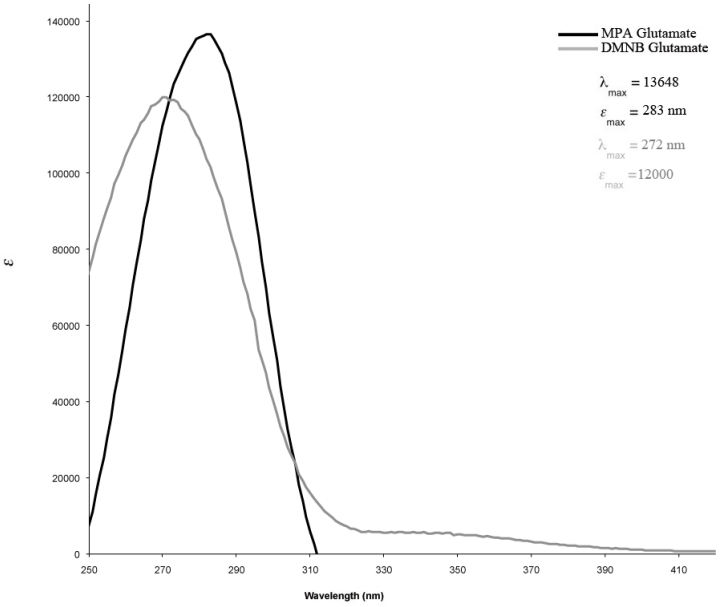

Figure 5.7: *Absorption characteristics of DMNB and MPA caged glutamate. The dimensionless extinction coefficient (ϵ) is plotted against wavelength to indicate where the compound absorbs most strongly. The absorption characteristics of the two compounds are very similar.*

must be selected for discrimination at short UV wavelengths around 250-270 nm and that the DMNB moiety is used for the selective activation of compounds with longer UV wavelengths around 400 nm. The possible pairings of cages is therefore with either a set of benzoin-DMNB or MPA-DMNB compounds.

Preliminary experiemnts involved the study of an orthogonaly caged pairing of DMNB glycine and benzoin GABBA. As shown in figure 5.8 absorption studies indicated that orthogonal photolysis of the compounds should be possible. Initial laser photolysis studies using 250 nm generated by an OPO and 405 nm generated by a CW laser diode (i-beam, Toptica) demonstrated successful orthogonal discrimination between the orthogonally caged pair of compounds as illustated by the partial NMR spectra (as discussed in chapter three) in figure 5.9. The partial NMR spectra in figure 5.9a show the result of illuminating an equimolar mixture of DMNB glycine and benzoin GABA at 250 nm resulted only in the generation of free GABA (50%) whilst the DMNB glycine remained intact. Figure 5.9b illustrates that under irradiation with 405 nm laser light only DMNB glycine is photolysed to produce free glycine (11%) whilst the benzoin GABA remained untouched. This preliminary study represents the first wavelength orthogonal photolysis of biologically relevant compounds.

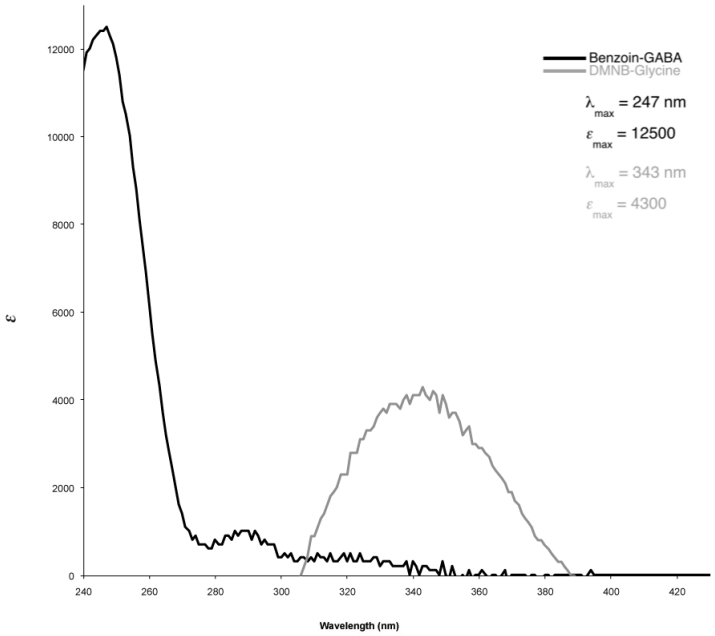

Figure 5.8: *The superimposed absorption profiles for benzoin GABA (black) and DMNB glycine (grey). The benzoin GABA compound exhibits maximum absorption at 247 nm where the DMNB glycine has none. The DMNB glycine has a maximum in absorption at 343 nm where the benzoin compound has very little. Wavelength orthogonal photolysis of the two compounds should be possible.*

Unfortunately, initial biological tests revealed unexpected benzoin-induced toxicity which has not been documented in the literature [126]. Therefore only a pairing of MPA and DMNB compounds was found to be suitable for application to *in vitro* studies.

As a result a pairing of MPA glutamate and DMNB GABA was adopted for biological application. The absorption characteristics illustrated in figure 5.10 suggested that wavelength orthoganality should be achieveable by illumination at 250-300 nm and 405 nm respectively. A preliminary photolysis study demonstrated that the MPA glutamate-DMNB GABA pair provided selective orthogonal photolysis with molecule discrimination discriminated by wavelength selection alone as illustrated in the partial NMR spectra in figure 5.11. Irradiation of a mixture of MPA-Glu and DMNB-GABA using a 405 nm diode generates photolysis of DMNB-GABA whilst MPA-Glu was unaffected. Irradiation of an identical mixture at 285 nm with a UV flashlamp & filterset only generates photolysis of MPA-Glu leaving the DMNB GABA intact. It can therefore be said that MPA-Glu is a suitable orthogonal partner for DMNB-GABA. Figure 5.12 illustrates the quantified selective photorelease

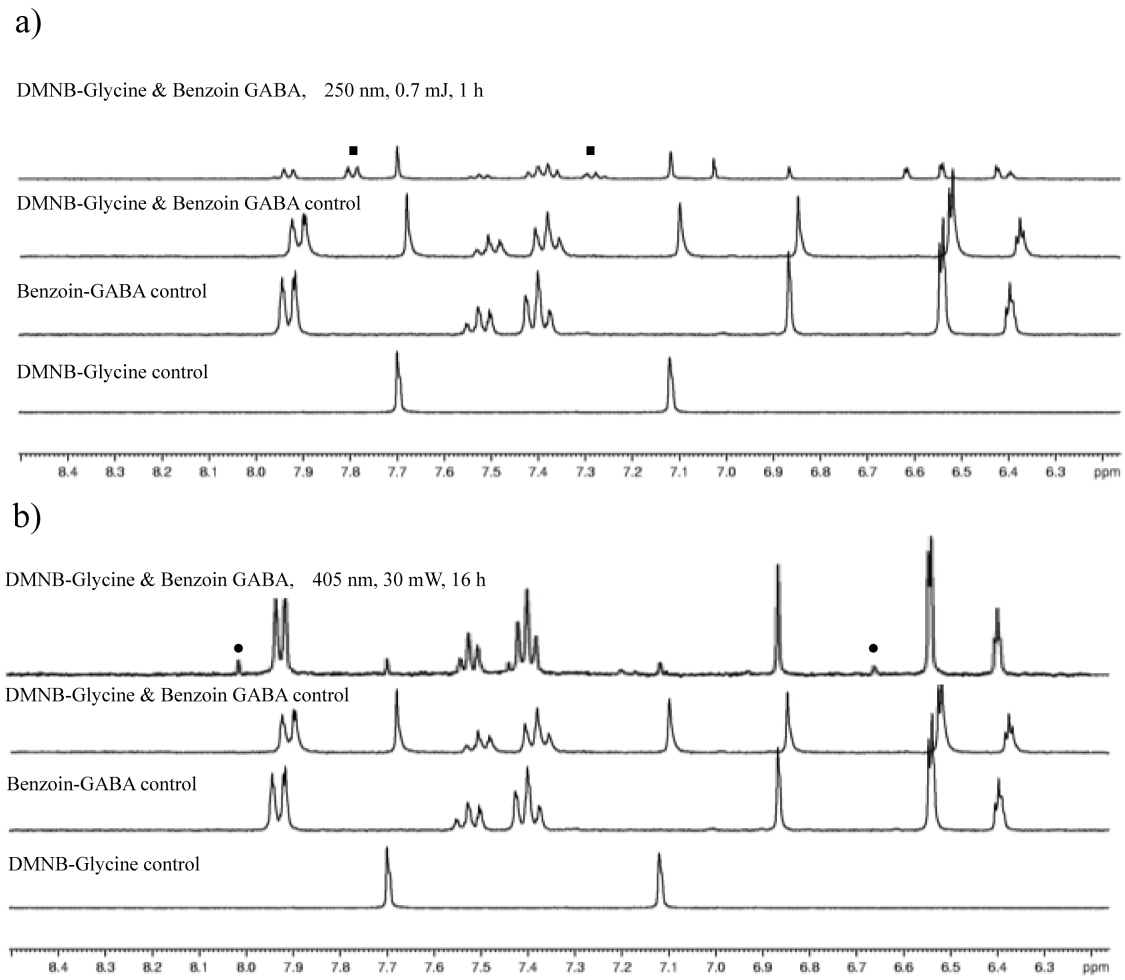

Figure 5.9: *Partial ^1H NMR spectra demonstrate selective photolysis of DMNB glycine and benzoin GABA. The generation of free GABA from an equimolar mixed solution is demonstrated by the peaks at 7.3 and 7.8 ppm in a (■). The generation of free glycine from an equimolar mixed solution is demonstrated by the peaks at 6.65 and 8.0 ppm in b (•).*

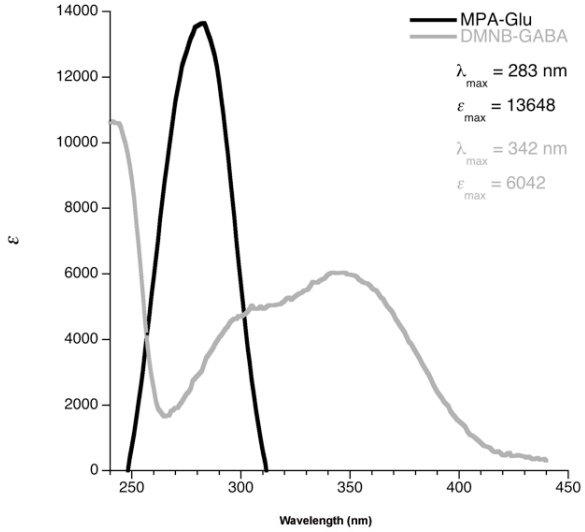

Figure 5.10: *Overlaid absorption characteristics of the MPA glutamate and DMNB GABA selected for orthogonal photolysis. The dimensionless extinction coefficient (ϵ) is plotted against wavelength to indicate where the compound absorbs most strongly. These characteristics indicate that the selective generation of free Glutamate from a mixture of the two compounds should be possible aroun 270 nm where DMNB GABA exhibits comparitively little absorption. Conversely, photolysis at longer wavelengths around 400 nm should permit selective generation of free GABA as the MPA glutamate demonstrates no absorption in this region. Figure modified from [1].*

of GABA from an equimolar solution of DMNB GABA and MPA glutamate was not observed under irradiation with 285 nm (a) but was successfully achieved through irradiation at 405 nm (b) as illustrated in figure 5.12. Initial application to biological samples showed that the caged compound itself evoked no unwanted biological activity demonstrated by no discernible increase in neural activity, firing of action potential or variation in holding potential. Neither of the compounds was observed to compromise cell viability.

5.4 Construction of the orthogonal photolysis microscope for *in vitro* studies

The *in vitro* orthogonal photolysis of the caged compounds was performed in the Department of Pharmacology, University of Oxford, using a commercially available inverted microscope (IX71, Olympus) incorporating a high numerical aperture (N.A) oil immersion objective (UPlanSApo 100x/1.4, Olympus) and a custom-built

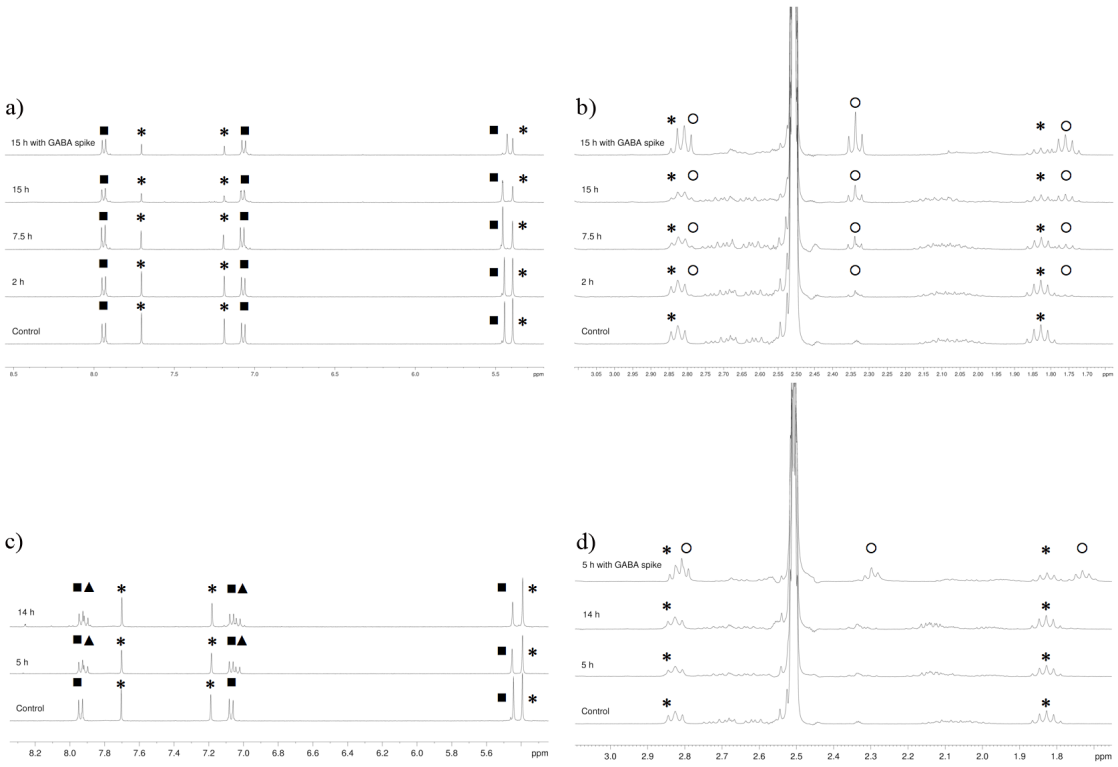

Figure 5.11: *Partial NMR spectra reveal the irradiation at 405 nm (a & b) provides selective photolysis of DMNB-GABA (*) to give free GABA (○) in the presence of MPA-Glu (■) which remains unchanged. Irradation at 285 nm (c & d) provides selective photolysis of MPA-Glu (■) in the presence of DMNB-GABA which remains unchanged. Generation of a photolysis by-product (▲) was observed observed (c). Spiking the sample with free GABA (d) confirms that no free GABA is formed following irradiation at this wavelength. Figure modified from [1].*

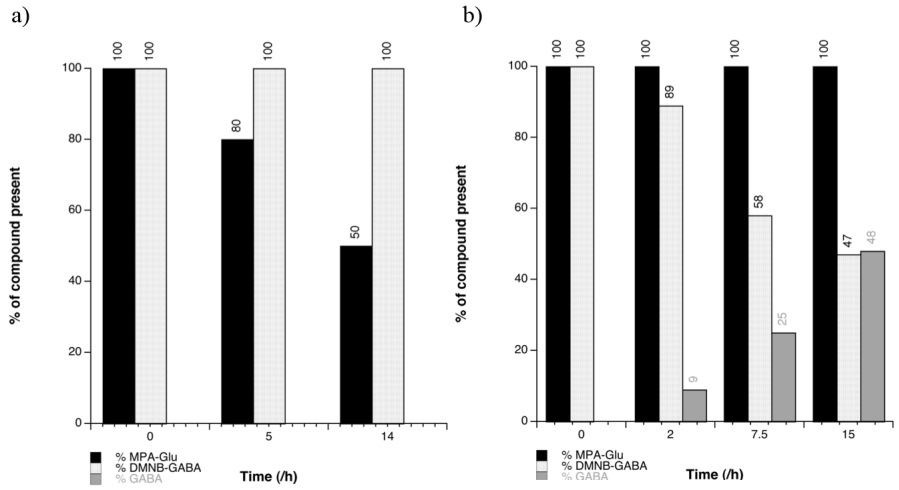

Figure 5.12: *Quantification as discussed in chapter three of the preliminary photolysis study provided a greater understanding of the selective release of GABA from an equimolar solution of DMNB GABA and MPA glutamate. Figure modified from [1] supplemental information.*

electrophysiology stage.

Biological samples were held in a perfusion chamber which provided the necessary physiological environment to maintain biological viability for the duration of the experiment while permitting access for the high N.A objective and electrophysiological equipment. As illustrated in figure 5.13 the microscope was adapted by myself to permit selective orthogonal photolysis of the caged compounds in solution by means of two independent light sources. Selective photolysis of the MPA-Glu was obtained with a mercury flash lamp (JML-C1, Rapp Optoelectronic) in combination with a 255 $\pm$8 nm interference bandpass filter (250FIB25, Knight Optical) mounted externally to the microscope assembly and focused to illuminate the entire sample region in the sample plane by an internal focusing lens. Orthogonal photolysis of the DMNB-GABA was accomplished with a 405 nm CW UV laser diode (PxLS, Toptica photonics) emitting 30 mW. The laser was co-aligned to the optical path of the microscope through the camera port of the microscope utilising a custom built optical cage plate system (Thorlabs). The optical system collimated the output of the diode laser and expanded the beam to match the back aperture of the high N.A objective. The external optics were designed to achieve efficient coupling of the laser into the microscope and comprised a x2 telescope for initial beam expan-

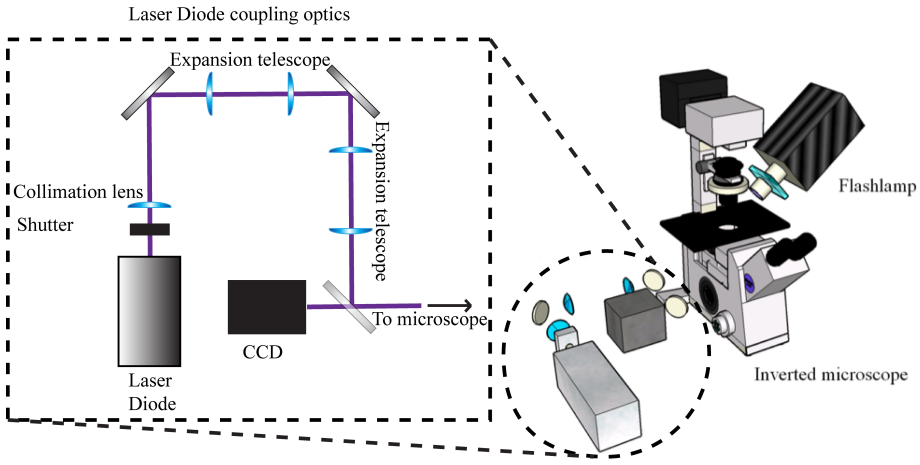

Figure 5.13: *The orthogonal wavelength photolysis was performed in a commercial inverted microscope (Olympus) modified with a 405 nm laser diode (Toptica) coupled to the sample plane and an external UV flashlamp (Rapp Optoelectronic) with a 255 ±8 nm interference bandpass filter (Knight Optical) mounted and focused upon the sample plane. In this way the sample plane could be selectively illuminated with either 405 or 255 nm.*

sion and collimation and a second x1.3 expansion telescope to ensure that the back aperture of the microscope objective was fully filled. A dichroic mirror (530 BK 16, Comar) permitted the introduction of the photolysis beam without interrupting image capture with an electron multiplying charge coupled device (EMCCD) camera (iXon DV887DCS-BV, Andor technology). A mechanical shutter (Uniblitz VS25, Rochester) provided temporal control of the 405 nm beam. The arrangement provided delivery of both wavelengths at the sample plane of the microscope with good control over exposure of the sample.

5.5 *In vitro* photorelease of wavelength orthogonal neurotransmitters

My collaborators in the Emptage group at the University of Oxford applied the orthogonally caged compounds to hippocampal pyramidal neurons whose response to photolysis was monitored by whole cell patch clamp recording as illustrated in figure 5.14 . Photolysis experiments were conducted in the commercial upright microscope which I had modified to provide 255 ± 8 nm and 405 nm illumination at the sample plane illustrated in figure 5.13.

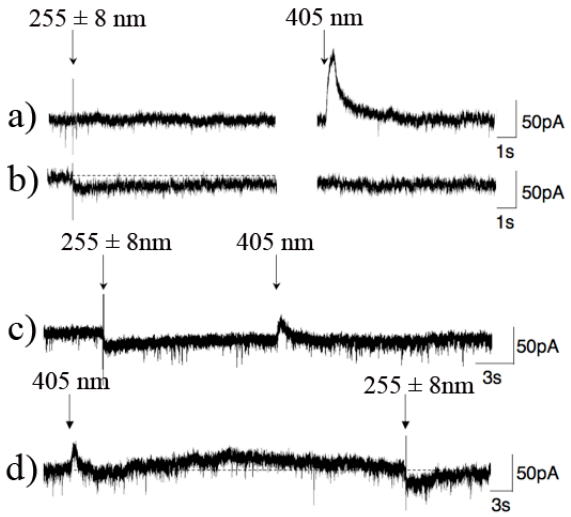

Figure 5.14: *In vitro application of the technique demonstrated full selective orthogonality between the two compounds descriminated by wavelength. Figures a-d show representative whole-cell patch-clamp recordings of cultured hippocampal pyramidal neurons bathed in a solution containing MPA-Glu (125 μM) and DMNB-GABA (50 μM). DMNB GABA only ilicits a response when illuminated by 405 nm (a) and MPA glutamate only ilicits a response when illuminated under 255 ± 8 nm (b). In a mixture of the compounds one compound can be preferentially activated in the presence of the other using wavelegth to discriminate the selection (c & d). Figure modified form [1].*

Initially the compounds were applied individually, it was shown that the *in vitro* application and illumination of application of DMNB GABA compound (50 μM) at 255 ± 8nm evoked no response whereas exposure to 405 nm generated the expected response (a). The observe large anion current generated upon irradiation at 405 nm is interpreted as photolysis of the DMNB compound, releasing free GABA and subsequent receptor activation. This behaviour was found typical in nine different cells a total of twenty two times.

It was then demonstrated that *in vitro* applicaiton and illumination of the the MPA glutamate (125 μM) at 255 ± 8nm generates a response, whereas none is observed at 405 nm (b). The observed large cation current response to illumination at 255 ± 8nm is interpreted as photolysis of the MPA glutamate compound, free glutamate generation and subsequent receptor activation. This behaviour was observed in nine different cells a total of twenty seven times. This selective wavelength photolysis of both compounds individually established the potential for wavelength selective orthogonal photolysis *in vitro*.

In vitro application and illumination of a mixture of the compounds at 255 ± 8nm evoked a large cation current consistent with activation of glutamate receptors. Subsequent 405 illumination generated a large anion current consistent with GABA receptor activation (c). This response was observed for n = 3 cells. The order of selective activation was then reversed, to ensure true orthogonality and not just selectivity was being achieved. Initial illumination with 405 nm caused GABA receptor activation and subsequent 255 ± 8nm elicited glutamate receptor activation (d). It was therefore shown for the first time *in vitro,* that controllable orthogonal wavelength-selective photolysis was successfully achieved [1].

5.6 Discussion & Conclusions

Caged compounds have been of great assistance in the quest for greater understanding of the biochemical processes but the inability to selectively activate one caged compound in the presence of another was previously a significant failing. Here, *in vitro* single-photon wavelength orthogonal photolysis has been demonstrated for the first time and represents a significant step forward in caging methodologies. The technique can potentially be applied to a large number of interesting biological systems [17, 18]. Orthogonal selective activation of the developed caged neurotransmitters will permit indepth studies into the processes behind memory and learning such as synaptic plasticity, synaptic integration and receptor mapping to be undertaken [1].

A single-photon system was developed as it provides a highly accessible method for the biological community. No expensive laser sources, microscopes or indepth optics knowledge is required. The methodology is of particular importance to neuroscience where the eludication of complex neuronal systems remains a significant challenge and control over the agonist and antagonist of a receptor under study is highly desireable.

Unlike the recent methodology developed by Kantevari *et al.* [123] the technique developed here maintains the concentrations, optical powers and regions of interest constant. True orthogonality was still observed even when the irradiation sequence

was reversed.

Chapter 6

Advanced techniques for femtosecond optical injection

In this chapter two techniqes for advanced femtosecond optical injection are presented. The first investigates the use of a relatively low cost IR femtosecond laser compared to the Ti:Al_2O_3 lasers traditionally employed for femtosecond optical injection applied to the optical injection of caged molecular probes. The ability to optically inject the caged precursor of a biological affector molecule for subsequent photolysis *in vitro* presents an attractive methodology for the all optical manipulation of a biological sample. The second demonstrates a methodology for the highly targeted placement of single gold nanoparticles at targeted regions within the interior of living mamallian cell.

6.1 Towards the optical delivery of caged molecular probes

The combination of optical injection and caging technologies has the potential to provide an unmatched level of control over a biological system. Such a technique is of interest as there is a trade-off in the synthesis of caged molecular probes of membrane permeability against the solubility of the compounds. As a result microinjection must often be employed to load cells with the caged molecular probes.

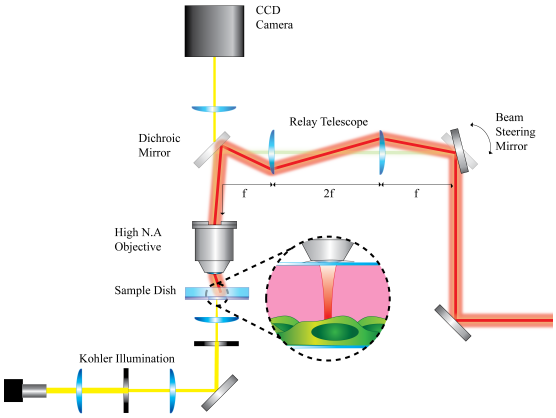

Figure 6.1: *An upright optical tweezers system utilising a femtosecond 1040 nm laser source was utilised for investigating optical injection of caged compounds.*

A methodology permitting the loading of cells and subsequent intracellular photolysis in one experimental setup is highly attractive.

Intuitively optical injection and photolysis of caged compounds appear to be incompatible. However, with intelligent laser selection optical injection can be undertaken without photolysing any caged compound present.

Wavelengths in the UV (CW or pulsed) and NIR around 800 nm (fs) must be avoided to prevent the single or multiphoton photolysis of any caged material [53]. Unfortunately these conditions represent those most commonly applied for successful optical injection [66, 67]. Alternatively, injection has also been successfully demonstrated at 532 nm (ns) [79], 1540 nm (fs) [127] and 2300 nm (fs) [128]. The nanosecond optical injection regime offers lower spatial selectivity and viability compared with femtosecond regimes [67].

Here a 1040 nm femtosecond laser source was employed to facilitate the targeted optical injection of caged compounds. In this chapter the results of a preliminary investigation into the optical injection of caged fluorescein are detailed.

6.2 Experimental arrangement

The experimental arrangement employed for optical injection is illustrated in figure 6.1 .

An upright optical tweezers arrangement based on the 1040 nm femtosecond laser

source (Elforlight , UK) was constructed. The laser is a 980 nm diode pumped vibronic laser system based on a Yb:KYW crystal and produces 1040 nm, 200 fs pulses at a 110 MHz repetition rate. Modelocking is achieved by use of a semiconductor saturable absorber mirror (SESAM). Pulsed operation was constantly monitored and verified using an autocorrelator (Timewarp, Elliot Scientific, UK).

The beam was attenuated by a $\frac{\lambda}{2}$ waveplate and beamsplitter cube arrangement. The beam was then expanded to overfill the back aperture of the Nikon 0.8 N.A, 100x, infinity-corrected air objective lens providing an approximately diffraction limited, sub-micron spot at focus. The objective transmission was measured to be 38 % at 1040 nm by the dual objective method [129]. For manipulation , the sample chamber was held on a precision xyz stage (Newport, USA). Temporal control of the laser beam was obtained using a high speed shutter (Newport , USA). The sample was illuminated by Köhler illumination to provide uniform illumination across the field of view. The sample plane was imaged by a CCD camera (Watec, Japan) connected to a computer by a dedicated video capture card.

For cell culture all reagents were purchased form Sigma (UK) unless specifically stated. Chinese Hamster Ovary K1 (CHO) cells were cultured in T25 tissue culture flasks in Modified Earles Medium (MEM) with 10% foetal calf serum (FCS) (Globepharm, UK), 20 enzyme units/ml of penicillin and 20 mg/ml of streptomycin (resulting medium referred to as "complete MEM") and kept in a humidified atmosphere of 5% CO_2/95% air at 37 ^{o}C. The cells were routinely passaged three times weekly. For experimentation, cells were prepared at a seeding density of 2.1 x10^4cells/ml in 30 mm diameter glass-bottomed culture dishes with a usable working area of 23 mm (World Precision Instruments, UK) in 2 ml of complete MEM. Once seeded in the dishes, cells were incubated for 24 hours to promote robust attachment to the bottom of the dish.

For the optical injection procedure, CHO cells were exposed to approximately 40 mW of laser power at sample (100 mW at back aperture) for ten seconds at focus whilst bathing in a solution containing fluorescein bis-(5-carboxymethoxy-2-nitrobenzyl) ether, dipotassium salt (CMNB caged fluorescein, Invitrogen, UK). Prior to exposure to the focused laser field, the 2 ml of complete MEM was re-

moved by aspiration and the cell mono-layer rinsed with Optimem (Invitrogen, UK) to remove any residual FCS which was shown to cause coagulation of the CMNB fluorescein. Cells were then bathed in a 20 µl solution composed of 1 mM CMNB fluorescein and 42.2 µm phenol red in OptiMEM (resulting medium subsequently referred to as "injection medium"). The experimental chamber was sealed by floating a sterile 22 mm type zero coverslip above the cell monolayer and encompassing bathing solution.

To permit identification of the targeted cells a central 1mm diameter region of interest was then circled using a custom fabricated diamond etching device. Following the optical injection event, the coverslip was removed by floating with OptiMEM and the cell monolayer was subsequently rinsed with OptiMEM. 2 ml complete MEM was then added and the cells returned to the incubator for for further incubation. Control cells were prepared in exactly the same manner, without laser irradiation. Cells were re-acclimatised in a CO_2 atmosphere for 10 minutes prior to the photolysis procedure.

For photolysis, the culture dish was hermetically sealed using parafilm immediately upon withdrawal from the CO_2 atmosphere. Prior to photolysis cells were imaged with a fluorescent microscope (Nikon, Japan) to asses post injection morphology and to ensure that no fluorescein was photolysed during the injection operation. The filter cube employed was previously shown to cause no photolysis of caged fluorescein whist providing excitation of free fluorescein. Cells were then transported to the confocal laser scanning microscope (CLSM, Leica TCS-SP2 AOBS). Photolysis was then evoked by exposure to a scan of 488 nm laser light. Subsequently an image stack was taken through the region of interest (ROI) to asses internalisation of the CMNB fluorescein post injection.

6.3 Results

Initial experiments with CMNB fluorescein in isolation demonstrated that photolysis and excitation of the free fluorescein generated was evoked by a mercury lamp in combination with a V-2A filter cube. A FITC filter cube was shown to cause no

photolysis but excitation of free fluorescein was possible. Therefore a combination of V-2A and FITC cubes could be used for photolysis and subsequent visualisation of free fluorescein generated without causing further photolysis. It was observed that the CMNB fluorescein itself binds to the surface of the CHO cells under study. Therefore internalisation had to be verified by CLSM as opposed to conventional fluorescent microscopy to demonstrate the photolysed fluorescent signal was originating from within the targeted cell and not the surface of the cell.

Before injection it was verified that the CMNB fluorescein was membrane impermeable in the system under study by bathing CHO cells in a solution of the caged dye for approximately 15 minutes. Subsequent CLSM imaging demonstrated no internalised dye. It was then confirmed that the optical injection source did not cause photolysis of the CMNB fluorescein by exposing a solution of the dye to 100 mW at the focus of the laser for several minutes. Fluorescent imaging confirmed no photolysis took place. Using a solution of OptiMEM, phenol red and Lucifer yellow the efficiency of optical injection was found to be approximately 50%.

The CLSM images in figure 6.2 show the result of an experiment in which 10 cells were targeted for optical injection. The images were acquired following a photolysis scan of high intensity UV light.

In figure 6.2a, the inset image illustrates the entire field of view in which the region of interest (ROI) targeted for optical injection is indicated by the dashed line. Figure 6.2b illustrates the confocal cross section of the cell indicated in the ROI in figure 6.2a. where the green face on each cube indicates the viewpoint.

Fluorescent signals are observed from cells outwith the targeted region from fluorescein bound to the cell membrane. Within the region targeted for injection, 5 of the targeted 10 cells appear far brighter than the others. This suggested that they contained free fluorescein throughout the cell in addition to that bound to the cell membrane. This injection efficiency is in agreement with injection experiemnts prevented in chapter seve, where an optical injection efficiency of 50 % was observed.

To confirm whether a more intense fluorescence signal corresponds to internalised fluorescein, a CLSM scan was taken to produce the cross section views in figure 6.2b. The CLSM images show that within the cell targeted for injection which exhibited

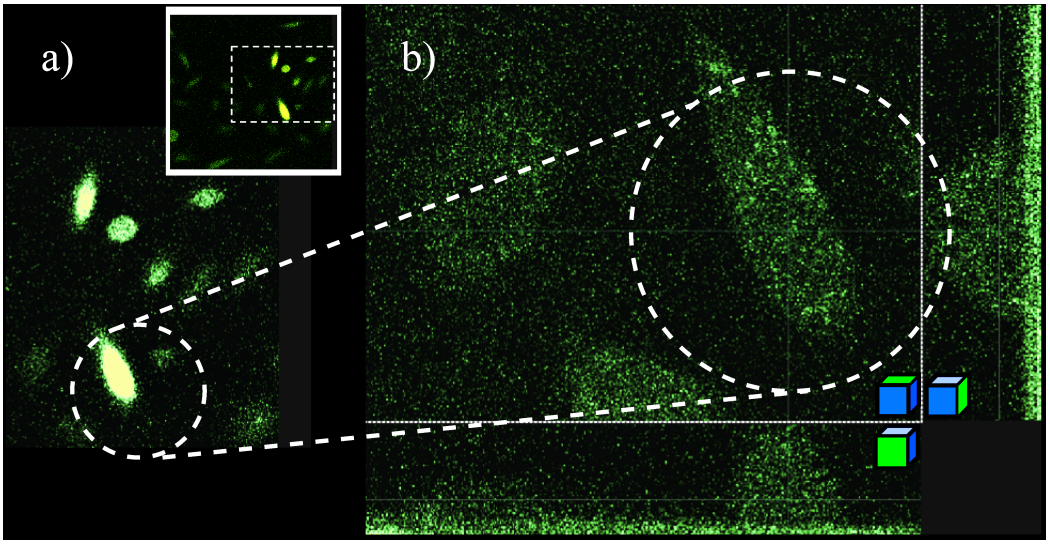

Figure 6.2: *Fluorescent images of cells optically injected with caged fluorescein and subsequently photolysed with UV light. A region of interest containing 10 cells (a) was targeted for optical injection within the field of view (inset a). The confocal cross section (b) demonstrates that free fluorescein is present uniformly throughout the targeted cell. This is interpreted as the caged compound being successfully injected to the cell interior and subsequently photolysed to generate free fluorescein. Other cells did exhibit fluoresence but from fluorescein bound to the cell membrane.*

an intense fluorescent signal the is signal is observed uniformly throughout the cell. Such a signal was not observed in cells which did not exhibit the intense fluorescence signal. It is noteworthy that photobleaching of the fluorescein caused a marked reduction in intensity between the initial scan (figure 6.2a) and the 3x averaged CLSM scan (figure 6.2b).

Initially it was unclear whether the viability of the cells was compromised by the optical injection, photolysis or the subsequent imaging. Subsequent experiments including only the injection and photolysis stages of the protocol remained viable under the conditions employed. This suggests that the repeated confocal imaging of the cells had compromised the viability of the cells.

6.4 Conclusions

The initial findings presented in this chapter indicate that the optical injection of caged compounds is a viable option for the targeted delivery of caged molecular probes. However, replication of the observed result remains to be undertaken before

firm conclusions can be made. Many challenges remain in the development of this methodology.

The binding of CMNB fluorescein to the cell membrane presented a significant problem and demanded CLSM scans to verify internalisation. The next step in development of this technique is the optical injection of a biologically relevant compound such as caged inositol 1,4,5-trisphosphate (IP_3). Photolysis of injected caged IP_3 should cause an influx of intracellular Ca^{2+}allowing internalisation of the compound may be provided with calcium imaging. Assuming the caged IP_3 did not bind to the cell membrane, CLSM could be avoided.

The ability to optically inject caged compounds into targeted regions of the cell interior presents a significant development in optical techniques for application to biological systems. In conjunction with optical tweezers techniques described in chapter seven, such a methodology presents a highly attractive photonic toolkit for the study of intracellular processes.

6.5 Targeted optical injection of gold nanoparticles

6.5.1 Introduction

In this section, a method for the targeted delivery of a single nanometer sized biosensor to the cell interior is presented. Such an injection event marks a significant step forward in the controlled analysis of cellular function and provides an elegant technique for the delivery of nanoparticles to chosen regions of the cell interior.

Single gold nanoparticles were selected due to their biological amiability, functionisability with chemical reagents and profound enhancement of spectroscopic signals, such as surface enhanced Raman spectroscopy (SERS). The method employs a dual-beam trap, with a CW tweezers beam coaligned to a femtosecond optical injection beam. Much like holding a nail between two fingers and using a hammer to drive it into a piece of wood, the CW tweezer is used to tweeze the nanoparticle above the region of interest on the target cell. Exposure to the coaligned fs injection

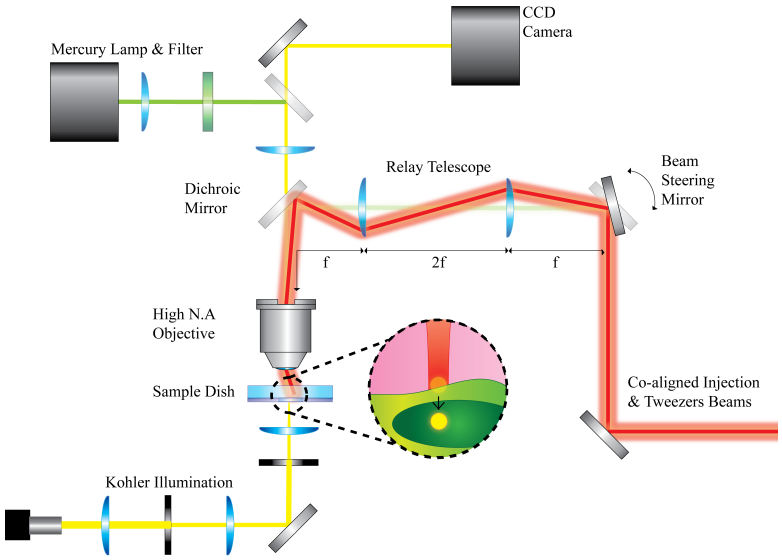

Figure 6.3: *An upright optical tweezers arrangement with additional epi-fluorescenct module was employed for the targeted optical injection of 100 nm gold nanoparticles into single mamallian cells. A 1064 nm laser source for CW optical tweezing of the nanoparticles was coaligned to a femtosecond optical injection beam for internalising the particles.*

beam results in the nanoparticle being propelled into the cell and internalised within the nucleus. Internalisation is confirmed by confocal microscopy.

6.5.2 Experimental

6.5.2.1 The optical tweezing and optical injection apparatus

An upright epi-fluorescent optical microscope was constructed as illustrted in figure 6.3. The home built femtosecond Ti:Al_2O_3 laser detailed in chapter three was used for optical injection and a continuous wave (cw) 1064 nm source (PIC, UK) for optical tweezing. Two laser sources were used in combination for the trapping and subsequent injection processes as the nanoparticle trapping was highly sensitive to laser modality being switched in modality from CW to femtosecond using the Ti:Al_2O_3 laser alone. As a result the simplified system developed in chapter seven could not be used. A mercury lamp and filter (543 nm) were used in combination for nanoparticle visualisation. Attenuation of the femtosecond injection beam was controlled by a pair of Glan Thomson prisms. Successful optical injection was observed for average powers between 25 mW and 70 mW at the focal plane which is consistent with the literature for successful viable optical injection exper-

iments [130]. A mechanical shutter was used to provide the short exposure time required for nanoparticle optoinjection. For optical tweezing of the nanoparticles the 1064 nm laser was used at an optical power of 25 mW at the sample plane.

This wavelength was selected as it too long to generate a plasmon resonance at the nanoparticle. Such plasmon resonances have been used to transfect cells [131] and could therfore poentially compromise cell viability through plasmon heating effects. This optical power was found to be biologically amiable for trapping and holding gold nanoparticles close to cells in viability studies. The power of the tweezing beam was attenuated by a half wave plate and polarising beamsplitter. The beam then passed through a quarter wave plate to generate circularly polarised light to provide a uniform field for trapping. The optical injection and tweezing beams were expanded and co-aligned to slightly overfill the back aperture of a 100 X Nikon oil immersion 1.4NA objective, providing a diffraction limited spot for each of the wavelengths. The objective was found to have 63 % transmission at 780 nm and 22 % transmission at 1064 nm by dual objective measurements [129]. Chromatic aberration was corrected for using a corrective telescope in the femtosecond optical injection beam path allowing both focal spots to be co-aligned in x, y and z.

6.5.2.2 Co-alignment of the optical traps

To ensure co-alignment in all three dimensions, a 1μm silica sphere was optically tweezed whilst manually switching between the two beams. Alignment was considered optimal when the trapped sphere did not move during toggling. Further confirmation of alignment was achieved by adhering a single nanoparticle to the bottom surface of a coverslip using the tweezing beam, and then immediately subsequently exposing it to the optical injection beam. Alignment was confirmed when the optical injection beam generated a bright reflectance signal.

Of critical importance was the optimisation of the refractive index matching immersion oil ("Series: A", n =1.5900 ± 0.0002, Cargille, USA) that enabled the full three-dimensional manipulation of 100 nm gold particles through the minimisation of spherical aberration [132].

A CCD camera was sited above the sample allowing direct observation and se-

lection of individual cells for targeted nanoparticle internalisation. Positioning of the laser beam focus was achieved by manipulating a precision xyz translation stage (Newport, USA) on which the sample dish was placed. Epi-illumination of the sample was achieved by directing a mercury lamp source through the objective for back scattered illumination of the nanoparticles. White light Köhler illumination from below enabled visualisation of the cell and nanoparticle simultaneously.

6.5.2.3 Cell culture

For cell culture all reagents were purchased form Sigma (UK) unless specifically stated. Chinese Hamster Ovary K1 (CHO) cells were prepared at a low seeding density (5 μl) in 30 mm diameter glass-bottomed culture dishes with a usable working area of 23 mm (World Precision Instruments, UK) in 2 ml of Modified Earles Medium (MEM) with 10% foetal calf serum (FCS) (Globepharm, UK), 20 enzyme units/ml of penicillin and 20 mg/ml of streptomycin (resulting medium referred to as "complete MEM") and routinely kept in a humidified atmosphere of 5% CO_2/95% air at 37 ^{o}C. A single cell of interest was selected for optical injection and circled using a diamond tip to score a region of interest on the bottom of the culture dish, such that the cell could later be located and identified for optical injection and confocal microscopy.

6.5.2.4 Nanoparticle imaging by confocal laser microscopy

Single cells were imaged both prior to and following nanoparticle injection. For the initial imaging, cells were first incubated in 2 ml complete MEM containing 10 mM HEPES for 10 minutes at 37 ^{o}C in 5% CO_2. Subsequently 500 ml of 5 mg/ml of the red fluorescent dye, FM 4–64FX (Molecular Probes, UK) was added to the dish and cells were incubated for a further 10 minutes in the same conditions. The culture dish was hermetically sealed using parafilm immediately upon withdrawal from the CO_2 atmosphere and transported to the confocal laser scanning microscope. An equivalent stack of planar images were taken in confocal laser scanning (CLSM) and confocal reflectance (CLSRM) modes.

The CLSM and CLSRM image stacks were then digitally merged using the cover

slip to verify alignment for analysis. The combined stack provided a reference control image upon which post-injection scans of the same cell could be compared. A Leica TCS-SP2 AOBS confocal system coupled to a Leica DMIRE2 inverted microscope using a Plan Apo 63x oil immersion objective (N.A = 1.4) was used for CLSM and CLSRM imaging of the cells. A double dichroic mirror (DD488/ 543) was used for CLSM imaging and an RT 30/70 (30% reflection, 70% transmission) dichroic mirror was used for CLSRM. Under CLSM, the FM 4– 64FX stained plasma membrane, cytosol and cytoplasm was excited by a 488 nm laser, with collection between 500 – 780 nm. Each image was scanned three times in photon counting mode. Under CLSRM, 100 nm gold nanoparticles were excited at 543 nm with collection between 533–553nm. Planar images were taken at 0.2 µm intervals through the cell of interest. The merging of the CLSM and CLSRM image stacks, quantification of membrane and nanoparticle intensities and 3D re-construction of the planar stacks were performed with the proprietary Leica Confocal Software supplied with the microscope system. To ensure that the CLSM and CLSRM image stacks were axially co-aligned, each scan included planar images of the coverslip-solution interface. The reflected signal from this interface, a few hundred nanometers in axial thickness, allowed the co-alignment of the two image stacks with submicron confidence.

The variance of the axial position of a repeatedly scanned nanoparticle was ± 115 nm. After initial imaging, cells were transported back to the incubator for approximately 30 minutes prior to the optical injection experiment taking place. This imaging procedure was then repeated after the optical injection experiment took place.

6.5.2.5 Optical manipulation of single gold nanoparticles

For the optical tweezing and subsequent optical injection of nanoparticles the complete MEM containing HEPES and stain was removed from the cell culture and set aside for later use during post-injection imaging. A manipulation chamber was constructed from the culture dish by adding a 20 µl volume of OptiMEM (Invitrogen, UK) containing 2.8 x 10^7/ml 100nm gold nanoparticles (BB International, UK) sealed by floating a sterile type-zero 22 mm diameter glass coverslip (VWR,

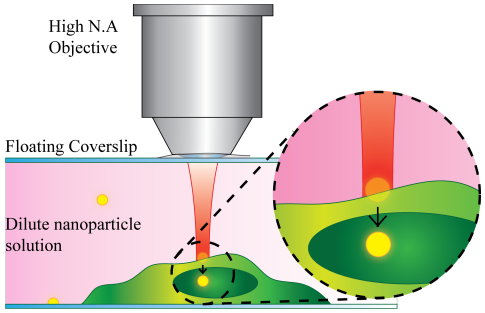

Figure 6.4: *A single 100 nm gold nanoparticle is tweezed and held above the targeted region of the mamallian cell. Subsequent introduction of the femtosecond beam initiates injection of the nanoparticle to the cell interior.*

UK) on top to protect the biological sample from the toxic immersion oil. The resulting solution of nanoparticles was very dilute solution meaning the probability of interaction between cells and nanoparticles without any active manipulation was extremely low.

For the injection a single gold nanoparticle was optically trapped in three dimensions using the tightly focused 1064 nm CW light field and moved to the top surface of the cell as illustrated in figure 6.4. While the 1064 nm tweezers were holding the nanoparticle against the top of the cell membrane the particle was exposed to a 40 ms pulse train of the co-aligned 780 nm fs laser light. After injection, the coverslip was carefully re-floated using the complete MEM containing 10 mM HEPES pH 7.4 previously set aside, the cell was re-acclimatised in a CO_2 atmosphere for 10 minutes, re-sealed hermetically, and imaged again as described previously.

6.5.3 Results

The three-dimensional spatial manipulation of nano/microparticles using optical tweezers in this way is well established [48]. A representative example of the subsequent novel injection of a single gold nanoparticle in conjunction with optical tweezing is illustrated in figure 6.5 which shows images captured with the CCD camera during the injection process. The nanoparticle annotated with the black arrow on the left hand side of figure 6.5 was optically injected into the live mammalian cell using a single 40 ms shuttered dose of 780 nm femtosecond laser light at an optical power of 25 mW at the sample plane. During the exposure to the femtosecond pulse

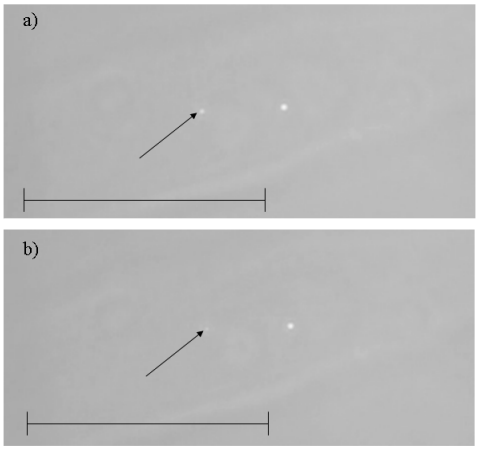

Figure 6.5: *Representative frames illustrating a typical injection event. A reference nanoparticle was positioned on the right hand side of the cell (a). A nanoparticle intended for injection was then tweezed and held over the targeted region of the cell as indicated by the arrow (a). Exposure to the femtosecond injection beam caused a drop in intensity from the nanoparticle signal and noticeable shift in position interpreted as injection to the cell interior (b). Figure modified from [3].*

train, a flash of reflected light was often observed to come from the nanoparticle.

The pulsed source causes a transient optical force upon the nanoparticle and this is believed to assist the nanoparticle to enter through the cell membrane. No photopore was observable during irradiation under the illumination conditions employed, but the backscattered light from the nanoparticle clearly dropped in intensity, and a shift in position was noticeable as illustrated in figure 6.5. The change in intensity whilst remaining focused on the same image plane was interpreted as a downwards movement of the nanoparticle in Z. Such an interpretation is unsatisfactory without further probing the position of the nanoparticle relative to the cell.

Figure 6.6 is a representative XZ cross section through a cell at the location of the optically injected nanoparticle formed with the confocal scans (CLSM & CLSRM), reconstructed using the Leica proprietary software. As shown both qualitatively by the cross section and quantitatively by the intensity signals, the nanoparticle is clearly located in the nucleus of the cell. Including this cell the optical injection of seven nanoparticles in the nuclei of five targeted cells was clearly demonstrated. In one case, two nanoparticles were injected into two separate locations in the nucleus.

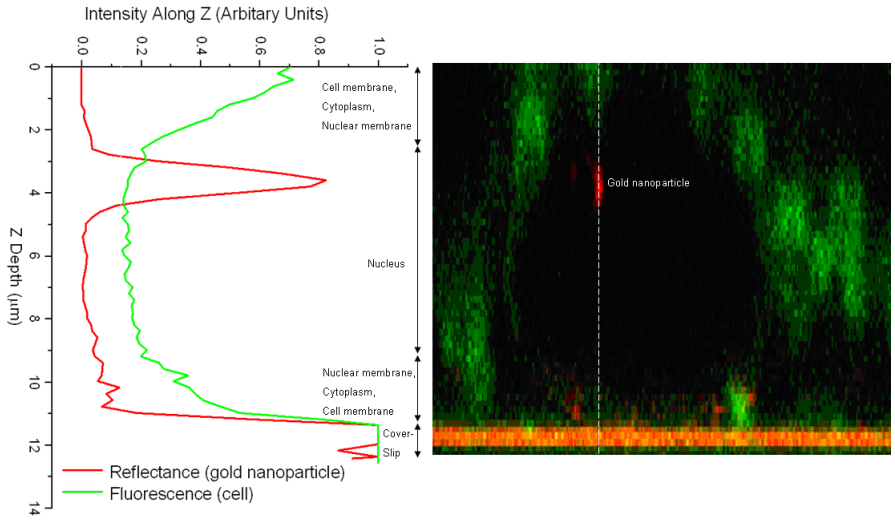

Figure 6.6: *A cross section of a representative cell at the location of the injected nanoparticle. The confocal image clearly indicates that the nanoparticle has been injected to the interior of the cell nucleus. Figure modified from [3].*

In another cell, two nanoparticles were simultaneously injected as an extra nanoparticle hopped into the trap by chance. Both particles were injected into the nucleus, ending up in the same spatial location. In the remaining three cases including the one shown in figure 6.6, a single nanoparticle was injected into the nuclei of the respective cell.

It is noteworthy that hundreds of examples of confocal scans which demonstrated nanoparticles embedded either on, in, or immediately below the plasma membrane were observed. However, with the limited axial (Z) resolution of a confocal laser scanning system it is difficult to determine whether a nanoparticle that is so close to the cell surface is on or in a cell. Consequently, attention focussed only on nuclear optical injection as when a nanoparticle resides in the nucleus, it is many microns from the plasma membrane and hence confidently resolvable with the 500 nm axial resolution inherent to a confocal system [133]. The nuclear optical injection efficiency was observed to be ~10% (n = 18). Note that as only nuclear injection of nanoparticles was considered a success, the optical injection of nanoparticles into a region of the cytoplasm was more efficient but less reliably quantified. It was also observed that if the nanoparticle was not correctly held directly against the cell membrane with the tweezing beam for the optoinjection event, the introduction of

the femtosecond pulse train caused the nanoparticle to become disassociated from the cell and no nanoparticle was seen in subsequent confocal scans. The overall injection efficiency could be potentially improved with further engineering refinements, providing a more stable mechanical and thermal environment for the process. However, there may be inherent limitations associated with manipulating a 100 nm object with a 380 nm (diffraction limited) tweezing spot co-aligned with a 286 nm (diffraction limited) optical injection spot.

6.5.4 Discussion

There are a number of experiments in the literature that investigate the use of lasers to internalise nano or micro particles into cells. Broadly speaking these experiments can be classified into three categories:

1. In the presence of high concentrations of particles, cells are raster scanned with a laser [134, 135]

2. In the presence of high concentrations of particles, cells are selectively targeted and dosed with a laser [78, 136]

3. In the presence of a low concentration of particles, a single particle is optically tweezed and delivered into the cell through a hole previously drilled by a laser [137, 138].

The method presented here adds a fourth category; the controlled placement and targeted delivery of single particles into a cell by simultaneously optically tweezing and optically injecting. The first two experimental categories use large numbers of spheres to settle passively onto or under cell monolayers before laser dosage. Nanosecond-pulsed lasers with an unfocused beam (a few millimeters in diameter) have been employed in this way to irradiate large populations of cells residing in a solution containing either 1 mm microspheres [134] or gold nanoparticles [135] in order to increase membrane permeability and allow exogenous molecules to enter. Femtosecond-pulsed, regeneratively amplified lasers with a focused beam have also demonstrated the internalisation of 200 nm polystyrene spheres [136]. Additionally,

optoinjection using a laser with a relatively large focal spot size of 14 μm has allowed delivery of nanocrystals [78] to single cells. It is key to note that although single cells have been targeted in these experiments, none addressed the potential to tweeze a sphere to a specific region onto a cell prior to injection.

With regards to the third category, there are no reports in the literature where a nanometer scale sized object was optically tweezed and actively inserted through the plasma membrane of a mammalian cell. However, there are interesting examples whereby plant cell walls [137] and the zona pellucida of oocytes [138, 139] have been laser drilled in order to assist the injection of larger extracellular particles by optically tweezing. In the case of plants, large objects such as 3 mm microspheres or even a single A. rhizogenes (bacterium), were optically tweezed and placed inside G. biloba callus (plant) cells, through a 2 – 4 mm hole which had previously been drilled using a frequency tripled 1064 nm Nd : YAG laser [137]. In the case of oocytes, it is possible to drill a hole (10 μm in diameter) in the zona pellucida in order to tweeze optically and insert a single sperm cell [138]. It is key to note that a plasma membrane was not penetrated by the laser field as in the presented technique, but rather a plant cell wall or a zona pellucida layer. A final experiment worth noting is that of Parkin *et al*, who used a femtosecond laser and optical tweezers in tandem. By prior exposure to a large dosage of fs laser light a bleb was generated upon a macrophage into which a trapped vaterite particle was inserted [140].

All of these methods described rely upon the natural ability of a cell to heal to heal itself after nanoparticle has been injected. Membrane disruption and resealing is common in vivo, and cells have naturally adapted to healing minor wounds induced by day to day mechanical stress [141]. The mechanism for resealing is in part thermodynamically mediated, as it is not energetically favourable to have a hydrophobic membrane pore rim exposed to the surrounding aqueous environment, but it is also an active event in live cells, whereby endomembranes structures “plug” the hole in a calcium dependent fashion [142–144].

Compared with other technologies for the delivery of gold nanoparticles to mamallian cells the efficiency of the presented optical injection technique is relatively low [145]. However, the significance in comparison with such methods is that this

novel all-optical technique provides the first precise placement of a single particle in a desired intracellular location and more specifically the nucleus of a targeted cell. Furthermore, the optical injection presented negates the requirement for complex chemical treatment of the nanoparticles to promote internalisation phagocytosis and enables precise delivery in cell types which do not exhibit a phagocytosis mechanism for the internalisation of extracellular materials. Moreover, nanoparticle internalisation by phagocytosis is highly non-targeted and will result in the internalised particle being engulfed in a lysosme obscuring any spectroscopic data.

6.5.5 Summary

All experiments described in this section were performed upon live mammalian cells. Cells were rigorously scanned many times post injection events to verify nanoparticle internalisation and no cells were observed to remain biologically viable after internalisation verification was completed. Sets of control cells were put through the same scanning process and found to survive. This includes those which had up-taken nanoparticles through phagocytosis. This indicates that nanoparticle-mediated heat effects as a result of scanning near the wavelength required for plasmon resonance were not responsible for cell death. Furthermore, optical tweezing and holding of nanoparticles next to cells at the parameters used for optical injection did not compromise viability. It was also shown that exposure to the optical injection beam in the absence of nanoparticles also did not lead to cell death. Viability of the cells was exclusively compromised when injection of a nanoparticle was targeted to the nucleus of the cell.

Previous experience whilst performing optical injection experiments have shown that optical injection events should not be targeted at the nucleus as doing so generally results in cell death. It seems reasonable therefore that injecting a metallic nanoparticle into the nucleus of a live mammalian cell would cause loss of viability.

As described in chapter two, it has been proposed that the mechanism of optical injection using ultrashort pulses (repetition rates > 1 MHz) involves the generation of a free electron mediated low density plasma adjacent to the lipid bilayer resulting in the generation of a transient pore [30]. It is clear from a number optical injection

experiments [130, 146] that bulk solutions of DNA (with a radius of gyration of 85–120 nm [147, 148]) do enter the nucleus upon optical injection. It is therefore tempting to imagine a simple model where a pore opens immediately below the nanoparticle, which is enshrouded by the free electron plasma cloud, and as the cloud dissipates the lipid bilayer closes behind it as it enters the cell. Alternatively I believe that the injection is more of a transfer of momentum from the injection beam to the particle, projecting the particle out of the trap and through the plasma membrane in a ballistic nature. This theory is supported by investigations I performed with no cell present, trapping and then ballistically ejecting nanoparticles from the trap with the optical injection beam. Consequently, much more work is required to investigate possible mechanisms behind the internalisation of the nanoparticle to the cell interior.

In the new method of nanoparticle internalisation described here, a 100 nm nanoparticle is placed onto a cell though optical tweezing with a cw laser, and propelled into the cell with a 40 ms burst of femtosecond laser. This method is entirely novel in its ability to target selectively individual regions within a cell for optical injection. I believe that in combination with spectroscopic studies this novel method will be of immense value for a variety of biophotonics applications.

6.6 Conclusions

The techniques for optical injection presented in this chapter provide all-optical methods for the internalisation of impermeable substances.

The initial demonstration of the *in vitro* optical injection of a caged molecular probe presented in this chapter presents an attractive all-optical methodology for the control of the cellular microenvironment. The ability to load cells with caged probes and subsequently generate highly localised concentration jumps of effector compound by photolysis in one microscope provides a significant relaxation of user ability. Further work in developing this methodology would involve the repetition of the observed results and application to biologically relevant compounds such as IP_3.

The targeted optical injection of gold nanoparticles provides the most precise technique for the placement of gold nanoparticles within targeted regions of mamallian cells demonstrated in the literature [3]. Development of a more sensitive method for the confirmation of internalisation is vital to allow internalisation at regions outside the cell nucleus to be confirmed and a complete viability study to be performed. A preliminary study into using the internalised nanoparticles for the surface plasmon enhanced Raman spectroscopy (SERS) of the cell interior was hamperd by spectra being dominated by the glass coverslip of the cell culture dish. Future work would involve the use of quartz based cultureware which would allow for the successfull aquisition of spectroscopic data.

Both of the presented techniques afford an increased level of control over currently available methodologies.

Chapter 7

Simpified optical micromanipulation and injection methodologies for application to biological systems

7.1 Single-cell assays

7.1.1 Introduction

Scaling biological assays from a global scale to an individual level is a problem in single-cell studies. Microfluidic technologies offer an ideally suited solution to this problem which are fully integratable with existing optical techniques including microscopy, spectroscopy and optical tweezing. However, microfluidics demands intelligent chip design, multiple fabrication steps and expensive pump systems. Consequently, in this section a relatively simple method for miniaturising a biological assay for application to single cells is presented.

The technique is based upon the use of square walled capillaries as reagent reservoirs and optical tweezers for sample transport. A sample may be serially dosed with multiple reagents without the requirement for fluid flow regimes. In this way a single-cell assay can be optimised quickly without requiring fabrication of an elab-

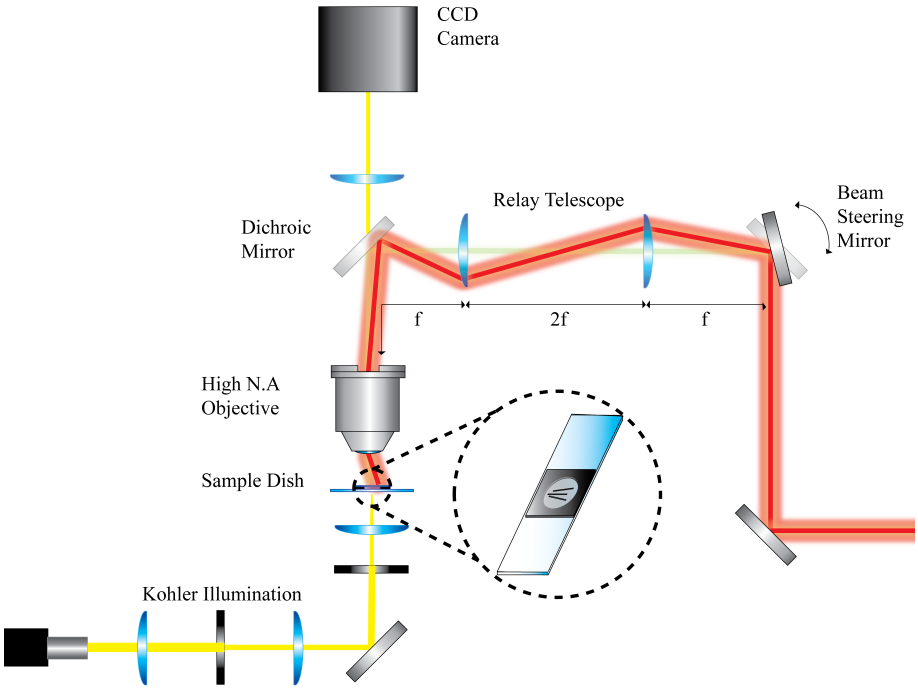

Figure 7.1: *An upright optical tweezers arrangement was employed. The Ti:Al_2O_3 laser source operated in CW modality.*

orate chip or use of associated pump devices.

This technique was developed as a control for the "tweeze-porate-tweeze" technique demonstrated in section 7.2. Optical tweezers are used to transport cells under static flow to perform fixation, permeablisation and staining of a single cell in a controlled manner.

7.1.2 Experimental

The experimental arrangement employed for optical injection is illustrated in figure 7.1. An upright optical tweezers setup with brightfield illumination was constructed. The laser source was the homebuilt Ti:Al_2O_3 laser, the design and construction of which was detailed in chapter three. This laser operated at a wavelength of 780 nm in CW modality. The objective was a Nikon high N.A 100x infinity corrected oil immersion lens providing an approximately 0.8 μm spot at focus. The objective was found to have 63 % transmission at 780 nm by dual objective measurements [129]. The sample chamber was held on a precision xyz stage (Newport, USA) which incorporated a doughnut Peltier (Melcore,USA) maintained at 37º C by a

temperature controller (Marlow, UK) for maintaining biological conditions during experiments. The sample was illuminated by Köhler illumination to provide uniform illumination across the field of view.

For cell culture all reagents were purchsed form Sigma (UK) unless specifically stated. The Human Leukaemia 60 (HL60) cells (EACC) were routinely cultured in a humidified atmosphere of 5% CO_2/95% air at 37^o C in Roswell Park Memorial Institute (RPMI) 1640 medium with 10% fetal bovine serum (Invitrogen, UK), 50 units/ml penicillin, 50 µg/ml streptomycin and 2 mM L-glutamine.

The optical manipulation chambers were constructed under aseptic conditions as described in chapter three. The chamber was pacified by addition and subsequent removal of Sigmacote. A 50 µl cell solution was loaded into the chamber. The capillary tubes containing reagents of interest were carefully placed in the chamber with precision metal tweezers which had been flame sterilised. The square capillary tubes (VitroCom, USA) had a 50 µm square inner diameter, 100 µm square outer diameter and were 4 mm in length.

The tubes were cut by the manufacturer to have a smooth edge to promote ease of transporting cells over the boundary. Tubes were loaded with the reagent of interest by capillary action. Square capillaries were required to minimise any deformation of the tweezers beam through the capillary wall, which would inhibit successful tweezing.

For the fixation and permeabilisation protocol, three capillaries were loaded. One containing 4 % formaldehyde for fixation, one 0.3 % triton X-100 in PBS for permeabilisation and another containing 0.4 % trypan blue solution, a membrane impermeable dye used to ascertain whether cells had been successfully permeabilised. Diffusion of the reagents into the bulk solution was not observed. As a precaution the capillaries containing the reagents of interest were located over millimeters apart, far beyond the range of any diffusion. The manipulation chamber was then sealed with a 23 mm diameter type zero cover slip to protect the sample form the toxic immersion oil used with the high N.A objective.

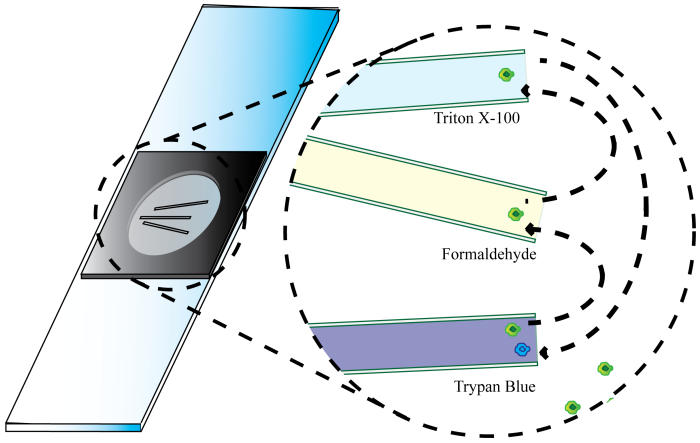

Figure 7.2: *Optical tweezing permits the selection of a single cell from bulk solution and treatment with numerous reagents housed in capilliary tubes in a static flow regime. In this way many large scale assays may be scaled down to the single cell level demanding reduced reagent volume without the requirement for microfluidics.*

7.1.3 Results

Prior to the fixation and permeabilisation steps, cells were tweezed into the capillary containing the membrane impermeable dye trypan blue to confirm the cells were not permeable before the procedure. For the fixation and permeabilisation of a large number of cells in a bulk sample, cells would first be fixed with 4 % formaldehyde and then permeabilised with triton X-100. In this experiment a single HL-60 cell was selected from the bulk solution far form the capillary tubes loaded with the reagents required for the protocol. HL-60 cells are a non adherent cell line making them ideally suited for optical manipulation with a tweezers setup. As illustrated in figure 7.2 the selected cell was tweezed from the bulk solution into the capillary containing the 4 % formaldehyde solution for the fixation step. The cell was then tweezed back into the bulk solution and into the capillary containing the 0.3 % Triton X-100 solution for the permeabilisation step. The cell was then tweezed to the capillary containing a 0.4 % solution of the membrane impermeable dye Trypan blue. Cells which then turned blue were confirmed as having been successfully permeabilised.

No tweezing-induced morphological changes were observed during the tweezing process, although it was noticed that tweezing became difficult after the chemical permeabilisation had taken place. Possible causes for the difficulty in trapping could

be a chemically induced change in refractive index working to reduce the refractive index contrast between the cell and surrounding medium or possibly some change in absorption characteristic of the cell leading to heating. For an assay on a large number of cells the protocol requires exposure to each of the reagents for a matter of minutes whereas successful permeabilisation was observed after relatively short exposures of a few seconds. Diffusion of liquids form the capillaries into the bulk solution was not observed however as an extra precaution the capillary tubes were placed far apart relative to the cell sizes and cells to undergo the protocol were selected from the other side of the sample chamber.

7.1.4 Discussion & Summary

The miniaturised assay resulted in successfully fixation and permeabilisation of the selected cell. The technique offers a simplistic alternative to microfluidics for reduction of assays to a single cell level. It is worth noting that the cell is dead upon fixation, so for this demonstration of the protocol a viability test after in not appropriate in this case.

Whilst I believe that microfluidic systems offer the most versatile and elegant solution to scaling down protocols to the single cell level, this technique using optical tweezing and capillaries as reservoirs offers an alternative for simple assays. It shares many of the advantages of microfluidics such as being highly integrateable with existing optical techniques, reduced sample and analyte volumes, reconfigurability, reproducible results and being disposable. Assuming the setup being used already includes an optical tweezers setup, it is far easier to implement than microfluidics and requires very little in terms of fabrication. The cost is greatly reduced as no mask, soft lithography or pumps are required. This method could be easily integrated into other experimental protocols where a bank of chemical reagents could be stored at the far end of a sample chamber to facilitate “on the fly” chemical processing of samples. For example, a quick viability assessment by exclusion could be carried out before going on to proceed with full optical manipulation.

Further work could involve the investigation of the difficulty in tweezing observed as a result of the chemical fixation process. Heat shock protein expressing cells could

be used to assess the heating caused by the process similar to studies conducted by Leitz *et al.* [41]. The use of dielectric tagging similar to that used by Muthunzi *et al.* [149] could also be employed to combat the difficulties caused by reduced trapping ability.

7.2 Tweeze-porate-tweeze

7.2.1 Introduction

It has been demonstrated that dual beam systems incorporating a CW optical tweezers and femtosecond surgery beam provide an all optical methodology for treatment of biological samples [150, 151]. Typically a single cell is selected, optically tweezed by the CW beam and held for imaging or surgery with the femtosecond beam. Here a similar technique is presented where a single beam is used to hold and then permeabilise the cell membrane for introduction of membrane impermeable substances. This method demonstrates a greatly simplified optical arrangement by exploiting the CW and femtosecond pulsed temporal modalities of the same laser source [5].

In 2004 Agate *et al.* demonstrated optical tweezing of silica microspheres coated with the fluorescent dye, firefly blue [152]. It was shown that both single and multiple-photon processes could be accessed by switching the operating regime of the laser source . Whilst mode locked producing femtosecond pulses, the microspheres could be successfully tweezed and the nonlinear absorption of the laser light by the dye resulted in the spheres fluorescing. Switching regimes to CW operation by disrupting the intracavity laser field momentarily resulted in tweezing continuing but with loss of fluorescence. Here the first use of a single laser to perform multi-photon and single-photon processes upon biological materials by switching the temporal operation modality of the laser source is demonstrated. The key to the versatility of the technique is the ability to switch laser operation from CW to femtosecond to access single-photon biologically amiable tweezing and then multiphoton based optical injection respectively. The technique provides a versatile technique with greatly simplified optical arrangement compared to that reported in the literature [150, 151].

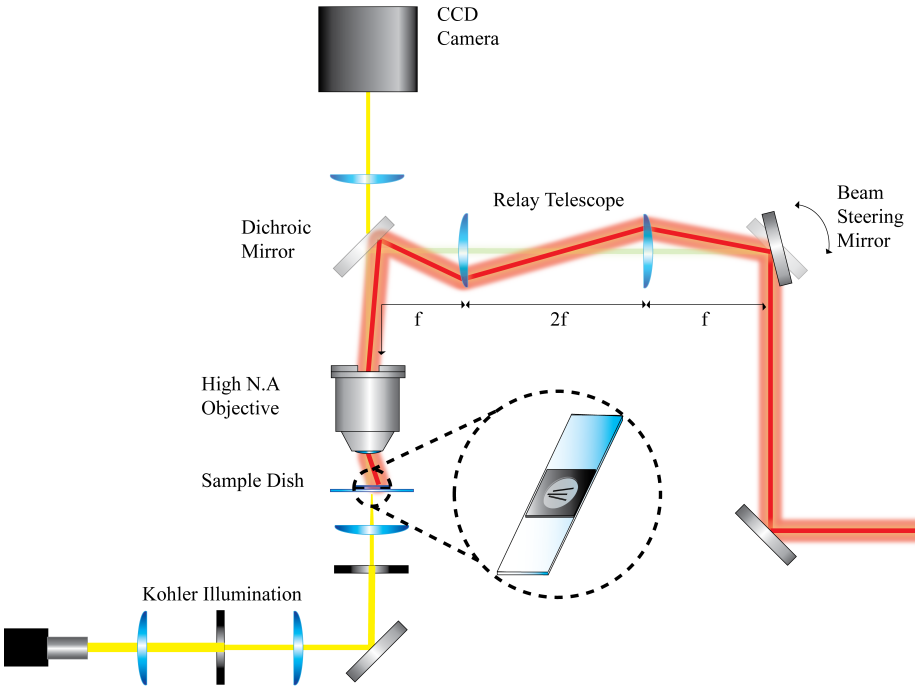

Figure 7.3: *An upright optical tweezrs arrangement was employed for the tweeze-porate-tweeze operation. The temporal modality of the laser was altered between CW and femtosecond regimes to achieve tweezing and membrane permeabilisation of the HL-60 cells respectively.*

7.2.2 Experimental

The experimental arrangement employed is illustrated in figure 7.3. The experimental arrangement was the same as that described in section 7.1, however for the tweeze-porate-tweeze operation it was possible to switch between femtosecond and CW operation by momentarily disrupting the intracavity laser field. The laser was aligned so that the switch from CW to femtosecond was achieved by introduction of a noise spike through tapping one of the cavity mirrors gently. A spectrum analyser (IST-Rees, UK) was used to distinguish between CW and femtosecond mode locked operation of the laser.

Similar to the chambers described in section 7.1, capillary tubes containing reagents of interest were carefully placed in the chamber with precision metal tweezers which had been flame sterilised. The square capillary tubes (VitroCom, USA) had a 50 μm square inner diameter, 100 μm square outer diameter and were 4 mm in length. The tubes were cut by the manufacturer to have a smooth edge to promote ease of transporting cells over the boundary. Square capillaries were required

to minimise any deformation of the tweezing/injection beam through the capillary wall, which would inhibit successful manipulation. Capillary tubes were loaded with the reagent of interest by capillary action.

For the tweeze-porate-tweeze operation a capillary was loaded with 0.4 % trypan blue solution, a membrane impermeable dye to be optically injected into a cell of interest. Two additional capillaries contained formaldehyde and triton X-100 required to chemically fix and permeabilise a cell to act as a control to the optical injection. The manipulation chamber was then sealed with a 23 mm diameter type 0 coverslip to protect the sample form the toxic immersion oil used with the high N.A objective.

7.2.3 Results

Prior to the tweeze-porate-tweeze experiment a single HL-60 cell was chemically fixed and permeabilised according to the procedure in section 7.1 to act as a control of a stained cells appearance. This stained cell was left in the capillary containing 4 % trypan blue solution for comparison to the optically injected cell. The procedure for a tweeze-porate-tweeze operation is illustrated in figure 7.4.

A single HL-60 cell was selected from the bulk solution and opticaly tweezed with the laser operating in CW mode (figure 7.4a). The laser was momentarily switched to mode locked operation by deliberate introduction of a noise spike. The cell was then exposed to a brief <100 ms train of femtosecond pulses (figure 7.4b). As can be seen the irradiance was deliberately high to allow observation of the generated photopore as indicated by the white arrow. The laser was then blocked over the next 6 minutes and the cell nucleus was observed to turn blue. The CW laser beam was then unblocked and used to tweeze the optically injected cell back into the bulk solution where it was compared to an untreated cell which had not undergone the operation. As figure 7.4c shows, the cell nucleus had clearly turned blue.

As a control another cell was selected from the bulk solution and tweezed into the capillary containing the 4 % trypan blue solution with the laser in CW mode. The cell was then left in the dye solution for a similar 6 minute period with the laser blocked subsequently tweezed back out of the capillary into the bulk solution. The

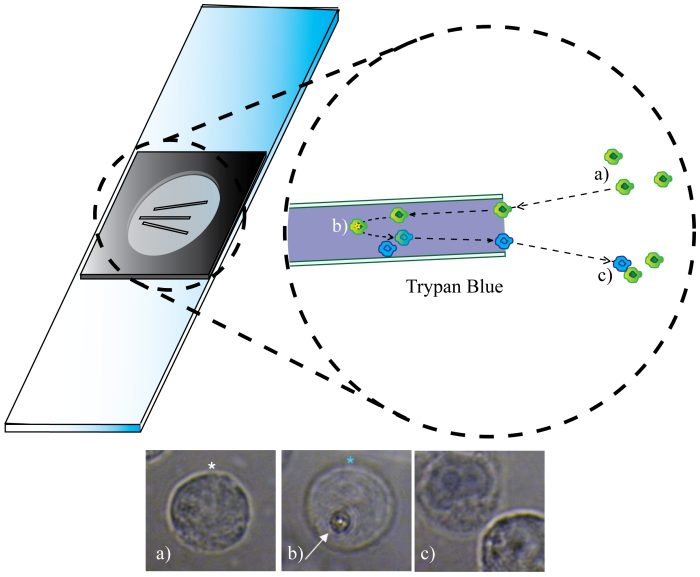

Figure 7.4: *Switching temporal modality of the laser system permits the selection and tweezing of a cell form bulk solution to a capilliary containing the reagent of interest in CW modality (a). Subsequent permeabilistaion and injection of membrane impermeable trypan blue is achieved through introduction of femtosecond operation (b). Switching to CW operation permits tweezing back to the bulk solution for comparison with untreated cells (c).*

cell which did not undergo exposure to the femtosecond injection beam did not turn blue with the stain.

This result was interpreted as the mode locked laser generating a photopore which permeabilised the cell membrane and allowed the membrane impermeable dye to enter the cell interior. It is noteworthy that the staining of the dead, chemically fixed, permeabilised and stained cell is uniform and concentrated whereas that of the optically injected cell is confined to the nucleus and took a longer period of time to stain. This difference indicates that the optically injected cell maintained a degree of permeability over the dead cell which is crucial to future viability. The cell demonstrated no morphological deformation during the CW optical tweezing phases and no apoptosis mechanisms such as blebbing (irregular protrusions in the cell membrane) or increased granularity where observed. The optically injected cell appeared to remain viable for some time after the experiment however the trypan blue dye which was injected is highly toxic and made any further viability studies inappropriate.

7.2.4 Discussion & Summary

This experiment highlighted the marked effect temporal modality can have upon the interaction between a laser source and a biological sample. Under CW conditions the cell of interest could be readily tweezed both in the bulk solution and within square capillaries containing reagents of interest by single-photon processes. The switch to mode locked operation enabled access to precise cellular nanosurgery and exposure to a short train of pulses resulted in permeabilisation of the cell. This technique could be used to deliver any number of membrane impermeable substances to a single cell in a highly selective and targeted manner. The ability to tweeze the cell of interest into a capillary of a selected reagent before permeabilisation adds another technique to the assay miniaturisation described in section 7.1. Any number of capillaries could house multiple reagents of interest permitting many imaginable processes without the requirement of microfluidics. Furthermore, the intelligent switching of laser operating modality from CW to femtosecond pulsed reduces the complexity of the optical setup and number of lasers required. It also ensures critical alignment between the tweezing and surgery sites as the two points are inherently located at the same focci.

Whilst no viability study was performed, laser irradiance and exposure times were consistent with those from the literature where around 50 % viability were reported [130]. At the time of this experiment I was unaware of lucifer yellow as a membrane impermeable non-toxic stain to act as an optical injection indicator. Repetition of the experiment using lucifer yellow as the injection indicator could be undertaken to perform a viability study.

7.3 Towards Long wavelength fs Optical injection

7.3.1 Introduction

For single-cell studies, high-repetition rate, mode locked femtosecond laser sources operating in the NIR have emerged as the prominent laser choice for optimal transfection efficiency and cell viability. Unfortunately, this operational regime dictates

the use of expensive vibronic crystal lasers such as the Ti:Al_2O_3. This preliminary study uses a lower cost, robust, small footprint femtosecond laser operating at a similar repetition rate, but emitting a longer wavelength deeper in the NIR at 1040 nm. The shift to a longer wavelength results in reduced absorption in the sample and surrounding medium and will have an effect upon the interplay between the laser field and sample. The objective of this experiment was to ascertain if cells could be successfully optically injected and indeed transfected using this longer wavelength laser source. Such a setup would represent a potentially simple to use, portable optical injection setup at a relatively low cost when compared to systems employing traditional commercially available femtosecond laser sources.

CHO cells were chosen for the injection operation as they remain a common cell type for investigating optical injection in the literature. The plasmid Mito-DsRed was chosen due to its relatively small size of 4.7 Kb for passing through the membrane, specificity to target the mitochondria of the cell and common use in the literature. Taking 12 hours to mature, the plasmid is expressed approximately 12 hours post injection. The DsRed protein is derived from red coral and fluoresces red when optically excited, demonstrating peak absorption at 558 nm.

7.3.2 Experimental

For optical injection, the upright 1040 nm femtosecond optical tweezers employed in chapter six section 6.1.2 were used as illustrated in figure 7.5.

For cell culture all reagents were purchased form Sigma (UK) unless specifically stated. Chinese Hamster Ovary K1 (CHO) cells were cultured in T25 tissue culture flasks in Modified Earles Medium (MEM) with 10% foetal calf serum (FCS) (Globepharm, UK), 20 enzyme units/ml of penicillin and 20 mg/ml of streptomycin (resulting medium referred to as “complete MEM”) and kept in a humidified atmosphere of 5% CO_2/95% air at 37 ^{o}C. The cells were routinely passaged three times weekly. For experimentation, cells were prepared at a seeding density of 2.1 x10^4cells/ml in 30 mm diameter glass-bottomed culture dishes with a usable working area of 23 mm (World Precision Instruments, UK) in 2 ml of complete MEM. Once seeded in the dishes, cells were incubated for 24 hours to promote robust attachment

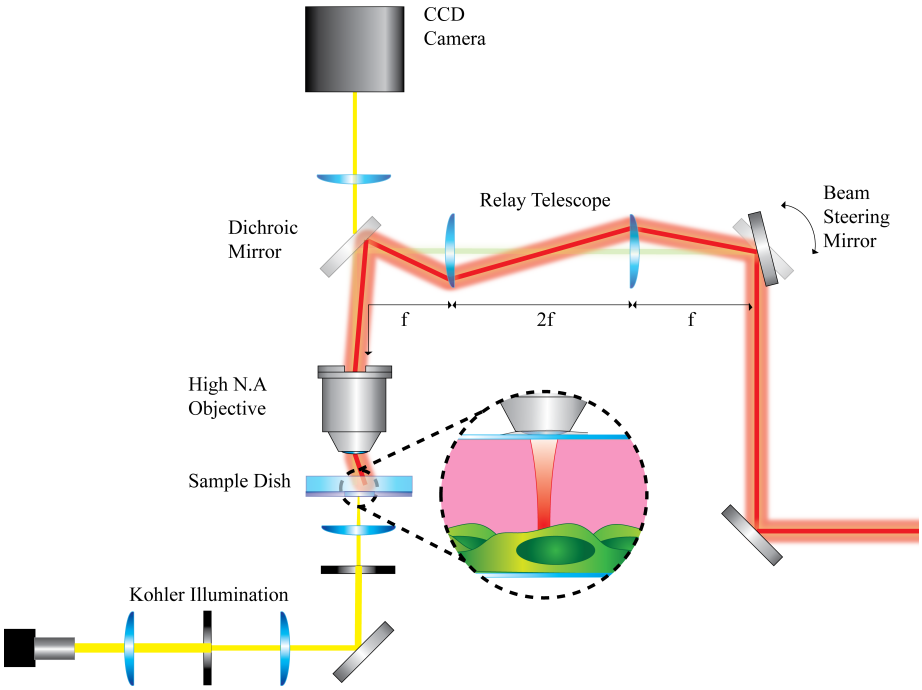

Figure 7.5: *An upright optical tweezers system utilising a 1040 nm mode locked femtosecond laser source was employed for investigating optical injection of membrane impermeable materials.*

to the bottom of the dish.

For the optimised optical transfection procedure, CHO cells were exposed to approximately 40 mW of laser power at the sample (100 mW at back aperture) for ten seconds at focus whilst bathing in a solution containing plasmid DNA. Prior to exposure to the focused laser field, the 2 ml of complete MEM was removed by aspiration and the cell mono-layer rinsed with Optimem (Invitrogen, UK) to remove any residual FCS which might deactivate the plasmid DNA. Cells were then bathed in a 20 μl solution composed of 10 μg/ml plasmid DNA which in this case encoded for Mito-DsRed (Clonetech), 42.2 μm phenol red, 5 mM ascorbic acid and 1 mM lucifer yellow in Optimem (the resulting medium is subsequently referred to as "injection medium"). The experimental chamber was sealed by floating a sterile 22 mm type zero coverslip above the cell monolayer and encompassing bathing solution. To permit identification of the targeted cells a central 1mm diameter region of interest was then circled using a custom fabricated diamond etching device. The optical injection was then undertaken after which the coverslip was removed by floating with OptiMEM and the cell monolyer subsequently rinsed with OptiMEM before

addition of 2 ml complete MEM for further incubation. After a ten minute re-acclimatisation in the incubator, cells were imaged with a fluorescent microscope to allow an optical injection efficiency to be calculated by uptake of lucifer yellow. The cells were then incubated for up to 72 hours post injection and routinely observed by fluorescent microscopy for expression of the Mito-Ds Red, indicated by production of the fluorescent Ds Red protein in the mitochondria of the cell. Control cells were prepared in exactly the same manner, without laser irradiation.

7.3.3 Results

Typically, 50 cells per dish were targeted for optical injection. This was carried out under brightfield illumination. Single cells were selected by manual manipulation of the xyz translation stage and shutter controlled exposure of the laser beam. Each cell was targeted on the plasma membrane in a region near to but not upon the cell nucleus. No morphological changes or cavitation was observed during the experiment.

The addition of the membrane impermeable, bio-compatible stain lucifer yellow to the injection medium permitted the optical injection efficiency to be decoupled form the transfection efficiency and was found to be around 50 %. Figure 7.6 illustrates a typical region of interest. The brightfield image in (a) illustrates the healthy apperance of the cells post injection. The fluorescence image (b) acquired at the same time demonstrates the successful injection of lucifer yellow. The lucifer yellow was then observed to be actively ejected from the cell as none was found 36 hours later (c) when assessing expression of the Mito-DsRed protein. This was taken as an additional viability indicator, used in conjunction with exclusion of the membrane impermeable stain trypan blue, and cell division which was seen as the absolute measure of viability. For the procedure described, viability was observed to be maintained for the majority of the cells which were targeted. A full statistical analysis of the viability as a result of the process was unfortunately not undertaken due to time constraints.

The subsequent transfection efficiency was found to be very low, at around 4 % which does not take into account cell doubling times. Spontaneous transfection,

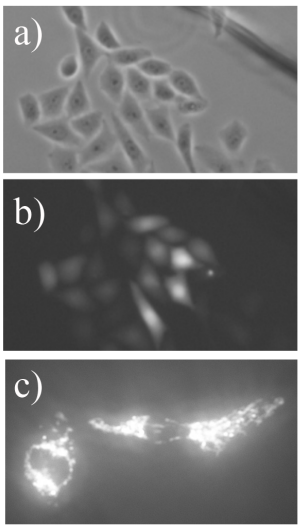

Figure 7.6: *A representative example of an optical injection experiment. Cells appear healthy following the injection procedure (a). Fluorescence imaging at the same time reveals successful optical injection of the membrane impermeable lucifer yellow stain (b) with 50% efficiency. At time >24 hours post experimentation the successful transfection of a small proprtion of the cells is observed (c) with 4 % efficiency.*

being when the cell expresses the encoded protein without experiencing laser irradiation, was not observed in the central region of interest. However, the level of optical transfection is not substantially greater than the spontaneous transfection expected or observed outside the region of interest. It was observed that the greatest levels of spontaneous transfection were present at the sample edges and where air bubbles had been present during the operation. Therefore careful sample preparation was crucial to this experiment to minimise such spontaneous transfection.

7.3.4 Discussion

There are two transfection studies conducted with femtosecond lasers at longer IR wavelengths reported in the literature. In 2003 Sagi *et al* reported the use of a 2 μm nanosecond laser to achieve 40 % transfection efficiency [128]. The ns nature of the laser indicates that the mechanism behind this transfection event was most likely mediated by propagation of a photomechanical shockwave. More recently and relevant to this work, *He et al* reported 77% transfection with a 1.5 μm femtosecond fibre laser [127]. Interestingly the exposure time was far longer than the typical ms doses employed with NIR fs optical transfection at 10 seconds. They attribute this

to the fact that at this wavelength more photons have to be absorbed to generate the free electron cloud responsible for permeabilising the cell membrane. This, however, assumes effective absorption of these photons in the plasma membrane. Furtheromore, plasma mediated optical injection events are driven by millisecond laser exposures not the tens of seconds observed. Therefore, I suspect that the mechanism behind this transfection event was not plasma mediated, but rather a thermal effect as indicated by the long exposure times.

The cell plasma membrane was targeted on a region of the cytoplasm near but not including the nucleus. When working with femtosecond cellular transfection, accurate alignment of the laser focus to the cell membrane is critical for the successful permeabilisation of the cell membrane. Doing so ensures that multiphoton effects which are closely confined to the focus of the beam are engaged in the generation of a low density free electron plasma driving the permeabilisation. Typically alignment of the laser focus to the correct position is achieved by tweezing a 1 μm sphere, and adjusting the laser expansion telescope until the image and laser planes are matched when the sphere is in focus. This technique however does not take into account that the optically trapped particle is held slightly below the focus of the laser spot. Therefore, the true focus of the laser beam will be slightly too high, resulting in a manual calibration to be performed by eye by the user.

The use of Bessel beams has been demonstrated to relax this requirement as illustrated in figure 7.7 [5, 146]. Figure 7.7a shows an optical arrangement I constructed to highlight the difference between the excitation characteristics of different beams [5]. The single-photon excitation of fluorescein with a 405 nm UV laser diode ($\circ$) demontrates excitation occurs throughout the entire focus. The multiphoton excitation of fluorescein by a Ti:Al_2O_3 laser is shown for a Bessel beam ($\blacksquare$) and Gaussian beam ($\square$) in figure 7.7a. The extended excitation region for the Bessel beam ($\blacksquare$) demonstrates why use of a Bessel beam relaxes the criteria for overlap of the laser focus with the cell membrane as demonstrated quantitatively in figure 7.7b which was modified from [146]. The extent of the effect of laser and image plane alignment upon a thermally mediated optical injection process is as of yet not investigated, however since the thermal heating is induced by multiphoton absorption,

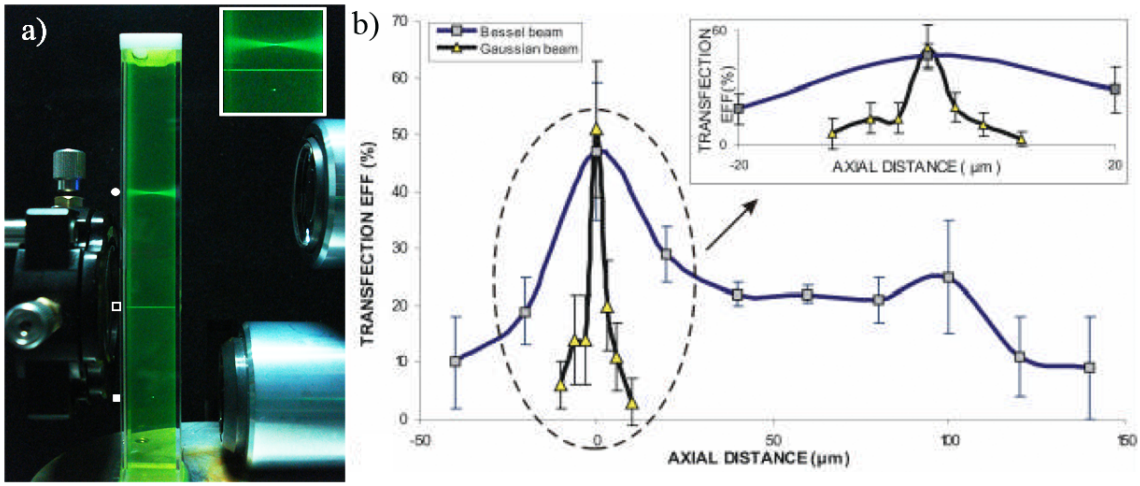

Figure 7.7: *The different excitation characteristics for single-photon Gaussian (∘), multiphoton Bessel (■) and multiphoton Gaussian (□) are shown in a, figure adapted from [5]. The use of multiphoton Bessel beams for fs transfection has been shown to relax the stringent requirement for overlap of the beam focus with the cell membrane as shown in b, figure adapted from [146].*

it is likely to be a similarly highly localised event similarly sensitive to deviations in focal region alignment. However, since the heating assumed to be responsible for permeabilisation occurs in the injection medium, it would be advantageous to have the focii aligned in the micron above the cell plasma membrane so the alignment procedure may be serendipitously optimally aligned.

7.3.5 Summary

The primary objective of this experiment was to assess the suitability of the laser source to optical injection and transfection. A rigorous statistical analysis has not been undertaken and all findings are preliminary.

This investigation finds the laser source to be suitable for optical injection of the membrane impermeable stain lucifer yellow. It has also been demonstrated that there is potential for developing a protocol for optical transfection, although work would have to be undertaken in improving efficiency. I believe the mechanism underpinning the injection events to be a thermally mediated, temporary premeabilisation of the cell membrane.

When developing NIR femtosecond optical injection protocols the starting point was typically the injection of the membrane impermeable, toxic stain trypan blue.

Typical dosage parameters for this would be tens of milliwatts laser light at focus for tens of milliseconds based upon reports in the literature [130]. In this way successful optical injection parameters were developed using membrane impermeable stains and then applied to injection medium containing the extracellular substance to be delivered. This was before development of the lucifer yellow protocol used here. When these conditions were recreated with the 1040 nm laser source, successful injection of trypan blue was observed. However, when the switch was made to optical injection medium, very little injection of around 8 % was observed. Indeed, even with the laser power and exposure duration increased far beyond a fatal dose, no interaction between the laser beam and biological sample was observed visually when one would normally observe cavitation and morphological change at 800 nm.

Based upon the existing work in the literature [69,70,72], the pH indicator phenol red which has an absorption centred at 550 nm was added to the injection medium to enhance absorption of the laser beam in the sample. As a result, visible laser/sample interaction and indeed injection was easily achievable. Coincidentally, phenol red can act as a fluorescent indicator for injection if the concentration is high enough. The protocol still includes the lucifer yellow as at the concentrations employed the phenol red fluorescence is not a reliable indicator and the lucifer yellow absorption was also found to enhance the injection in experiments using phenol red as the injection indicator. The 42.2 μm concentration used is consistent with that reported for absorption enhancement using CW laser diodes reported in the literature [70,72]. The addition of the phenol red saw the injection efficiency rise form 8 % to around 50 % and fully supports the thermally mediated mechanism theory.

Further evidence supporting a thermally mediated mechanism is that the injection events are only successful when performed in small volumes of injection medium. With the parameters described, effective injection was not observed in volumes greater than 25 μl. 20 μl is the smallest usable volume allowing reliable refloating of the coverslip without causing detachment of the cell monolayer and as such was used for the protocol. Greater volume of liquid provides a larger effective heatsink to cool the interaction region between the laser and sample, suggesting that the heating is responsible for the injection event. These facts all seem to suggest that

localised heating of the plasma membrane results in a temporary premeabilisation permitting the delivery of extracellular materials. The thermal effect appears to be mediated by multiphoton absorption in the optical injection medium as no injection was observed when the laser was deliberately misaligned to run in CW.

The relatively long exposure times employed result in the formation of harmful reactive oxygen species (ROS) which are harmful to the cell resulting in loss of viability. Marked improvement in cell viability was observed through the addition of the antioxidant ascorbic acid (vitamin C) although no quatitative data has been recorded. This observation was supported by the work of Nikolskaya *et al.* [68]. As a result 5 mM ascorbic acid was added to the injection medium to act as a ROS absorber, whilst demonstrating no effect upon injection efficiency.

The laser power and exposure duration parameters came as a result of much investigation. Duration was based upon the work of He *et al*, by varying the duration and powers a single dose of ten seconds was found to be most suitable. There is great interplay between the power and exposure duration, experience and experimentation resulted in moving towards longer exposures of lower power rather than short sharp burst of higher powers. For example powers of 60 mW at sample saw 100 % optical injection but 100 % loss of viability. Reducing the power to 40 mW at the sample saw the reasonable 50 % optical injection efficiencies achieved whilst maintaining the viability of most of the cells as verified by the ability to continue dividing. Viability was observed to be far lower in the absence of ascorbic acid in the injection medium. This is believed to act as a antioxidant, removing harmful energetic free radicals generated during such long irradiation periods.

This proof-of-principle experiment has demonstrated that more economical longer wavelength mode locked femtosecond laser sources have potential as optical injection sources. The mechanism of permeabilisation appears to be thermal, different to those for laser operation around 800 nm whose injection events are mediated by plasma formation. Preliminary optical injection efficiencies of around 50 % were observed whilst injecting membrane impermeable stains and optical transfection was achieved albeit with very low efficiencies. Moving forward from this preliminary study much work must be done for the development of a fruitfull technique. There

must be further investigation into optimising the injection parameters. Further work must be done in a robust statistical analysis of the optical injection and transfection including a full viability study. Moreover, further investigation into the alignment of the laser focus to the cell membrane must be undertaken. Once this work has been completed, there will be a far more robust picture of the role such laser sources have to play in the field of optical injection.

7.4 Conclusions

In this chapter the development of three techniques for the manipulation of single cells has been presented. Two of the the techniques employ capilliary tubes as reservoirs for reagents and permit the controlled serial dosing of single cells in a static flow regime. These techniques are simple to implement and require no complicated chip fabrication or microfluidic pumps. The third presents a simplified approach to optical injection employing a less complicated optical arrangement.

In section 7.1 cells were optically tweezed between reagents with the laser in CW modality. This approach has the potential to be scaled to any number of reagents or treatments upon the cell of interest. In this way any chemical assay could be reduced to a single-cell assay. Individual cells of interest could be selected from the bulk solution and treated.

In section 7.2 the role the temporal nature of the laser field was exploited. A methodology providing the ability to optically tweeze and perform laser microsurgery upon a cell under study using a single laser source was developed.

These methods are easily integratable with existing experients. Capillaries containing reagents could be placed into sample chambers and accessed during experimentation. I believe this approach offers a simple and cost effective alternative to microfluidics for the treatment of individual cells with reagents.

In section 7.3 a preliminary study into the use of a mode locked 1040 nm femtosecond laser for optical injection indicated that the laser is a viable source for optical transfection of mamallian cells. A 50 % optical injection efficiency was observed for the fluorescent stain Lucifer yellow, without compromising cell viability.

Successful transfection transfection of CHO cells with Mito-DsRed was also demonstrated whilst maintaining cell viability, but the observed efficieney was extremely low at 4 %. Further development of the methodolgy could yield a relatively low cost and portable technique of fs cellular transfection when compared with traditional techniques based upon Ti:Al_2O_3 laser sources.

Chapter 8

Conclusions

8.1 Summary

The main theme of this thesis has been the development of photonic techniques for the enhanced control over biological samples under study. More specifically, the work has been directed at the development of methodologies for application to the study of single mammalian cells.

The thesis began with an introduction to the use of light as a tool in the life sciences. The requirement for tools with greater spatial and temporal control of biological systems for the investigation and correction of dysfunctional cellular behaviour was identified as the motivation for the work presented in this thesis. Optical tweezers, laser scalpels and caged compounds were introduced as the three underpinning technologies behind the work within this thesis. An introduction was given to the structure of the eukaryotic mammalian cell. Finally, the factors regulating the interaction between an incident laser field and a biological sample were discussed.

The second chapter provided the theoretical basis of the optical tweezers and optical injection techniques employed in this thesis.

In the third chapter the experimental methods used throughout the thesis were detailed to prevent repetition. This included the design and construction of a fs laser system, a generic scheme for the construction of an optical tweezers setup, a description of the techniques associated with the preparation, characterisation and application of caged compounds and the biological techniques employed.

The experimental work conducted in the lab was detailed in chapters four through seven.

More specifically, chapter four described the development of caged molecular probes for application to biological systems. In this work the characterisation techniques described in chapter three where used to asses the suitability of the caged molecular probes for application to *in vitro* studies.

In chapter five, the first wavelength orthogonal caging of biologically relevant compounds was demonstrated. The ability to activate one compound in the presence of another provides a solution to the major failing of caged technologies of the lack of an "off switch" by the orthogonal caging of the agonist and antagonist of the biological target.

Chapter six exhibited the development of two advanced techniques for the optical injection of membrane impermeable substances based on mode locked femtosecond laser sources.

The first of these was the optical injection of caged molecular probes. The motivation for such a technique is that there is a trade off between synthesising a compound to be membrane permeable whilst maintaining a usable level of solubility. As such caged compounds are often applied to the cell interior by microinjection. The preliminary work presented in this chapter demonstrated the optical injection and subsequent activation of caged fluorescein in CHO cells. This technique if extended to biologically relevant compounds potentially affords the ability to inject and activate a compound of choice with one instrument.

The second optical optical injection study presented in chapter four details the use of a modelocked Ti:Al_2O_3 femtosecond laser for optical injection in conjunction with a CW 1064 nm trapping beam coaligned in an upright optical tweezers configuration. This arrangement provided the targeted placement and internalisation of single 100 nm gold nanoparticles within selected regions of mammalian cells. In this way nanometer sized biosensors could be located to distinct intracellular regions.

In the seventh and final experimental chapter three techniques for the simplified micromanipulation of biological samples were presented.

The first of these used capillary tubes as reservoirs for reagents of interest to scale

a chemical assay to the single-cell level in a static flow regime. Such a methodology has potential in single-cell studies where information masked by global ensembles of cells may be lost.

The second technique exploited the change from tweezing to ablation caused by varying the peak power of the trapping laser. This was achieved by switching the tweezers laser source from CW to mode locked pulsed operation. It was demonstrated that a cell may be tweezed to capillary holding a reagent of interest and optically injected using the same laser beam. This simplified setup permitted the transport and nanosurgery of cells to be undertaken.

The third technique employed a mode locked Yb:KYW femtosecond laser source as an alternative to the Ti:Al_2O_3 typically utilised for femtosecond optical injection. This laser is more compact, robust, affordable and provides improved ease of use compared to Ti:Al_2O_3 laser sources. Whilst successful injection was observed with a 50 % efficiency, transfection of the Mito-DsRed was observed to be highly inefficient with a 4 % transfection efficiency. It is possible that this injection is thermally mediated by two photon absorption within the injection medium as opposed to the generation of a low density free electron cloud which is believed to be the mechanism for MHz femtosecond optical injection.

The work presented in this thesis has contributed to the field of biophotonics with new techniques for the manipulation of biological samples.

The innovative caged molecular probes developed in the presented work demonstrate great potential in their respective areas. Caged AG10 provides a powerful tool for the highly localised disruption of mitochondria function. In this way the role mitochondria play in intracellular signalling can be probed. The caged TRPV1 compounds will find application in the study of TRPV1 receptor dynamics which are involved in studies of pain and noiception. The developed methodology of orthogonally caged neurotransmitters has great potential in the study of fundamental processes underpinning memory and cognitive function. The single photon nature of the technique makes it highly accessible to researchers in the life sciences.

The presented optical injection techniques provide new approaches for the introduction of membrane impermeable substances. The optical injection of a caged

molecular probe to the cell interior was demonstrated for the first time. The presented optical injection of gold nanoparticles remains the most precise targeted injection of a single nanoparticle in the literature, however the complexity of the optical system will likely hamper its widespread adoption.

The simplified optical trapping techniques provide elegant means for the serial dosing of single cells with reagents in static flow and negates the need to use microfluidics for simple operations. The use of switching laser modality to vary the laser-tissue interaction demonstrates a more accessible approach to the combination of optical tweezing and cellular nanosurgery which has now been adopted by other groups [153]. The longer wavelength NIR femtosecond optical injection appears to offer some potential as a low cost alternative to the optical arrangements typically emplyed for femtosecond optical injection techniques.

8.2 Future work

Based on the work presented in this thesis, there is scope for the further development of the presented techniques.

The next stages of development for the caged molecular probes involves assessment of the multiphoton characteristics of the developed compounds. These would include measurements of the efficiency of photolysis assessed by the quantum yields of the compounds and the measurement of two photon cross sections should be assessed. The development of a multisite photolysis system employing holographic optical tweezers techniques based on spatial light modulator devices should then be undertaken. The combination of a multisite photolysis system with the wavelength orthogonal methodology will provide a powerful system for the study of crucial processes in the central nervous system.

The presented work into the optical injection of caged molecular probes should be further developed as the technique shows great promise for enabling simplified delivery and photolysis of caged molecular probes in an all optical arrangement. Injection should be extended to biologically relevent caged molecular probes. With regards to the optical injection of gold nanoparticles a new system should be devel-

oped for the confirmation of particle internalisation, most likely through the use of a stain which only targets the cell membrane. It would not then be necessary to target the cell nucleus for injection and a full viability study of the process could be undertaken. Work also remains in eludicating the exact mechanism for the nanoparticle insertion into the cell interior. The use of quartz culture-ware should also be undertaken to allow studies into the use of the internalised gold nanoparticles for enhanced spectroscopic studies (SERS) of the cell interior.

Further work development of the simplified optical tweezers techniques could involve the use of lucifer yellow to confirm optical injection as opposed to the toxic trypan blue. In this way a full viability study into the tweeze-porate-tweeze operation could be performed. The initial studies into long wavelength femtosecond optical injection should be further investigated to find if there are steps to increase the observed transfection efficiency.

8.3 Final thoughts

The work presented in this thesis has demonstrated the strength and flexibility offered by optical manipulation technologies, specifically in biophotonics. The field has grown quickly since the advent of the laser fifty years ago, providing novel methodologies for researchers in the life sciences. The benefits of collaborative work across disciplines has also been highlighted within the work presented. The interdisciplinary nature of work in the field of biophotonics remains its greatest strength and shall hopefully continue to be so.

References

[1] Stanton-Humphereys.M, Taylor.R, McDougall.C, Hart.M, Brown.C.T.A, Emptage, N, and Conway.S, "Wavelength-orthogonal photorelease of neurotransmitters in vitro," In review

[2] VanRyssen.M, Avlonitis.N, Giniatullin.R, McDougall.C, Carr.J, Stanton-Humphereys.M, Borgstrom.E, Brown.C.T.A, Fayuk.D, Surin.A, Niittykoskis.M, Khiroug.L, and Conway.S, "Synthesis,photolysis studies and in vitro photorelease of caged TRPV1 agonists and antagonists," *Org-BiomolChem*, volume 7, pp. 4695–4707, 2009

[3] McDougall.C, Stevenson.D.J, Brown.C.T.A, Gunn-Moore.F.J, and Dholakia.K, "Targeted optical injection of gold nanoparticles into single mammalian cells," *JBiophoton*, volume 2, pp. 736–743, 2009

[4] Avlonitis.N, Chalmers.S, McDougall.C, Stanton-Humphereys.M, Brown.C.T.A, McCarron.J, and Conway.S, "Caged AG10:new tools for the spatially predefined mitochondrial uncoupling," *MolBiosyst*, volume 5, pp. 450–457, 2009

[5] Brown.C.T.A, Stevenson.D.J, Tsampoula.X, McDougall.C, Lagatsky.A.A, Sibbett.W, Gunn-Moore.F.J, and Dholakia.K, "Enhanced operation of femtosecond lasers and applications in cell transfection," *JBiophoton*, volume 1, pp. 183–199, 2008

[6] McDougall.C, Stevenson.D.J, Brown.C.T.A, Gunn-Moore.F.J, and Dholakia.K, "Targeted optical injection of gold nanoparticles into single mammalian cells," *CLEO, Munich (WB1)*, CLEO, 2009

[7] Brown.C.T.A, McDougall.C, Stevenson.D.J Gunn-Moore.F.J Dholakia.K, "Laser assisted delivery of membrane impermeable materials to targeted cells," *Topical problems in Biophotonics, Russia*, 2009

[8] Hooke.R, *Micrographia:Or, Some physiological descriptions of minute bodies made by magnifying glasses. With observations and inquiiries thereupon*, Martyn.J and Allestry.J, 1665

[9] Maiman.T.H, "Optical and microwave experiments in ruby," *PhysRevLett*, volume 4, pp. 564–566, 1960

[10] Ashkin.A, "Acceleration and Trapping of Particles by Radiation Pressure," *PhysRevLett*, volume 24, no. 4, pp. 156–159, Jan 1970

[11] Bessis.M, Gires.F, Mayer.G, and Nomarski.G, "Irradiation of cellular organisms with a ruby laser," *CRAcadSci*, volume 255, pp. 1010–1012, 1962

[12] Berns.M.W, "A history of laser scissors (microbeams)," *MethodsCellBiol*, volume 82, pp. 1–58, 2007

[13] Sato.S, Higurashi.E, Taguchi.Y, and Inaba.H, "Achievement of laser fusion of biological cells using UV pulsed dye laser beams," *ApplPhysB*, volume 54, pp. 531–533, 1992

[14] Guck.J, Ananthakrishnan.R, ans Moon.T.J, Mahmood.H, Cunninham.C.C, and Kas.J, "The optical stretcher:a novel laser tool to micromanipulate cells," *BiophysJ*, volume 81, pp. 767–784, 2001

[15] Kreysing.M.K, Kiebling.T, Fritsch.A, Dietrich.C, Guck.J, and Kas, "The optical cell rotator," *OptExpress*, volume 16, pp. 16984–16992, 2008

[16] Kaplan.J.H, Forbush.B, and Hoffman.J, "Rapid photolytic release of Adensine 5'Triphosphate from a protected Analog- Utilization by Na-K Pump of Human Red Blood Cell Ghosts," *Biochem*, volume 17, pp. 1929–1935, 1978

[17] Lee.H, Larson.D.R, and Lawrence.D.S, "Illuminating the Chemistry of Life: Design, Synthesis, and Applications of Caged and Related Photoresponsive Compounds," *ACS ChemBiol*, volume 4, pp. 409–427, 2009

[18] Mayer.G and Heckel.A, "Biologically Active Molecules with a Light Switch," *AngewChemIntEd*, volume 45, pp. 4900–4921, 2006

[19] Monroe.W.T, McQuain.M.M, Chang.S.M, Alexander.J.S, and Haselton.R.F, "Targeting Expression with Light Using Caged DNA," *JBiolChem*, volume 274, pp. 20895–20900, 1999

[20] Engert.F, Paulus.G.G, and Bonhoeffer.T, "A low cost UV lasers for flash photolysis of caged compounds," *JNeurosciMethods*, volume 66, pp. 47–54, 1996

[21] Denk.W, "Two photon scanning photochemical microscopy:Mapping ligand gated ion channel distributions," *ProcNatlAcadSciUSA*, volume 91, pp. 6629–6633, 1994

[22] Pettit.D.L, Wang.S.S.H, Gee.K.R, and Augustine.G.J, "Chemical Two Photon Uncaging:a Novel Approach to Mapping Glutamate Receptors," *Neuron*, volume 19, pp. 465–471, 1997

[23] Mason.A, *Cell biology and genetics*, Edinburgh:Mosby, 2002

[24] Campbell.N and Reece.J, *Biology*, Benjamin Cummings, 2004

[25] Singer.S.J and Nicolson.G.L, "The Fulid Mosaic Model of the Structure of Cell Membranes," *Science*, volume 175, pp. 720–731, 1972

[26] Liang.H, Vu.K.T, Krishnan.P, Trang.T.C, Shin.D, Kimel.S, and Berns.M.W, "Wavelength dependence of cell cloning efficiency after optical trapping," *BiophysJ*, volume 70, pp. 1529–1533, 1996

[27] Niemz.M.H, *Laser Tissue Interactions:Fundamentals and Applications*, New York:Springer-Verlag, 1996

[28] Venugopalan.V, III.A, Guerra, Nahen.K, and Vogel.A, "Role of laser-induced plasma formation in pulsed cellular microsurgery and micromanipulation," *PhysRevLett*, volume 88, p. 078103, 2002

[29] Vogel.A, Linz.N, Freidank.S, and Paltauf.G, "Femtosecond laser induced nanocavitation in water:implications for optical breakdown threshol in cell surgery," *PhysRevLett*, volume 100, p. 038102, 2008

[30] Vogel.A, Noack.J, Huttman.G, and Palatauf.G, "Mechanisms of femtosecond laser nanosurgery of cells and tissues," *ApplPhysB*, volume 81, pp. 1015–1047, 2005

[31] Vogel.A, Noack.J, Nahen.K, Theisen.D, Busch.S, Parlitz.U, Hammer.D.X, Noojin.G.D, Rockwell.B.A, and Birngruber.R, "Energy balance of optical breakdown in water at the nanosecond to femtosecond time scales," *ApplPhysB*, volume 68, pp. 271–280, 1999

[32] Vogel.A, Schweiger.P, Freieser.A, Asiyo.M.N, and Birngruber.R, "Intraocular Nd:YAG Laser Surgery:Light Tiss Interaction, Damage Range, and Reduction of Collateral Effects," *IEEEJQantumElect*, volume 26, pp. 2240–2260, 1990

[33] Vogel.A and Venugopalan.V, "Mechanisms of Pulsed Laser Ablation of Biological Tissues," *ChemRev*, volume 103, pp. 577–644, 2003

[34] Zeigler.M.B and Chiu.D.T, "Laser selection significantly affects cell viability following single cell nanosurgery," *PhotochemPhotobiol*, volume 85, pp. 1218–1224, 2009

[35] Hammer.D.X, Jansen.E.D, Frenz.M, Noojin.G.D, Thomas.R.J, Noack.J, Vogel.A, Rockwell.B.A, and Welch.A.J, "Shielding properties of laser induced breakdown in water for pulse durations form 5 ns to 125 fs," *ApplOpt*, volume 36, pp. 5630–5640, 1997

[36] Koenig.K., "Multiphoton Microscopy in life sciences," *JMicroscOxford*, volume 200, pp. 83–104, 2000

[37] Ashkin.A, Dziedzic.J.M, and Yaman.T, "Optical Trapping and Manipulation Of Single Cells Using Infared-Laser Beams," *Nature*, volume 330, pp. 769–771, 1987

[38] Tschachotin.S, "Die mikroskopische Strahlenstichmethode, eine Zelloperationsmethode," *BiolZentrabl*, volume 32, pp. 623–630, 1912

[39] Vorobjev.I.A, Liang.H, Wright.W.H, and Berns.M.W, "Optical trapping for chromosome manipulation:a wavelength dependence of induced chromosome bridges," *BiophysJ*, volume 64, pp. 533–538, 1993

[40] Neuman.K.C, Chadd.E.C, Liou.G.F, Bergman.K, and Block.S.M, "Characterisation of photodamage to Escherichia coli in Optical Traps," *BiophysJ*, volume 77, pp. 2856–2863, 1999

[41] Leitz.G, Fallman.E, Tuck.S, and Anxer.O, "Stress response in Caenorhabditis elegans Caused by Optical Tweezers:Wavelength, Power, and Time Dependance," *BiophysJ*, volume 82, pp. 2224–2231, 2002

[42] Ramser.K, Enger.J, Goksor.M, Hanstorp.D, Logg.K, and Kall.M, "A microfluidic system enabling Raman measurements of the oxyenation cycle in single optically trapped red blood cells," *Lab Chip*, volume 5, pp. 431–436, 2005

[43] Mirsaidov.U, Timp.W, Timp.K, Mir.M, Matsudaira.P, and Timp.G, "Optimal optical trap for bacterial viability," *PhysRevE*, volume 78, p. 021910, 2008

[44] Schafer.C.B, Garcia.J.F, and Mazur.E, "Bulk heating of transparent materials using a high repetition rate femtosecond laser," *AppPhysA*, volume 76, pp. 351–354, 2003

[45] Heisterkamp.A, Maxwell.I.Z, Mazur.E, Underwood.J.M, Nickerson.J.A, Kumar.s, and Ingber.D.E, "Pulse energy dependence of subcellular dissection by femtosecond laser pulses," *OptExpress*, volume 13, pp. 3690–3696, 2005

[46] Liu.Y, Sonek.G.J, Berns.M.W, Konik.K, and Tromberg.B.J, "Two photon fluorescence excitation in continuous wave infared optical tweezers," *OptLett*, volume 20, pp. 2246–2248, 1995

[47] Chen.I.H, Chu.S.W, Sun.C.K, Cheng.P.K, and Lin.B.L, "Wavelength dependent damage in biological multiphoton confocal micrsocopy:A microspectrocsopic comparison between Ti:sapphire and Cr:forsterite laser sources," *OptQuantumElectron*, volume 34, pp. 1251–1266, 2002

[48] Ashkin.A, Dziedzic.J.M, Bjorkholm.J.E, and Chu, "Observation of a single beam gradient force optical trap for dielectric particles," *OptLett*, volume 11, pp. 228–290, 1986

[49] Kuo.S.C, "Optical tweezers: A practical guide," *MicroscMicroanal*, volume 1, pp. 65–74, 1995

[50] Lang.M.J and Block.S.M, "Resource letter:LBOT-1:Laser based optical tweezers," *AmJPhys*, volume 71, pp. 201–215, 2006

[51] Svboda.K and Block.S.M, "Biological applications of optical forces," *AnnuRevBiophysBiomolStruct*, volume 23, pp. 247–285, 1994

[52] Padgett.M, Molloy.J, and McGloin.D, editors, *Optical tweezers methods and applications*, CRC Press, 2010

[53] Maxwell.J.C, *Treatise on electricity and magnetism*, Clarendon Press, 1873

[54] Lebedev.P.N, "Experimental Examination of Light Pressure," *Ann Der Physik*, volume 6, p. 433, 1901

[55] Einstein.A, "Zur Quantentheorie der Stahlung (On the Quantum Mechanics of Radaiation)," *Physikalische Zeitschrift*, volume 18, pp. 121–128, 1917

[56] Ashkin.A, "Optical trapping and manipulation of neutral particles using lasers," *PNatlAcdSciUSA*, volume 94, pp. 4853–4860, 1996

[57] Ashkin.A and Dziedzic.J.M, "Optical levitation by radiation pressure," *ApplPhysLet*, volume 19, pp. 283–286, 1971

[58] Ashkin.A, "Forces of a single beam gradient laser trap on a dielectric sphere in the ray optics regime," *BiophysJ*, volume 61, pp. 569–582, 1992

[59] Hansen.P.M, Bhatia.V.K, Harrit.N, and Oddershede.L, "Expanding the optical trapping range of gold nanoparticles," *NanoLett*, volume 5, pp. 1937–1942, 2005

[60] Gouesbet.G, Maheu.B, and Gehan.G, "Light scattering from a sphere arbitrarily located in a Gaussian beam, using a Bromwich formulation," *JOptSocAmA*, volume 5, pp. 1427–1443, 1988

[61] Mie.G, "Beitrage zur Optik truber Meide, Speziell Kolloideler Metalosurgen," *Ann der Physik*, volume 25, pp. 377–452, 1908

[62] Nieminen.T.A, Loke.V.L.Y, Stilgoe.A.B, Knoner.G, Branczyk.A.M, Heckenberg.N.R, and Rubinsztein-Dunlop.H, "Optical tweezers computational toolbox," *JOptAPureApplOpt*, volume 9, pp. 196–203, 2007

[63] Chiou.A.E, Wang.W, Sonek.G, Hong.J, and Berns.M.W, "Interferometric optical tweezers," *OptCommun*, volume 133, pp. 7–10, 1997

[64] MacDonald.M.P, Spalding.G.C, and Dholakia.K, "Microfluidic sorting in an optical lattice," *Nature*, volume 426, pp. 421–424, 2003

[65] Tsukakoshi.M, Kurata.S, Nomiya.Y, Ikawa.Y, and Kasuya.T, "A novel method of DNA transfection by laser microbeam cell surgery," *ApplPhysB*, volume 35, pp. 135–140, 1984

[66] Stevenson.D.J, Gunn-Moore.F.J, Campbell.P, and Dholakia.K, *Transfection by optical injection*, chapter 3, CRC Press, 2010

[67] Stevenson.D.J, Gunn-Moore.F.J, Campbell.P, and Dholakia.K, "Single cell optical transfection," *JRSocInterface*, volume 7, pp. 863–871, 2010

[68] Nikolskaya.A.V, Nikolski.V.P, and Efimov.I.R, "Gene printer: Laser scanning targeted transfection of cultures cardiac neonatal rat cells," *CellCommunAdhes*, volume 13, pp. 217–222, 2006

[69] Palumbo.G, Caruso.M, Crescenzi.E, MF, Tecce, Roberti.G, and Colasanti.A, "Targeted gene transfer in eucaryotic cells by dye assisted laser optoporation," *JPhotochemPhotobiolB*, volume 36, pp. 41–46, 1996

[70] Paterson.L, Agate.B, Comrie.M, Ferguson.R, Lake.T, Morris.J, Carruthers.A, Brown.C.T.A, Sibbett.W, Bryant.P, Gunn-Moore.F.J, Riches.A, and Dholakia.K, "Photoporation and cell transfection using a violet diode laser," *OptExpress*, volume 13, pp. 595–600, 2005

[71] Schneckenburger.H, Hendinder.A, Sailer.R, Strauss.W.S, and Schmitt.M, "Laser assisted optoporation of single cells," *JBiomedOpt*, volume 7, pp. 41–416, 2002

[72] Torres-Mapa.M.L, Angus.L, Ploschner.M, Dholakia.K, and Gun, "Transient transfection of mammalian cells using a violet diode laser," *JBiomed*, volume 15, p. 041506, 2010

[73] Paterson.L, Papagiakoumou.E, Milne.G, Garces-Chavez.V, Tatarkova.S.A, Sibbett.W, Gunn-Moore.F.J, Bryant.P, Riches.A, and Dholakia.K, "Light induced cell separation in a tailored optical landscape," *ApplPhys Lett*, volume 87, p. 123901, 2005

[74] Badr.Y.A, Kereim.M.A, Yehia.M.A, Fouad.O.O, and Bahieldin.A, "Production of fertile transgenic wheat plants by laser micropuncture," *PhotochemPhotobiolSci*, volume 4, pp. 803–807, 2005

[75] Guo.Y, Liang.H, and Berns.M.W, "Laser mediated gene transfer in rice," *PhysiolPlant*, volume 93, pp. 19–24, 1995

[76] Shirahata.Y, Ohkohchi.N, Itagak.H, and Satomi.S, "New technique for gene transfection using laser irradiation," *JInvestigMed*, volume 49, pp. 184–190, 2001

[77] Tao.W, Wilkinson.J, Stanbridge.E.J, and Berns.M.W, "Direct gene transfer into human cultures cells facilitated by laser micropuncture of the cell membrane," *PNAS*, volume 84, pp. 4180–4184, 1987

[78] Clark.I.B, Hanania.E.G, Stevens.J, Gallina.M, Fleck.A, Brandes.R, Palsson.B.O, and Koller.M.R, "Optoinjection for efficient targeted delivery of a broad range of compounds and macromolecules into diverse cell types," *JBiomedOpt*, volume 11, p. 014034, 2006

[79] Soughayer.J.S, Krasieva.T, Jacobson.S.C, Ramsey.J.M, Tromberg.B.J, and Allbritton.N.L, "Characterization of cellular optoporation with distance," *AnalChem*, volume 72, pp. 1342–1347, 2000

[80] Knoll.T, Trojan.L, Langbein.S, Sagi.S, Alken.P, and Michel.M.S, "Impact of holmium:YAG lasers on the efficiency of DNA delivery in transitional cell carcinoma," *LasersMedSci*, volume 19, pp. 33–36, 2004

[81] Mohanty.S.K, Sharma.M, and Gupta.P.K, "Laser assisted microinjection into targeted animal cells," *Biotechnol Lett*, volume 25, pp. 895–899, 2003

[82] Albers.P, Stark.E, and Huber.G, "Continuous-wave laser operation and quantum efficiency of titanium-doped sapphire," *JOptSocAmB*, volume 3, pp. 134–139, 1986

[83] Kane.D.M, "Astigmatism compensation in off axis laser resonators with two or more coupled foci," *OptCommun*, volume 71, pp. 113–118, 1989

[84] Kogelnik.H, Ippen.E, Dienes.A, and Shank.C, "Astigmatically compensated cavities for cw dye lasers," *IEEEJQuantumElectron*, volume 8, pp. 373–379, 1972

[85] Magni.V, Cerrulo.G, and Silverstri.S, De, "Closed form gaussian beam analysis of resonators containing a Kerr medium for femtosecond lasers," *OptCommun*, volume 101, pp. 365–370, 1993

[86] Spence.D.E, Kean.P.N, and Sibbett.W, "60-fsec pulse generation form a self mode locked Ti:sapphire laser," *OptLett*, volume 16, pp. 42–44, 1991

[87] Magni.V, Cerullo.G, and Silverstri.S, De, "ABCD matrix analysis of propagation of gaussian beams through Kerr media," *OptCommun*, volume 96, pp. 348–355, 1993

[88] Fork.R.L, Martinez.O.E, and Gordon.J.P, "Negative dispersion using pairs of prisms," *OptLett*, volume 9, pp. 150–152, 1984

[89] Block.S.M, *Construction of optical tweezers*, chapter C 7, Cold spring harbour laboratory press, 1997

[90] Lee.W.M, Reece.P.J, Marchington.R.F, Metzger.N.K, and Dholakia.K, "Construction and calibration of an optical trap on a fluorescence optical microscope," *NatProtoc*, volume 2, pp. 3226–3238, 2007

[91] Wei.S, Yi-Qui.W, and Chong-Ming.G, "Construction of an optical tweezers-calculation and experiments," *ChinPhys*, volume 9, pp. 856–860, 2000

[92] Dholakia.K and Reece.P, "Optical micromanipulation takes hold," *Nano Today*, volume 1, pp. 18–27, 2006

[93] Beer.A, "Bestimmung der Absorption des rothen Lichts in farbigen Flüssigkeiten," *AnnalPhysChem*, volume 86, pp. 78–88, 1852

[94] Martin.B, *Tissue culture techniques:An introduction*, Birkhauser, Boston, 1994

[95] Mather.J and Roberts.P, *Introduction to cell and tissue culture:Theory and technique (Introductory cell and molecular biology techniques)*, Springer, 1998

[96] Neumann, E, Schaefer-Ridder, M, Wang, Y, and Hofschneider, P, "Gene transfer into mouse lyoma cells by electroporation in high electric fields," *EMBO*, volume 1, pp. 841–845, 1982

[97] Sanford, J, Smith, F, and Russel, J, "Optimising the biolistic process for different biological applications," *METHOD ENZYMOL*, volume 217, pp. 483–509, 1993

[98] Shimada.T, Watanabe.W, Matsunaga.S, Higashi.T, Ishii.H, Fukui.K, Isobe.K, and Itoh.K, "Intracellular disruption of mitochondria in living HeLa cell with a 76-MHz laser oscillator," *OptExpress*, volume 13, pp. 9869–9880, 2005

[99] Watanabe.W, Matsunaga.S, Shimada.T, Higashi.T, Fukul.K, and Itoh.K, "Femtosecond laser disruption of mitochondria in living cells," *MedLaserAppl*, volume 20, pp. 185–191, 2005

[100] Soltoff.S.P, "Evidence that tryphostins AG10 and AG18 are mitochondrial uncouplers that alter phosphorylation dependent cell signalling," *JBiolChem*, volume 279, pp. 10910–10918, 2004

[101] Walpole.C, Wrigglesworth.R, Bevan.S, Campbell.E, Dray.A, James.I, Masdin.K, Perkins.M, and Winter.J, "Analogs of capsaicin with agonist activity as novel analgesic agents-structure activity studies.2.The amide bond B-region," *JMedChem*, volume 36, pp. 2373–2380, 1993

[102] Walpole.C, Wrigglesworth.R, Bevan.S, Campbell.E, Dray.A, James.I, Masdin.K, Perkins.M, and Winter.J, "Analogs of capsaicin with agonist activity as novel analgesic agents-structure-activity studies.3. The hydrophobic side chain C region," *JMedChem*, volume 36, pp. 2381–2389, 1993

[103] Walpole.C, Wrigglesworth.R, Bevan.S, Campbell.E, Dray.A, James.I, Perkins.M, Reid.D, and Winter.J, "Analogs of capsaicin with agonist activity as novel analgesic agents-structure ativity studies.1.the aromatic A-region," *JMedChem*, volume 36, pp. 2362–2372, 1993

[104] Conway.S, "TRPing the switch on pain: an introduction to the chemistry and biology of capsaicin and TRPV1," *ChemSocRev*, volume 37, pp. 1530–1545, 2008

[105] Caterina.M, Schumacher.M, Tominaga.M, Rosen.T, Levine.J, and Julius.D, "The capsaicin receptor:A heat activated Ion channel in the pain pathway," *Nature*, volume 389, pp. 816–824, 1997

[106] Szallasi.A and Blumberg.P, "Vanilloid (capsaicin) receptors and mechanisms," *PharmacolRev*, volume 51, pp. 159–211, 1999

[107] Szallasi.A, Cortright.D, Blum.C, and Eid.S, "The vanilloid receptor TRPV1: 10 years from channel cloning to antagonist proof of concept," *NatRevDrugDiscov*, volume 6, pp. 357–372, 2007

[108] Zemelman.B, Nesnas.N, Lee.G, and Miesenbock.G, "Photochemical gating of heterologous ion channels:Remote control over genetically designated populations of neurons," *ProcN*, volume 100, pp. 1352–1357, 2003

[109] Katritzky.A, Vakulenco.A, Wilcox.A, and Bley.K, "Model compounds of caged capsaicin:Design,synthesis and photoreactivity," *JouOrgChem*, volume 68, pp. 9100–9104, 2003

[110] Carr.J, Wease.K, VanRyssen.M, Paterson.S, Agate.B, Gallagher.K, Brown.C.T.A, Scott.R, and Conway.S, "In vitro photo releaser of a TRPV1 agonist," *BioorgMedChemLett*, volume 16, pp. 208–212, 2006

[111] Zhao.J, Gover.T, Muralidharan.S, Auston.D, Weinreich.D, and Kao.J, "Caged vanilloid ligands for activation of TRPV1 receptors by 1 and 2 photon excitation," *Biochem*, volume 45, pp. 4915–4926, 2006

[112] Hagen.V, Dekowski.B, Kotzur.N, Lechler.R, Wiesner.B, Briand.B, and Beyermann.M, "7-[bis(carboxymethyl)amino]coumarin-4-ylmethoxycarbonyl derivatives for photorelease of carboxylic acids,alcohols/phenols, thioalcohols/thiophenols and amines," *ChemEurJ*, volume 14, pp. 1621–1627, 2008

[113] Appendino.G, Daddario.N, Minassi.A, Moriello.S, Petrocellis.L, and DiMarzo.V, "The taming of capsaicin. Reversal of the vanilloid activity of N-acylvanillamines by aromatic iodination," *JMedChem*, volume 48, pp. 4663–4669, 2005

[114] Appendino.G, Harrison.S, DePetrocellis.L, Daddario.N, Bianchi.F, Moriello.S, Trevisani.M, Benvenuti.F, Geppetti.P, and Marzo.V, "Halogenation of a capsaicin analogue leads to novel vanilloid TRPV1 receptor antagonists," *BritJPharmacol*, volume 139, pp. 1417–1424, 2003

[115] Simonetti.M, Fabbro.A, Zweyer.M, D'Arco.M, Nistri.A, and Giniatullin.R, "Comparison of P2X and TRPV1 receptors in ganglia or primary culture of trigeminal neurons and their modulation by NGF or serotonin," *MolPain*, volume 2, 2006

[116] Walpole.C, Bevan.S, Boverman.G, Boelstreli.J, Breckenridge.R, Davies.J, Hughes.G, James.I, Oberer.L, Winter.J, and Wrigglesworth.R, "The discovery of capsazepine, the first competitive agonist of the sensory neuron exitants capsaicin and resiniferatoxin," *JMedChem*, volume 37, pp. 1942–1954, 1994

[117] Blanc.A and Bochet.C, "Wavelength controlled orthogonal photolysis of protecting groups," *JOrgChem*, volume 67, pp. 5567–5577, 2002

[118] Bochet.C, "Chromatic orthogonality in organic synthesis," *Synlett*, pp. 2268–2274, 2004

[119] Bochet.C, "Orthogonal photolysis of protecting groups," *AngewChemIntEdEngl*, volume 40, pp. 2071–2073, 2001

[120] Bochet.C, "Wavelength selective cleavage of photolabile protecting groups," *Tetrahedron Lett*, volume 41, pp. 6341–6346, 2000

[121] Kessler.M, Glatter.R, Giese.B, and Bochet.C, "Sequentionally photocleaveable protecting groups in solidpphase synthesis," *OrgLett*, volume 5, pp. 1179–1181, 2003

[122] DelCampo.A, Boos.D, Spiess.H, and Jonas.U, "Surface modification with orthogonal photosensitive silanes for sequential chemical lithography and site selective particle deposition," *AngewChemIntEd*, volume 44, pp. 4707–4712, 2005

[123] Kantevari.S, Matsuzaki.M, Kanemoto.Y, Kasai.H, and Ellis-Davis.G, "Two colour, two photon uncaging of glutamate and GABA," *NatMethods*, volume 7, pp. 123–125, 2009

[124] Anwyl.R, "Synaptic Plasticity:A molecular switch for memory," *CurrBiol*, volume 4, pp. 854–856, 1994

[125] Riedel.G, Platt.B, and Micheau.J, "Glutamate receptor function in learning and memory," *BehavBrainRes*, volume 140, pp. 1–47, 2003

[126] Thirlwell.H, Corrie.J, Reid.G, Trentham.D, and Ferenczi.M, "Kinetics of relxation from rigor of permeabilized fast twitch skeletal fibers from the rabbit using novel caged ATP and Apyrase," *BiophysJ*, volume 67, pp. 2436–2447, 1994

[127] He.H, Kong.S.K, Lee.R.KY, Suen.YK, and Chan.K.T, "Targeted photoporation and transfection in human HepG2 cells by a fibre femtosecond laser at 1554 nm," *OptLett*, volume 33, pp. 2961–2963, 2008

[128] Sagi.S, Knoll.T, Trojan.L, Schaaf.A, Alken.P, and Michel.S, "Gene delivery into prostate cancer cells by holmium laser application," *ProstateCancerProstaticDis*, volume 6, pp. 127–130, 2003

[129] Misawa.H, Kooshioka.m, Sasaki.K, Kitamura.N, and Masuhara.H, "Three dimensional optical trapping and laser ablation of a single polymer latex particle in water," *JApplPhys*, volume 70, pp. 3829–3836, 1991

[130] Stevenson.D.J, Agate.B, Tsampoula.X, Fischer.P, Brown.C.T.A, Sibbett.W, Riches.A, Gunn-Moore.F.J, and Dholakia.K, "Femtosecond optical transfection of cells:viability and efficiency," *OptExpress*, volume 14, pp. 7125–7133, 2006

[131] Schomaker.M, JBaumgart.J, Ngezahayo.A, Bullerdiek.J, Nolte.I, Escobar.M, Lubatschowski.H, and Heisterkamp.A, "Plasmonic perforation of living cells using ultrashort laser pulses and gold nanoparticles," volume 7192, SPIE, 2009

[132] Nader.S, Reihani.S, and Oddershede.L, "Optimizing immersion media refractive index improves optical trapping by compensating spherical aberrations," *OptLett*, volume 32, pp. 1998–2000, 2007

[133] Punge.A, Rizzoli.S.O, Jahn.R, Wildanger.J.D, Meyer.L, Schonle.A, Kastrup.L, and Hell.S.W, "3D reconstruction of high-resolution STED microscope images," *MicroscResTech*, volume 71, pp. 644–650, 2008

[134] Umebayashi.Y, Miyamoto.Y, Wakita.M, Kobayashi.A, and Nishisaka.T, "Elevation of plasma membrane permeability on laser irradiation of extracellular latx particles," *JBiolChem*, volume 134, pp. 219–224, 2003

[135] Yao.C.P, Rahmanzadeh.R, Endl.E, Zhang.Z.X, Gerdes.J, and Huttman.G, "Elevation of plasma membrane permeability by laser irradiation of selectively bound nanoparticles," *JBiomedOpt*, volume 10, p. 064012, 2005

[136] Yamaguchi.A, Hosokawa.Y, Louit.G, Asahi.T, Shukunamni.C, Hiraki.Y, and Masuhara.H, "Nanoparticle injection to single animal cells using femtosecond laser induced impulsive force," *ApplPhysA*, volume 93, pp. 39–43, 2008

[137] Buer.C.S, Gahagan.K.T, Grover.A, and Weathers.P.J, "Insertion of Agrobacterium rhizogenes into Ginko biolboa using lasers as optical tweezers and scalpel," *PlantPhysiol*, volume 114, pp. 1613–1613, 1997

[138] Schutze.K, Clement-Sengewald.A, and Ashkin.A, "Zona drilling and sperm insertion with combined laser microbeam and optical tweezers," *Fertilsteril*, volume 61, pp. 783–786, 1994

[139] Chen.G and Yao.S.Q, "Lighting up cancer cells with dots," *The Lancet*, volume 364, pp. 2001–2003, 2004

[140] Parkin.S.J, Knoner.G, Nieminen.T.A, Heckenberg.N.R, and Rubinsztein-Dunlop.H, "Picolitre viscometry using optically rotated particles," *PhysRevE*, volume 76, p. 041507, 2007

[141] McNeil.P.L and Steinhardt.R.A, "Loss, restoration and maintenance of plasma membrane integrity," *JCell Biol*, volume 137, pp. 1–4, 1997

[142] McNeil.P.L, "Repairing a torn cell surface:make way, lysosomes to the rescue," *JCell Sci*, volume 115, pp. 873–879, 2002

[143] McNeil.P.L, Miyake.K, and Vogel.S.S, "The endomembrane requirement for cell surface repair," *PNAS*, volume 100, pp. 4592–4597, 2003

[144] Terasaki.M, Miyake.K, and McNeil.P.L, "Large plasma membrane disruptions are rapidly resealed by Ca2+ dependent vesicle-vesicle fusion events," *JCell-Biol*, volume 139, pp. 63–74, 1997

[145] Levy.R, Shaheen.U, Cesbron.Y, and See.V, "Gold nanoparticles delivery in mammalian live cells:a critical review," *Nano Reviews*, volume 1, 2010

[146] Tsampoula.X, Garces-Chavez.V, Comrie.M, Stevenson.D.J, Agate.B, Brown.C.T.A, Gunn-Moore.F.J, and Dholakia.K, "Femtosecond cellular transfection using a nondiffracting light beam," *ApplPhysLett*, volume 91, p. 053902, 2007

[147] Cunha.S, Woldringh.C.L, and Odijk.T, "Polymer merdiated compaction and internal dynamics of isolated Escherichia coli nucleoids," *JStructBiol*, volume 13, pp. 53–56, 2001

[148] Vologodskii.A.V and Cozzarelli.N.R, "Conformational ad thermodynamic properties of supercoiled DNA," *AnnuRev*, volume 23, pp. 609–643, 1994

[149] Mthunzi.P, Lee.W.M, Riches.A, Brown.C.T.A, Gunn-Moore.F.J, and Dholakia.K, "Intracellular dielectric tagging for inmproved optical manipulation of mammalian cells," *IEEEJSelTopQuant*, volume 16, pp. 608–618, 2010

[150] Goksor.M, Enger.J, and Hanst.D, "Optical manipulation in combination with multiphoton microscopy for single cell studies," *ApplOpt*, volume 43, pp. 4831–4837, 2004

[151] Scrimgeour.J, Eriksson.E, and Go, "Laser surgery and optical trapping in a laser scanning microscope," *MethodsCellBiol*, volume 82, pp. 629–646, 2007

[152] Agate.B, Brown.C.T.A, Sibbett.W, and Dholakia.K, "Femtosecond optical tweezers for in-situ control of two-photon fluorescence," *OptExpress*, volume 12, pp. 3011–3017, 2004

[153] Ando.J, Bautista.G, Smith.N, Fujita.K, and Ricardo.D, "Optical trapping and surgery of living yeast cells using a single laser," *RevSciInstrum*, volume 79, p. 103705, 2008